R395

Technical Report

DYNAMIC SHEAR STRENGTH OF REINFORCED CONCRETE BEAMS

PART I

December 1965

U. S. NAVAL CIVIL ENGINEERING LABORATORY
Port Hueneme, California

DYNAMIC SHEAR STRENGTH OF REINFORCED CONCRETE BEAMS - PART I

Y-F008-08-02-110

Type C

by

William A. Keenan

ABSTRACT

A series of reinforced concrete beams were tested to study shear and diagonal tension in beams under dynamic load. The tests constitute the first phase of a study designed (1) to determine criteria for the minimum amount of web reinforcement required for developing the ultimate flexural resistance of beams and (2) to evaluate the difference between these criteria for static and dynamic loading.

Nine beams were tested; three were loaded statically and six dynamically. Each beam was simply supported at its ends; all loads both static and dynamic were uniformly distributed along the span. Major variables were stirrup spacing, peak load, load-duration, and rate of loading.

It was found that (1) the shear resistance at diagonal tension cracking and at first yielding of the stirrups increased under dynamic load, and (2) the formulas presented in a definitive report by a joint committee of the American Concrete Institute (ACI) and the American Society of Civil Engineers (ASCE) adequately predicted the static shear resistance but grossly underestimated the dynamic shear resistance. Evidence is cited which attributes the increase in shear resistance under dynamic load to an increase in the tensile strength of the concrete and yield strength of the stirrups. An effective amount of web reinforcement (rf_y), 69 percent less than the amount required by the ACI-ASCE formula, resulted in flexure failures under static and dynamic load.

Equations are presented which permit prediction of the dynamic shear resistance corresponding to diagonal tension cracking and first yielding of the stirrups. A dynamic response chart is developed for estimating the maximum shear at the supports of a simply supported beam under a uniform dynamic load.

CONTENTS

INTRODUCTION

Current design procedures for resisting shear and diagonal tension in reinforced concrete (R/C) beams are similar whether the load is applied slowly or rapidly. In practice, beams are generally proportioned to provide enough dynamic flexural resistance and ductility to limit the deflection under dynamic load to a value less than the acceptable maximum deflection. Design procedures developed for static loads then are applied to determine the minimum amount of web reinforcement required to develop this dynamic flexural resistance and prevent a sudden, premature failure in shear. Whether this approach is conservative for designing R/C beams to resist dynamic shear and diagonal tension depends on the relative increase in the flexural and shear resistance under dynamic loads and the degree of conservatism of the static design procedure.

The objectives of this study are (1) to develop criteria for the minimum amount of vertical web reinforcement required to develop the ultimate flexural resistance of beams, and (2) to study the difference between these criteria for static and dynamic loading.

Defining the shear resistance of R/C beams is a complex problem involving several variables. These include beam geometry, nature of loading, amount and distribution of longitudinal and web reinforcement, and the mechanical properties of the reinforcement and concrete. The relationships between the variables are almost entirely empirical in nature; little is known regarding the underlying basic phenomena.

A summary of present knowledge of the shear resistance of R/C beams under static loading is presented in the report of the ACI-ASCE Committee 426(326), "Shear and Diagonal Tension."[1] The report summarizes the vast amount of experimental data and presents empirical procedures to determine the minimum amount of web reinforcement required to produce a flexural failure. The procedures are based on the empirical observation that the effective amount of web reinforcement required to produce a flexural failure is a function of the difference between the shears corresponding to the ultimate flexural resistance and the diagonal tension-cracking resistance.

A systematic study of the data in the ACI-ASCE Committee report indicated that the diagonal tension cracking resistance depends primarily on the percentage of longitudinal reinforcement, effective depth of beam, tensile strength of the concrete, and the moment-shear ratio at the critical section. Thus, the minimum amount of web reinforcement is in part a function of the yield strength of the stirrups and longitudinal tensile reinforcement, the tensile strength of the concrete, and the moment-shear ratio at the critical section. Each of these quantities differs between static and dynamic loading.

Dynamic loading complicates the problem of measuring and relating the effect of the variables; it also introduces additional variables such as peak dynamic load level, load duration, and inertia forces resulting from acceleration of the beam's mass. These inertia forces change the magnitude and distribution of shear and moment along the span and thus change the moment-shear ratio along the span. At the same time, the rapid rate of loading or rapid rate at which the materials of the beam must develop resistance changes the mechanical properties of the longitudinal and web reinforcement as well as those of the concrete. Thus, the variation along the span in moment and shear and resistance to shear and diagonal tension is different under static and dynamic loading. Therefore, the amount and distribution of web reinforcement required to force a flexural failure are different for static and dynamic loading. The magnitude and importance of these differences are unknown and need study.

Knowledge of the shear resistance of beams under dynamic loading is meager. Although there is considerable test data for the behavior of beams subjected to dynamic load, essentially none of such beams were designed or instrumented for study of dynamic shear. There is no experimental data on the shear resistance of beams with or without web reinforcement under any type of dynamic load.

Present knowledge of the shear resistance and behavior of beams subjected to uniform loading is very limited. Nevertheless, uniform loading is the type most commonly encountered by the designer of blast-resistant construction. All available experimental data on beams under uniform load pertains to static loads and beams without web reinforcement; no data involving uniform loads pertains to beams with web reinforcement.

SCOPE AND APPROACH

To study the cited problems, an experimental and analytical program consisting of four phases is contemplated. Lack of knowledge of the effect of dynamic loading on the relationship between the variables makes it essential that each phase of the study be planned and carried out step by step; the scope and approach for each phase must be based on the results of previous phases.

The first phase of the study, described here in Part I, comprises tests wherein peak dynamic load level, load duration, and stirrup spacing are varied. All beams used were identical except for the amount of web reinforcement. The yield strength and size of the vertical stirrups were selected such that a stirrup spacing no greater than one-half the effective depth of the beam was required to produce a shear failure.

Nine beams were tested. Each beam was simply supported at its ends; all loads, both static and dynamic, were uniformly distributed along the length of the beam.

An important consideration in planning the first phase was the proper distribution of web reinforcement along the span. Theoretically, the distribution of web reinforcement in beams under uniform static load should be varied linearly from a maximum at the critical section near the supports to zero somewhere near midspan. Although this distribution may be optimum for static loads (a probability not actually substantiated by tests), there was no assurance that the variation in dynamic moment and shear or in the resistance to dynamic shear and diagonal tension would vary in the same way. Therefore, it was difficult to justify a linear distribution of web reinforcement.

The other alternatives were to vary the web reinforcement in some arbitrary manner or to provide uniform web reinforcement throughout the span. The former course would involve a variation in either the size or spacing of the stirrups along the span. Either of these variations would have undoubtedly confused the interpretation of the test results and increased the number of variables. Uniform spacing of web reinforcement would not in itself be undesirable from the standpoint of its contribution to shear resistance, since it would simply ensure that the critical section be near the end of the beam.

After careful consideration of each of the two alternatives, uniform spacing of web reinforcement was adopted; the size and spacing of stirrups provided at the critical section were maintained uniform out to a distance one-third of the span (L/3). Only nominal web reinforcement (or ties) was provided throughout the middle third of the span.

The same size of stirrup was used in all beams, but a different stirrup spacing was used at each end of each beam between the support and the L/3 point of the span. This procedure was adopted after conducting pilot tests to weigh the possible disadvantages of the procedure against the advantages of reduction in instrumentation and availability of two different stirrup spacings for study from one beam test. The pilot tests indicated that the stirrup spacing at one end of the beam had little effect on the shear resistance of the other, and that unsymmetrical distribution of web reinforcement had little effect on the response and behavior of beams under dynamic load (the transient variation in the measured reaction at each end of the pilot beams under dynamic load being essentially the same).

The overall approach was to start with beams having a small effective amount of web reinforcement to ensure their failure in shear under static loading. Then, similar beams were to be tested under dynamic loading to obtain information regarding the amount of increase or decrease in shear resistance. The first phase of the study following this approach has been completed, with results presented here.

Based on the relative shear resistance observed in the dynamic tests as compared to the static tests, another set of beams will be tested in the next phase of the program. This procedure will be repeated until the minimum amount of web reinforcement required to force a beam to fail in flexure under static and dynamic loading is determined.

EXPERIMENTAL WORK

Test Specimen

Approximately fifty different beam designs were considered in an attempt to select a practical design in which (1) the geometry and resistance of the beams were within the limitations of the Naval Civil Engineering Laboratory (NCEL) Blast Simulator, (2) the failure mode of the beam without web reinforcement was diagonal tension and not shear compression, (3) the difference between the diagonal tension cracking resistance and ultimate flexural resistance was large enough to study the effective contribution of several different amounts of web reinforcement, and (4) the beam had ample ductility and an elasto-plastic flexural resistance diagram to simplify the analysis of the dynamic test data.

Description. Details of the test beam selected for Phase 1 are shown in Figure 1 and Table I. The width, depth, overall length, and clear span of each beam were 7.75, 15, 154, and 144 inches, respectively. Reinforcement in each beam consisted of two No. 9 deformed bars for longitudinal tensile steel, two No. 7 deformed bars for longitudinal compression steel, and No. 2 deformed bars for vertical web reinforcement or stirrups. The stirrups were the box type, hooked to the compression steel and spaced 6 inches on centers at one end and 4 inches on centers at the other end of the beam as shown in Figure 1. The ends of each beam were supported on and bolted to 10-inch-long by 1-inch-thick bearing plates which were free to rotate and translate.

The beams were designated WD1 through WD9. Several of the beams were loaded dynamically more than once, in which case an additional "dash" number was added to the beam designation to indicate the cycle of loading. For example, WD8-4 means beam number 8, fourth dynamic loading.

Material Properties. The average properties of the steel reinforcing bars in each beam are summarized in Table I. All bars of each size were from the same lot and satisfied the deformation requirements of Specification A305-56T of the American Society for Testing and Materials (ASTM).

The No. 7 and No. 9 bars satisfied the requirements of ASTM A432. Typical stress-strain curves for these bars are shown in Figure 2. As indicated, the No. 7 and No. 9 bars exhibited a linear stress-strain relationship up to a well-defined minimum yield stress of 66,000 and 70,000 psi respectively. The yield range was flat to a minimum strain of 1.3 percent.

The No. 2 bars were of intermediate grade steel. These are not commonly available commercially. The typical stress-strain curves for them are shown in Figure 2. The yield strength was about 65,000 psi as rolled and delivered. The bars were annealed in an oven at 1,800°F and cooled to room temperature in the oven over an 8-hour period to reduce the yield strength to between 30,000 and 40,000 psi. The yield range of the annealed bar was flat to a minimum strain of 1.0 percent.

The effect of strain rate on the tensile yield strength of the No. 9 steel reinforcing bars is shown in Figure 3. The data in this figure are the results of rapid load tests of a series of tensile specimens machined from the No. 9 deformed bars. As indicated, the yield strength increased with increasing strain rate; the increase was about 26 percent when the steel was strained at a rate of about 0.35 in./in./sec. These tests are described in detail in Appendix A.

The beams were cast using a 3000-psi concrete mix made from Type I portland cement, 3/4-inch maximum size San Gabriel aggregate and San Gabriel sand having a fineness modulus of 2.82. Mix proportions were 1.00 : 3.82 : 3.66 by weight, with a water-cement ratio of 0.71 by weight or 7.98 gallons per sack. The cement factor was 4.7 sacks per cubic yard.

Average properties of the concrete in each beam are summarized in Table I.

The effect of stress rate on the tensile splitting strength of the concrete is shown in Figure 4. Data in this figure are the results of rapid load tests on a series of 4- by 8-inch cylinders cast from the same mix used in the beams. The mode of failure was the same under static and dynamic loading. However, the tensile splitting strength of the cylinders increased with an increase in loading rate. As indicated, the tensile splitting strength increased about 70 percent when the concrete was stressed at a rate of 300,000 psi per second. These tests are described in detail in Appendix B.

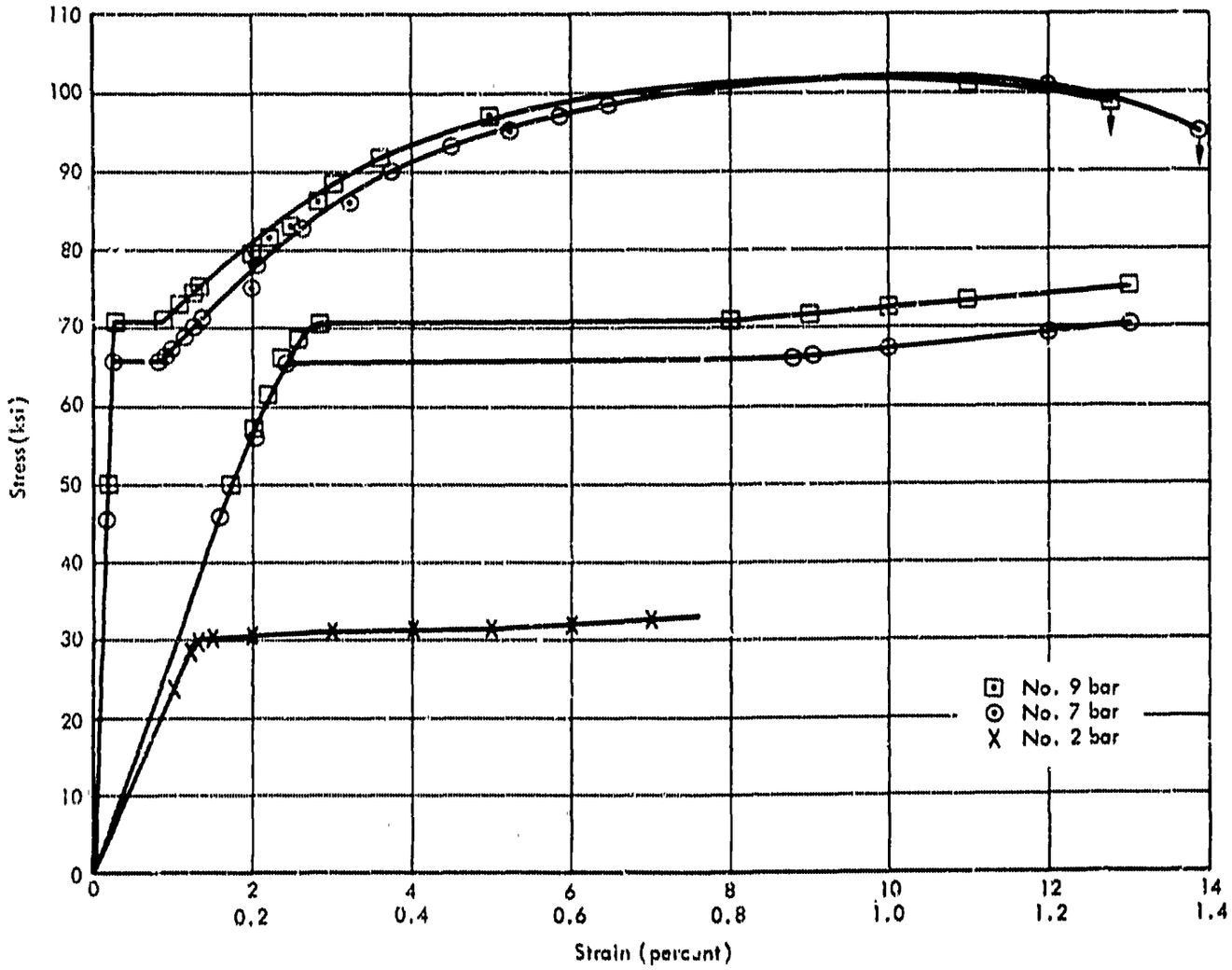

Figure 2. Typical stress-strain curves for reinforcing bars.

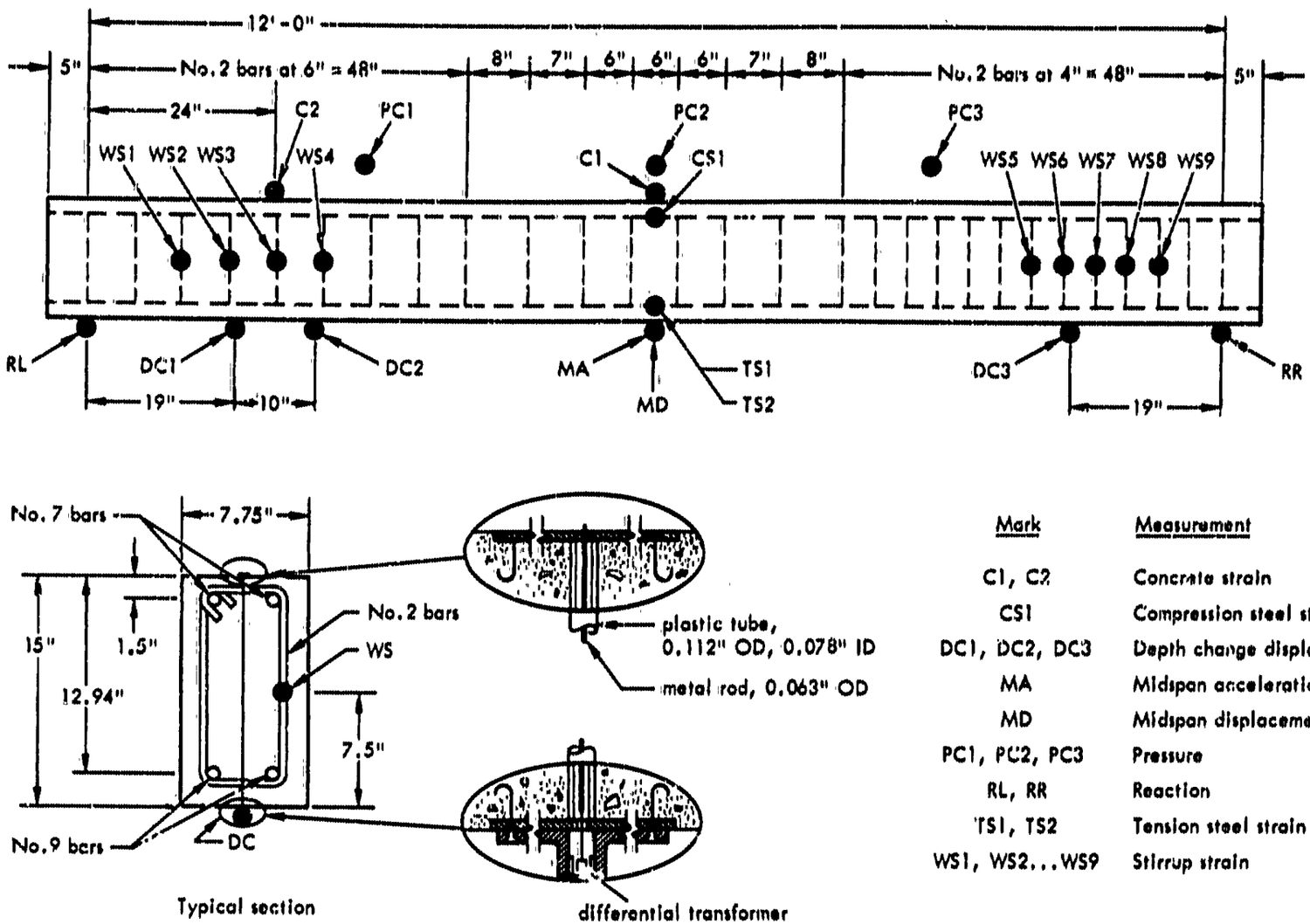

Mark	Measurement
C1, C2	Concrete strain
CS1	Compression steel strain
DC1, DC2, DC3	Depth change displacement
MA	Midspan acceleration
MD	Midspan displacement
PC1, PC2, PC3	Pressure
RL, RR	Reaction
TS1, TS2	Tension steel strain
WS1, WS2...WS9	Stirrup strain

Figure 1. Beam details and instrumentation, series WD.

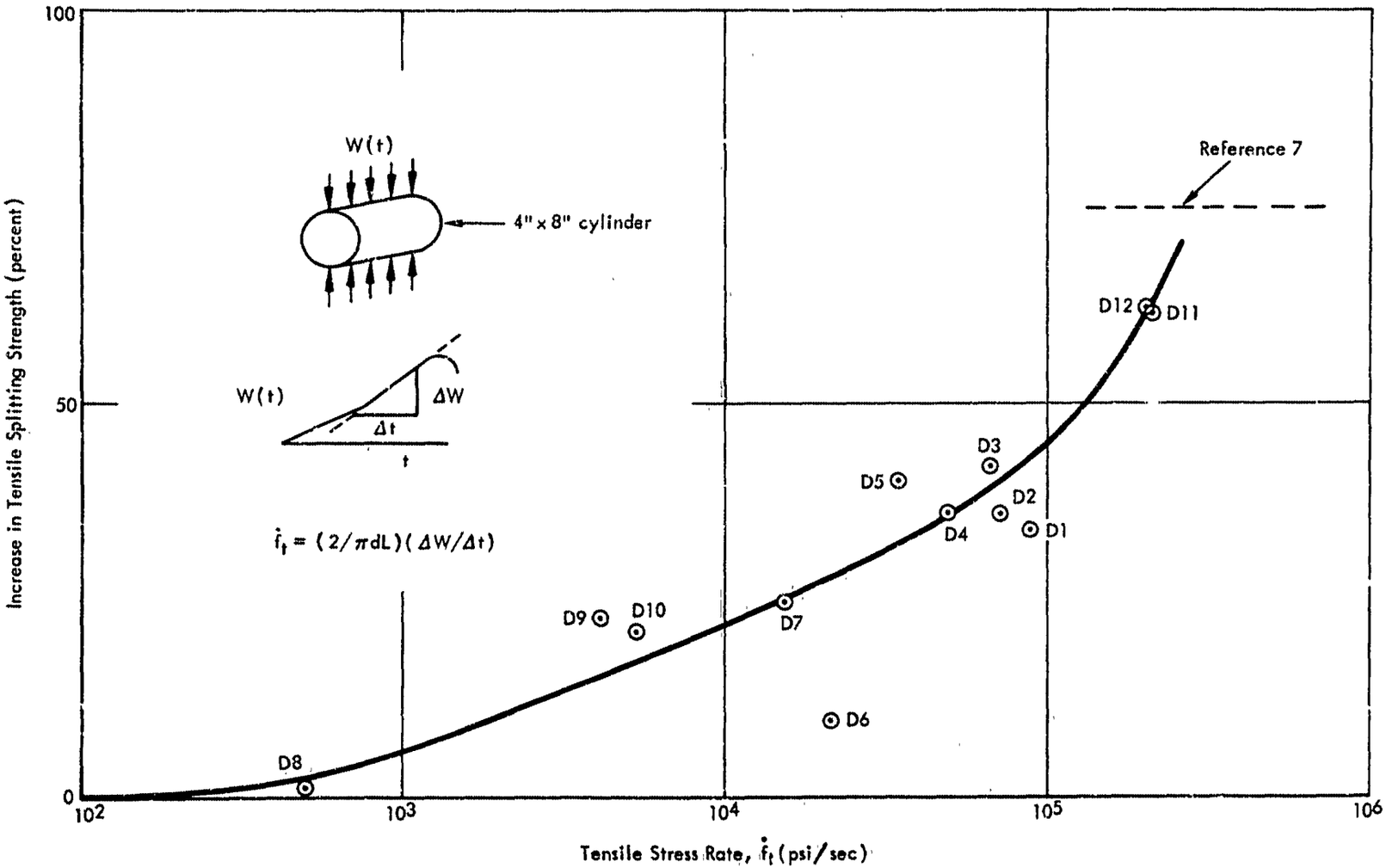

Figure 4. Increase in tensile splitting strength versus tensile stress rate curve.

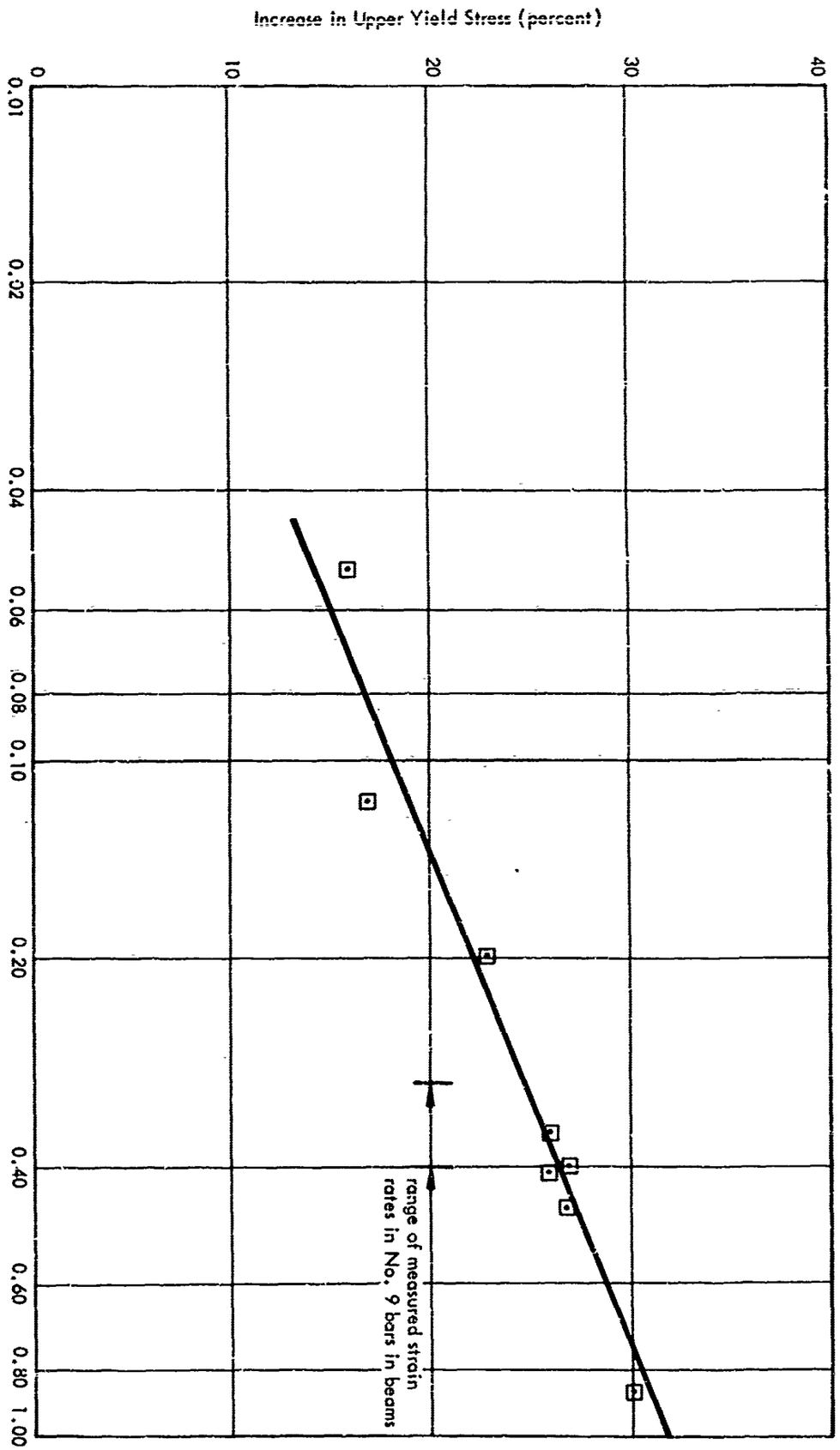

Figure 3. Increase in upper yield stress versus strain rate curve for No. 9 bars.

Table I. Geometric and Material Properties of Beams

Beam No.	Concrete Strength			Beam Dimensions				Longitudinal Reinforcement				Web Reinforcement					
								Tension		Compression		Left End			Right End		
	Age (days)	f_c' [1] (ksi)	f_t' [2] (psi)	b (in.)	h (in.)	d (in.)	L/d	p (%)	f_y (ksi)	p' (%)	f_y (ksi)	s (in.)	f_y (ksi)	rf_y (psi)	s (in.)	f_y (ksi)	rf_y (psi)
WD1	21	3.44	360	7.75	15	12.94	11.1	1.99	70.0	1.20	66.3	6	41.0	88	4	40.5	130
WD2	20	3.31	338	7.75	15	12.94	11.1	1.99	70.1	1.20	65.5	6	39.0	84	4	41.5	133
WD3	20	2.95	322	7.75	15	12.94	11.1	1.99	69.1	1.20	67.2	6	33.0	71	4	33.0	106
WD4	21	3.33	336	7.75	15	12.94	11.1	1.99	70.0	1.20	68.4	6	34.0	73	4	44.0	141
WD5	20	2.95	303	7.75	15	12.94	11.1	1.99	70.0	1.20	66.4	6	31.0	67	4	31.0	99
WD6	22	3.14	362	7.75	15	12.94	11.1	1.99	65.5	1.20	65.8	6	30.0	65	4	31.0	99
WD7	20	3.21	346	7.75	15	12.94	11.1	1.99	72.1	1.20	66.4	6	40.5	87	4	40.5	130
WD8	20	2.59	293	7.75	15	12.94	11.1	1.99	64.5	1.20	69.1	6	37.3	80	4	38.0	122
WD9	20	2.69	311	7.75	15	12.94	11.1	1.99	71.4	1.20	65.2	6	39.5	85	4	38.0	122

$E_s = 28.3 \times 10^6$ psi average

$E_s' = 29.0 \times 10^6$ psi average

$E_v = 25.1 \times 10^6$ psi average

1/ f_c' = average from three cylinder tests

2/ f_t' = average from three split cylinder tests

Fabrication. The reinforcing cage was assembled and positioned in a steel form by hydrostone spacers placed at the middle and at each end of the cage. The stirrups were wired to the top and bottom longitudinal reinforcement, and lifting hooks were wired to the stirrups as a means for transporting the finished beam.

Three plastic tubes, 0.11 inches in outer diameter, were positioned vertically in the form to provide holes of 0.078-inch inner diameter through the depth of the beam. The plastic tubes were made rigid during the casting operation by inserting a metal rod through them. A tube was placed 24 inches from each end of the beam and 34 inches from the end having the larger stirrup spacing as shown in Figure 1.

Four metal tubes were positioned vertically in the form to provide 1.060-inch-diameter bolt holes through the depth of the beam; one 2 inches and one 8 inches from each end of the beam. These holes permitted the beam to be bolted to its bearing plates prior to testing.

All beams were cast in a steel form in the upright position. The concrete was mixed in a 16-cubic-foot capacity horizontal, nontilting, drum-type mixer. One batch of concrete was required for each beam and six concrete control cylinders. The concrete was vibrated internally with a rod vibrator.

The forms were stripped from the beam and cylinders 5 days after casting, and subsequently both the beams and the control cylinders were covered with wet burlap and moist cured until tested. The test age of each beam and its companion cylinders is listed in Table I.

Test Equipment

Loading Machine. The beams were tested in the NCEL Blast Simulator (Figure 5), which is capable of applying a uniformly distributed static or dynamic load.[2] In this facility, dynamic load is applied to the beam by generating expanding gases in the simulator from the detonation of Primacord by means of two blasting caps. The peak dynamic pressure is controlled by the amount of Primacord; the decay time, by opening a series of valves which vent the gases to the atmosphere. A static load is applied by admitting compressed air into the simulator by means of a compressor. The design capacity of the simulator is 185 psi.

Instrumentation. Instrumentation was located as shown in Figure 1. Applied load, PC1, PC2, and PC3, was measured with Statham pressure cells. Each support reaction, RL and RR, was measured with a 60,000-pound-capacity Kulite-Bytrex load cell mounted between the plates of each support cart (Figure 6). Midspan displacement, MD, was measured with a 6-inch-capacity Bourns potentiometer; the changes in beam depth at the critical section for shear, DC1, DC2, and DC3, were measured with 0.02-inch-capacity Crescent differential transformers. Midspan acceleration, MA, was measured with a 100-g-capacity Statham accelerometer. Strains in the longitudinal steel, TS1, TS2, and CS1, were measured with two Baldwin-Lima-Hamilton electric foil strain gages, type FA-100-12, placed diametrically opposite each other on the bar and wired to form opposite arms of a Wheatstone bridge circuit. Strains in the stirrups, WS1 through WS9, were measured with Micro Measurements electric foil strain gages, type EA-06-500EH. Strains in the top fiber of the concrete, C1 and C2, were measured with type A9-2, SR-4 electric strain gages.

All measurements were recorded with Consolidated Electrodynamics Corporation (CEC) System D equipment and two CEC 5-119 oscillographs.

Test Procedure

Strain gages, C1 and C2, were bonded to the face of the concrete, and the transducers, DC1, DC2, and DC3, were fastened to the beam. (See Figure 1.) Then, the vertical faces of the beam were whitewashed to emphasize the crack patterns in the concrete during the test, and lined with black paint to indicate the location of the stirrups and longitudinal reinforcement. After the beam was positioned and bolted on the reaction carts, the whole unit was positioned in the blast simulator and anchored to the concrete foundation. Finally, transducers MA and MD were fastened to the beam, all electrical connections were made, and a strip of neoprene was placed over the top of the beam to seal the pressure chamber of the simulator. A beam ready for testing is shown schematically in Figure 7.

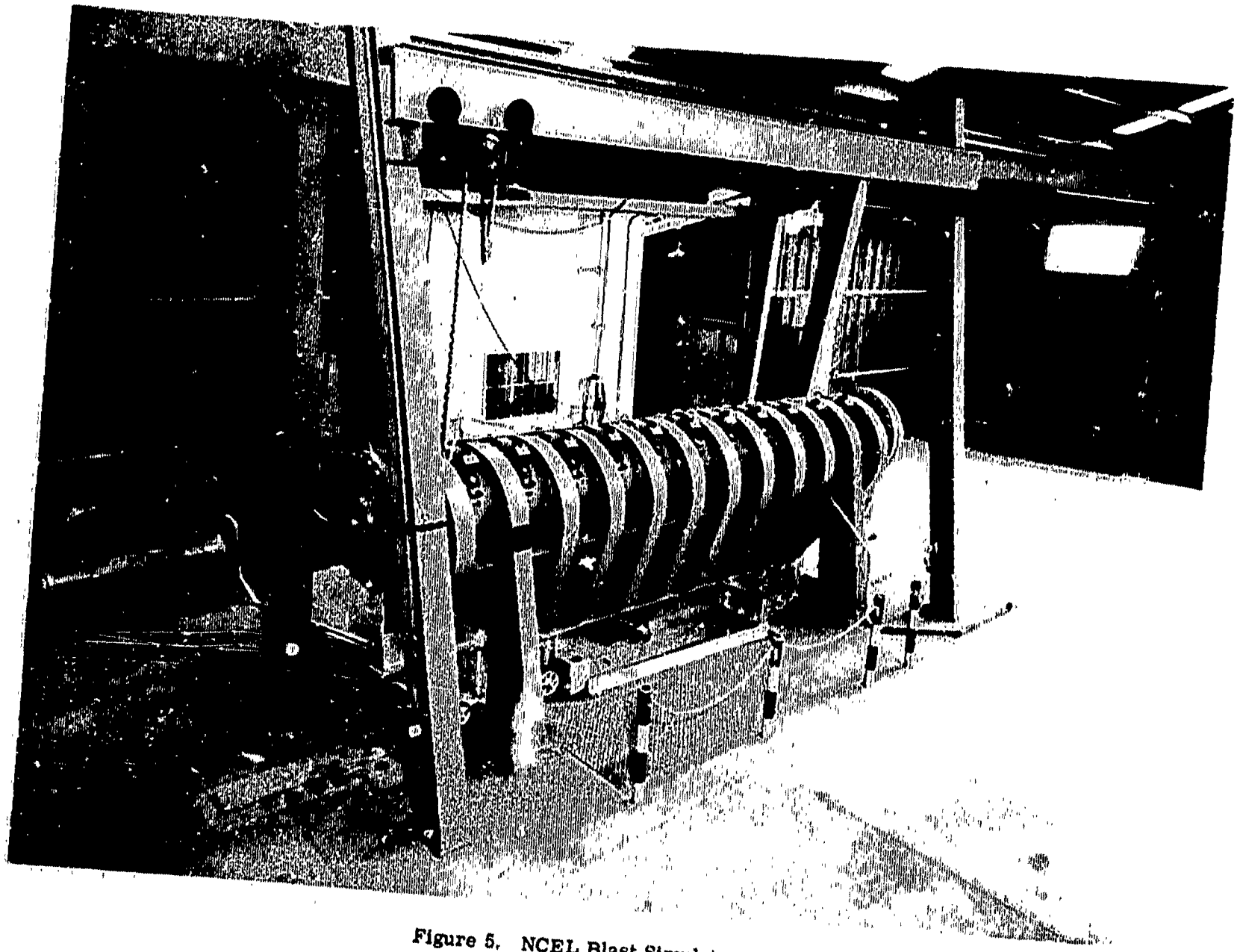

Figure 5. NCEL Blast Simulator.

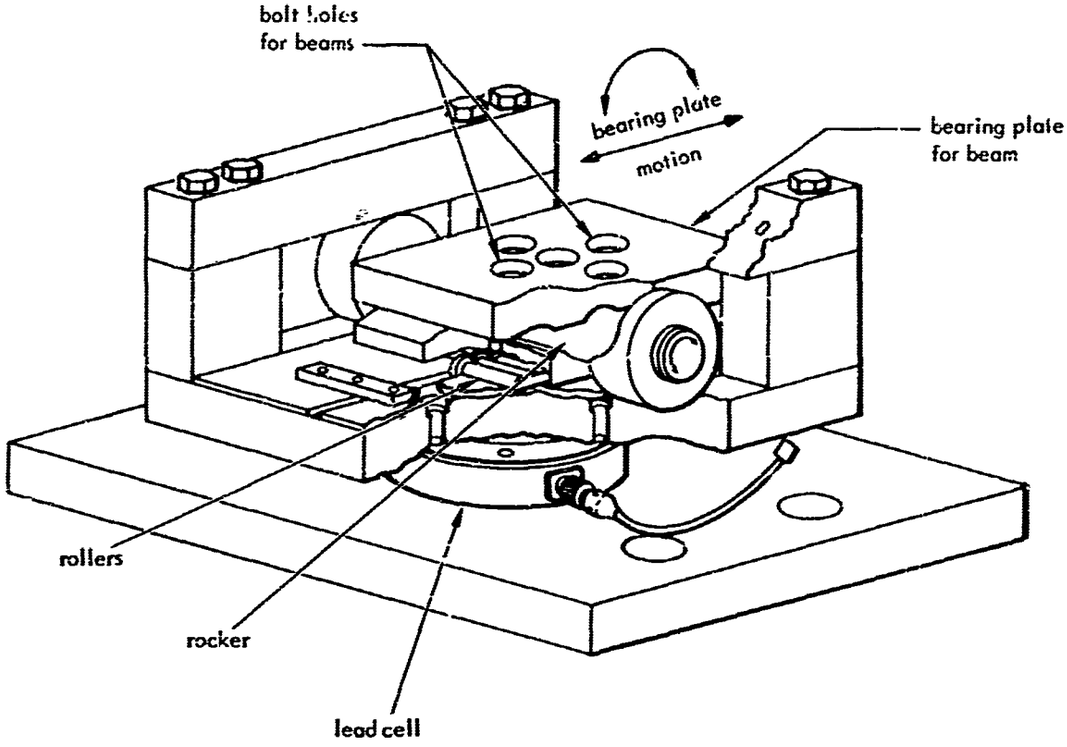

Figure 6. Support configuration.

A static test was conducted by gradually and continuously increasing a uniformly distributed load on the beam until it collapsed. The uniform load was applied to the beam by admitting air pressure into the simulator by means of an air compressor. The level of pressure was noted visually by use of an Emery pressure gage (375 psi capacity). Recordings of pressures, deflections, reactions and strains were taken on the oscillograph at each 5 psi increment of pressure until a pressure of 25 psi was developed; thereafter, the pressure increment was 2 psi until the ultimate resistance of the beam was overcome.

A dynamic test was conducted by first loading the firing tube with the amount of Primacord required to obtain the desired peak pressure and presetting the firing sequence and delay time of the air vents to obtain the desired decay rate of the pressure. A blasting cap was then inserted in each end of the firing tube and wired to the master control circuit. Finally, a switch was closed to start an electromechanical programmer which in turn started the recording equipment, ignited the explosive charge, controlled the opening of the air vents and stopped the recording equipment. After the shot, permanent strains and deflections were recorded and the beam was visually inspected and photographed. If the dynamic load was not large enough to fail the beam in flexure or shear, the above procedure was repeated at a higher load level.

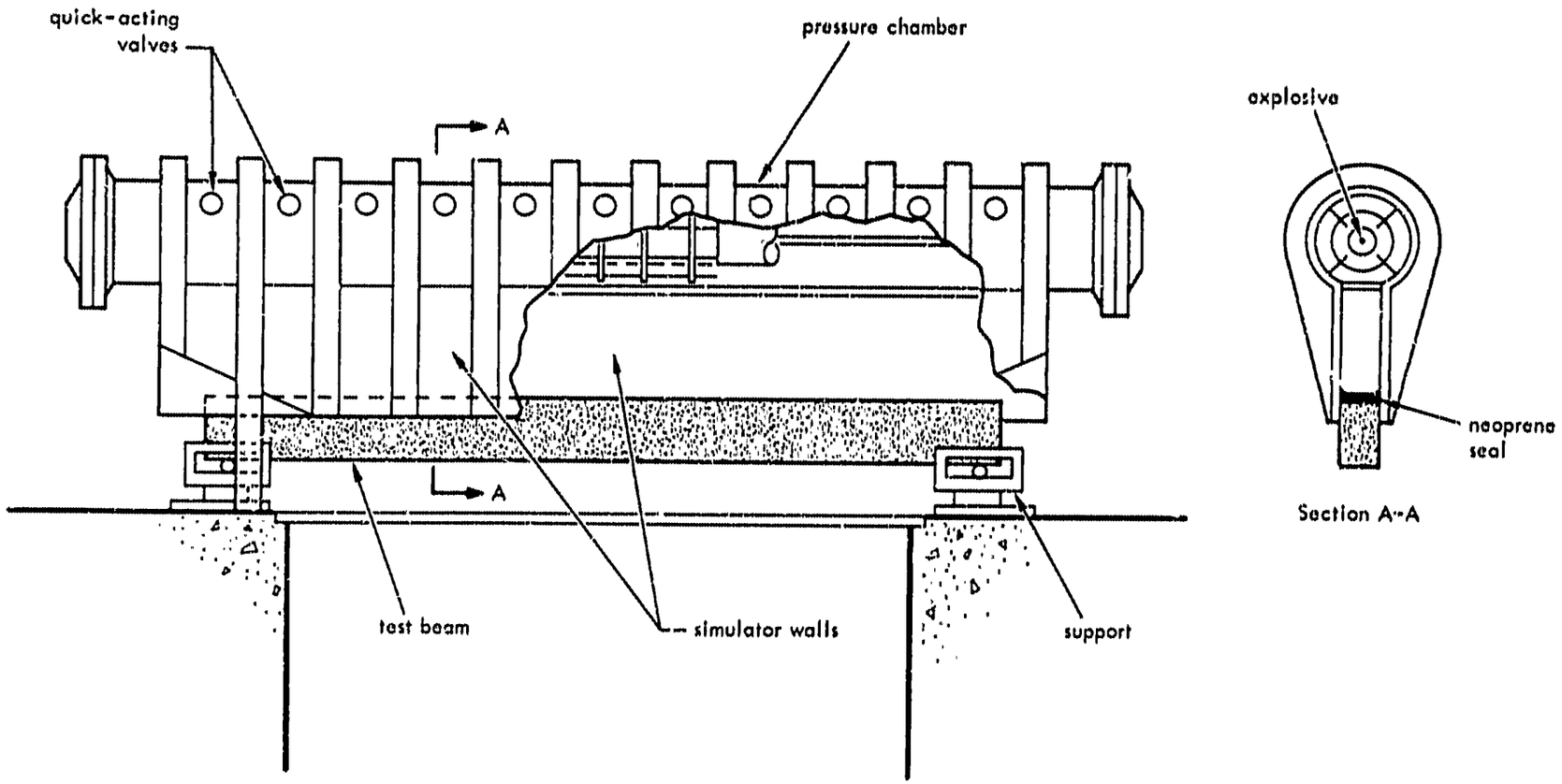

Figure 7. Schematic of beam in NCEL Blast Simulator.

RESULTS AND ANALYSIS OF DATA

Three beams, WI [1] through WD3, were tested under an increasing static load to failure. The measured and idealized static resistance diagrams for these beams are shown in Figure 8. Six beams, WD4 through WD9, were tested under dynamic load. Typical oscillograms showing the time variation in the measured quantities are presented in Figures C1 through C6 (Appendix C). The magnitude and duration of the dynamic loads, maximum midspan deflection, and average maximum shear at the supports are listed in Table II. Photographs of the beams after failure are included as Figures D-1 and D-2 (Appendix D).

All beams failed in flexure even though the effective amount of web reinforcement (rf_y) was 69 percent less than the ACI Code[3] requirement. Despite the unexpected persistence of the beams to fail in flexure, considerable information about the shear resistance was derived from the data. The data related to resistance and behavior in shear are presented and analyzed in the following sections.

In the material which follows, the terms right and left span, reaction, crack, and the like, refer to the end of the beam with the 4- and 6-inch stirrup spacing, respectively.

Critical Diagonal Crack

The critical diagonal cracks are shown in Figures D1 and D2 (Appendix D). The growth of these cracks in the beams loaded dynamically could not be recorded. The resolution of the available high-speed camera was inadequate for the size of the cracks. However, crack growth was observed in the beams loaded statically.

The typical path and growth of a critical diagonal crack observed under static loading are illustrated in Figure 9. As the applied load approached the cracking resistance of the beam, crack A (Figure 9) developed and slowly propagated to about the mid-depth of the beam. This was the only visible crack near the support up to this stage of loading. A slight increase in load developed crack B, the critical diagonal tension crack, which suddenly propagated from near the edge of the bearing plate and rapidly spread across three stirrups (at the left end) and into the compression zone of the concrete. The propagation of this crack retarded further growth of crack A and suddenly increased the strains, WS1 through WS4, in the stirrups and the relative displacement, DC1 and DC2, between the top and bottom faces of the beam.

Crack B continued to grow with increasing load but at a lesser inclination as it slowly approached the level of the compression reinforcement. This phenomenon continued until the ultimate resistance of the beam was overcome. All beams failed at midspan in flexure except beam WD3 (Figure D1, Appendix D) which appeared to fail simultaneously in flexure and shear. Removal of the load caused flexural tension cracks to open near the top of the beam as it deflected upward. These cracks (Figures D1 and D2) extended to the level of the compression reinforcement in the vicinity of the head of the critical crack.

The measured location of the critical diagonal crack is listed in Table III for beams WD1 through WD9. The measured location is defined by the distance from the center of the support to the point of intersection of the critical diagonal crack and the longitudinal tension reinforcement. This definition is compatible with that of other investigators.[1]

There was no measurable change in the location of the critical diagonal crack (Table III) under dynamic load. Both static and dynamic loading caused a critical crack at the left end of the beam between 0.55d and 0.70d from the support. The crack appeared suddenly, spread rapidly across three stirrups, and eventually intersected the compression reinforcement between 1.7d and 2.3d from the support. At the right end, the crack developed between 0.31d and 0.93d from the support, crossed four stirrups, and eventually intersected the compression reinforcement between 1.9d and 2.5d from the support. The variation in critical crack location was greater at the right end but the variation at either end was about the same for static and dynamic loading. This finding suggests that the greatest amount of web reinforcement is required at the same location for dynamic loads as for static loads.

Table II. Dynamic Test Results - Load, Deflection, and Shear

Beam No.	Load Characteristics				Midspan Deflection				Shear at Support (Average) 3/				
	Peak Load		Duration		Maximum		Time to Max		Maximum			Time to Max	
	w_0 (lb/in.)	w_0/r_y'	T (msec)	T/T_n 1/	y_m (in.)	y_m/y_y'	t_m (msec)	t_m/T_n	V_m (kips)	V_m/V_y' 2/	DSF_m	t_m (msec)	t_m/T_n
WD4-1	390	0.630	490	14.3	1.00	1.09	17.2	0.51	45.7	1.02	1.62	17.2	0.51
WD4-2	526	0.850	350	10.3	1.50	1.64	21.3	0.63	54.2	1.21	1.43	11.4	0.33
WD5	569	0.917	490	14.4	1.84	2.00	25.5	0.75	56.0	1.25	1.30	13.3	0.39
WD6	585	0.943	460	13.5	1.98	2.15	26.2	0.77	53.6	1.20	1.27	11.2	0.33
WD7-1	364	0.586	720	21.2	0.81	0.89	17.0	0.50	48.8	0.96	1.64	16.0	0.47
WD7-2	580	0.935	500	14.7	1.89	2.05	26.6	0.78	57.0	1.28	1.37	11.5	0.34
WD8-1	552	0.890	139	4.1	1.49	1.62	22.5	0.66	52.3	1.17	1.32	13.6	0.40
WD8-2	502	0.810	140	4.1	1.40	1.52	20.8	0.61	49.0	1.09	1.35	12.2	0.36
WD9-1	332	0.535	47	1.4	0.75	0.81	15.3	0.45	35.7	0.80	1.49	15.0	0.44
WD9-2	555	0.895	47	1.4	1.45	1.58	18.0	0.53	53.6	1.20	1.34	11.6	0.34

1/ T_n = 34 milliseconds (see Figures C1 and C2).

2/ V_y' = 44.6 kips (see Figure 8).

3/ Average of left and right supports.

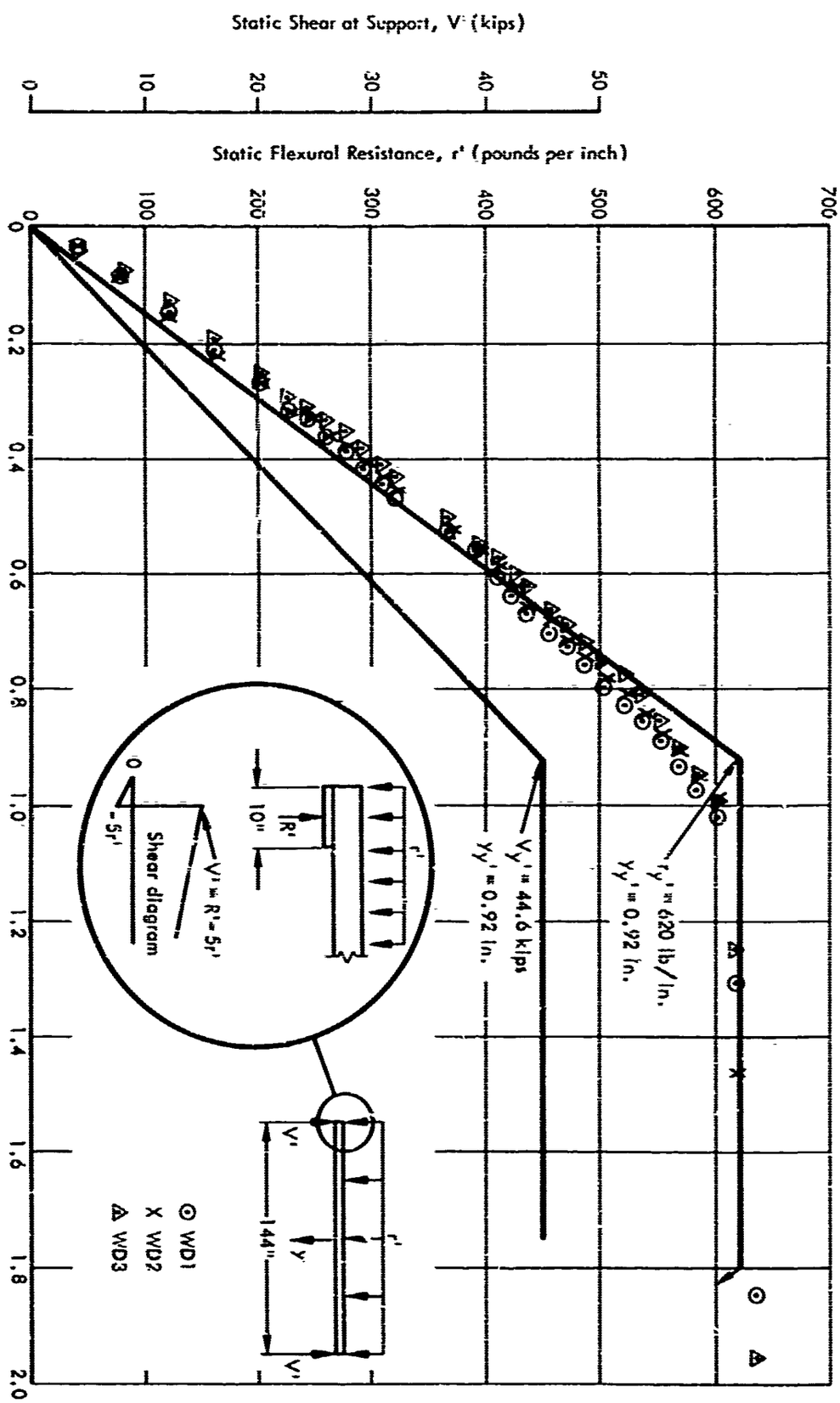

Figure 8. Measured and idealized static flexural resistance diagrams.

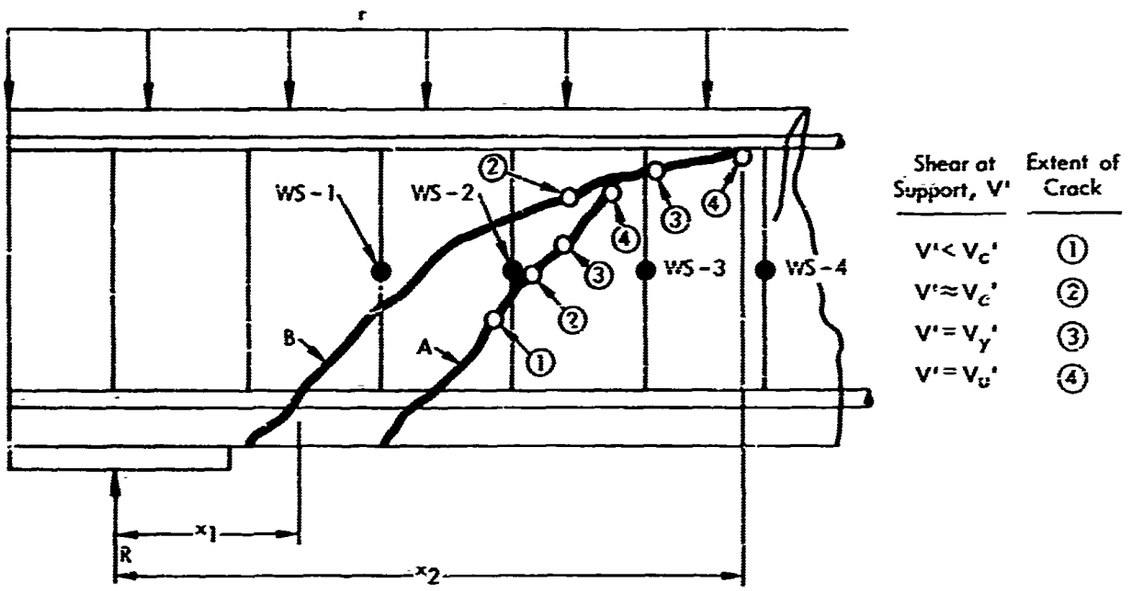

Figure 9. Typical path and growth of critical diagonal crack.

The critical crack at each end of the beam intersected the compression reinforcement nearly the same distance from each support. In other words, the critical crack crossed more stirrups at the right end where the stirrups were more closely spaced. This suggests that the path of the critical crack is independent of the number of stirrups it crosses, and that the closer the stirrup spacing, the greater the number of stirrups effective in resisting shear. However, this latter point is not substantiated by test data because the beams failed in flexure before the ultimate shear resistance of either end was overcome. It is interesting to note that the critical crack crossed mid-depth of the beam about 16 inches (1.1d) from the center of each support.

Shear at Supports

Measured shear at the supports and measured deflection at midspan are plotted in Figures E-1 through E-10 (Appendix E) as a function of time. For convenience in interpreting the data, the shear and deflection are plotted in nondimensional form as ratios of the static shear at the support corresponding to the static flexural yield resistance (V_y') and the static flexural yield deflection (y_y') (Figure 8), respectively. Time is plotted as a ratio of the measured fundamental period of vibration, T_n = 34 milliseconds (see Figures C-4 through C-6, Appendix C). The magnitude *and* time of maximum shear and deflection for each test are listed in Table II.

Dynamic load produced a greater shear at the supports than the same peak load applied statically. For example, a peak dynamic load of $0.586r_y$' applied to WD7-1 produced a maximum shear of $0.96V_y$' (Figure E-5, Appendix E) while the same peak load produced a static shear of only $0.586V_y$' (Figure 8). Therefore, the shear was $0.96V_y'/0.586V_y'$ or 1.64 times greater under dynamic load. In other words, the maximum dynamic shear factor (DSF_m) for WD7-1 was 1.64; this was the largest DSF_m recorded in the tests.

The DSF_m was always greater than one (see Table II) and greatest in the elastic range of response ($y_m < y_y$). In the plastic range ($y_m > y_y$), the DSF_m decreased as the peak dynamic load, w_0, increased. For example, when w_0 increased from $0.850r_y$' (WD4-2) to $0.943r_y$' (WD6), the DSF_m decreased from 1.43 to 1.27. The DSF_m decreased because the maximum shear approaches a limiting value in the plastic range, regardless of the magnitude of the applied load.

Table III. Measured Location of Critical Diagonal Crack

Beam No.	Left End						Right End					
	x_1 (in.)	$\frac{x_1}{d}$	$\frac{x_1}{L}$	x_2 (in.)	$\frac{x_2}{d}$	$\frac{x_2}{L}$	x_1 (in.)	$\frac{x_1}{d}$	$\frac{x_1}{L}$	x_2 (in.)	$\frac{x_2}{d}$	$\frac{x_2}{L}$
WD1	7	0.55	0.049	28	2.17	0.194	4	0.31	0.028	25	1.93	0.174
WD2	8	0.62	0.055	28	2.17	0.194	8	0.62	0.055	28	2.17	0.194
WD3	8	0.62	0.055	22	1.71	0.154	8	0.62	0.055	28	2.17	0.194
WD4	9	0.70	0.063	-	-	-	10	0.77	0.070	27	2.09	0.188
WD5	9	0.70	0.063	30	2.32	0.210	8	0.62	0.055	27	2.09	0.188
WD6	9	0.70	0.063	30	2.32	0.210	4	0.31	0.028	26	2.01	0.181
WD7	7	0.55	0.049	27	2.09	0.188	8	0.62	0.055	-	-	-
WD8	7	0.55	0.049	30	2.32	0.210	12	0.93	0.083	32	2.47	0.222
WD9	8	0.62	0.055	27	2.09	0.188	12	0.93	0.083	30	2.32	0.210

The maximum shear at the supports approached a limiting value when the longitudinal tensile steel yielded (see Figures C-2, C-3, and C-5, Appendix C) even though the midspan deflection continued to increase. In other words, the maximum dynamic shear at the supports approached a limiting value when the flexural yield resistance of the beam was overcome by the load. Apparently, flexural yielding at midspan dampens out the higher modes of vibration and changes the fundamental mode shape enough to significantly reduce the shear at the supports.

When the tensile steel yielded, the ratio of the maximum dynamic shear to maximum static shear (V_m/V_y') ranged from 1.09 to 1.28 and increased as the peak load increased. Thus, the ratio depended not just on the dynamic flexural yield resistance of the beam but also on the load on the beam at the instant the tensile steel yielded. In other words, the ratio was a function of the dynamic flexural yield resistance (r_y), peak load (w_0), load duration (T), and time when the tensile steel yielded (t_y).

The shear at the support and time when the critical diagonal crack formed and when the first stirrup yielded are listed in Tables IV and V, respectively. The criteria for measuring these quantities are illustrated in Figure 10. It is to be noted that mean values corresponding to a smooth curve through the measured reaction-time curve were used to compute V_c and V_y. If the actual reaction-time curve were used, small errors in measuring t_c would result in large errors in the computation of V_c and V_y because of the large oscillations in the reaction caused by the higher modes of vibration.

The shear at the supports corresponding to diagonal cracking and yielding of the stirrups increased substantially under dynamic load (Tables IV and V). The cracking shear averaged 15.2 kips under static load and increased to 28.5 kips (average) or 88 percent under dynamic load. The cracking shear differed as much as 18 percent between supports under dynamic load, but the difference was no greater than under static load. The shear at first yielding of the stirrups at the left end averaged 26.1 kips under static load and increased to 45.5 kips or 74 percent under dynamic load. The shear at first yielding of the stirrups at the right end averaged 34.5 kips under static load and increased to 49.8 kips or 44 percent under dynamic load.

Effectiveness of Stirrups

The measured stirrup strains in the beams under static load (Figures 11 through 13) and under dynamic load (Figures C-1 through C-6, Appendix C) indicate practically no stress in the stirrups prior to formation of the critical diagonal crack. In other words, the stirrups had no apparent effect on the behavior of the beam prior to diagonal cracking or on the static or dynamic cracking resistance.

The stirrups were effective only after the critical diagonal crack developed. Under both static and dynamic loading, formation of the critical diagonal crack immediately increased the measured strain in the stirrups. The gage closest to the critical crack, WS2 at the left end and WS6 or WS7 at the right end, strained first, and adjacent stirrups strained shortly afterward.

As the resistance of the beam increased, the measured strains in all stirrups continued to increase until the beam failed. However, care must be exercised in interpreting the magnitude of these strains. They are typical of the maximum strain in the stirrup only if the crack crosses through or very near the gage. Generally, WS2 yielded first and then WS7. This is apparent from Figures D-1 and D-2, Appendix D, which show that the critical crack propagated closest to the location of the gages on these stirrups (mid-depth of the beam). It is to be noted that WS2 and WS7 were located 18 and 16 inches, respectively, from the nearest support. This suggests that the first stirrup to yield depends primarily on its distance from the support.

Yielding of the stirrups did not trigger collapse of the beam. In fact, even after one or more stirrups yielded at each end of the beam, adjacent stirrups provided enough shear resistance to force a flexural failure in all beams under static and dynamic load.

Table IV. Measured Shear and Time When Critical Diagonal Crack Formed

Beam No.	Measured Shear at Support				Measured Time			
	Left		Right		Left		Right	
	V_c (kips)	V_c/bd (psi)	V_c (kips)	V_c/bd (psi)	t_c (msec)	t_c/T_n	t_c (msec)	t_c/T_n
WD1	14.2	142	13.8	138	-	-	-	-
WD2	14.4	144	16.4	164	-	-	-	-
WD3	15.0	150	17.8	178	-	-	-	-
WD4	33.7	337	27.8	278	9.1	0.27	7.0	0.21
WD5	28.8	288	30.1	301	5.2	0.15	5.5	0.16
WD6	30.7	307	31.5	315	6.0	0.18	5.3	0.16
WD7	28.8	288	31.0	310	8.3	0.24	8.9	0.26
WD8	26.9	269	26.6	266	5.5	0.16	6.0	0.18
WD9	22.1	221	25.7	257	7.2	0.21	8.0	0.24

Table V. Measured Shear and Time When First Stirrup Yielded

Beam No.	Measured Shear at Support				Measured Time			
	Left		Right		Left		Right	
	V_v (kips)	V_v/bd (psi)	V_v (kips)	V_v/bd (psi)	t_v (msec)	t_v/T_n	t_v (msec)	t_v/T_n
WD1	27.8	278	36.0	360	-	-	-	-
WD2	26.4	264	35.2	352	-	-	-	-
WD3	24.0	240	32.4	324	-	-	-	-
WD4	40.6	406	55.1	551	11.5	0.34	12.0	0.35
WD5	46.3	463	47.6	476	10.0	0.29	9.0	0.26
WD6	42.9	429	49.1	491	9.4	0.28	9.3	0.27
WD7	52.6	526	50.1	501	11.1	0.33	9.6	0.28
WD8	45.9	459	44.8	448	11.5	0.34	11.0	0.32
WD9	44.4	444	52.1	521	10.1	0.30	10.5	0.31

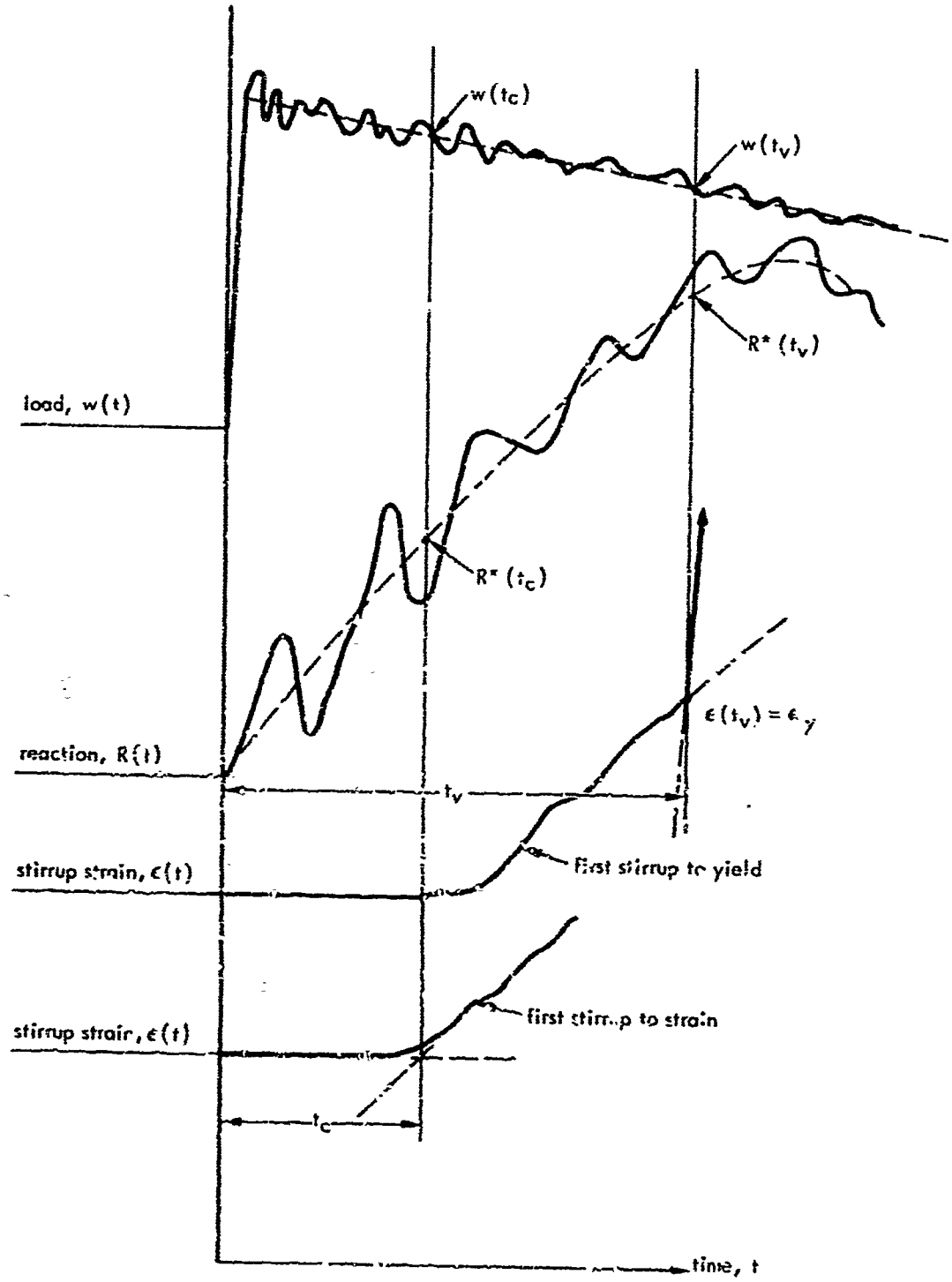

$$V_c = R^*(t_c) - 5w(t_c)$$

$$V_v = R^*(t_v) - 5w(t_v)$$

Figure 10. Illustrated technique for measuring support shear at times of critical cracking and stirrup yielding.

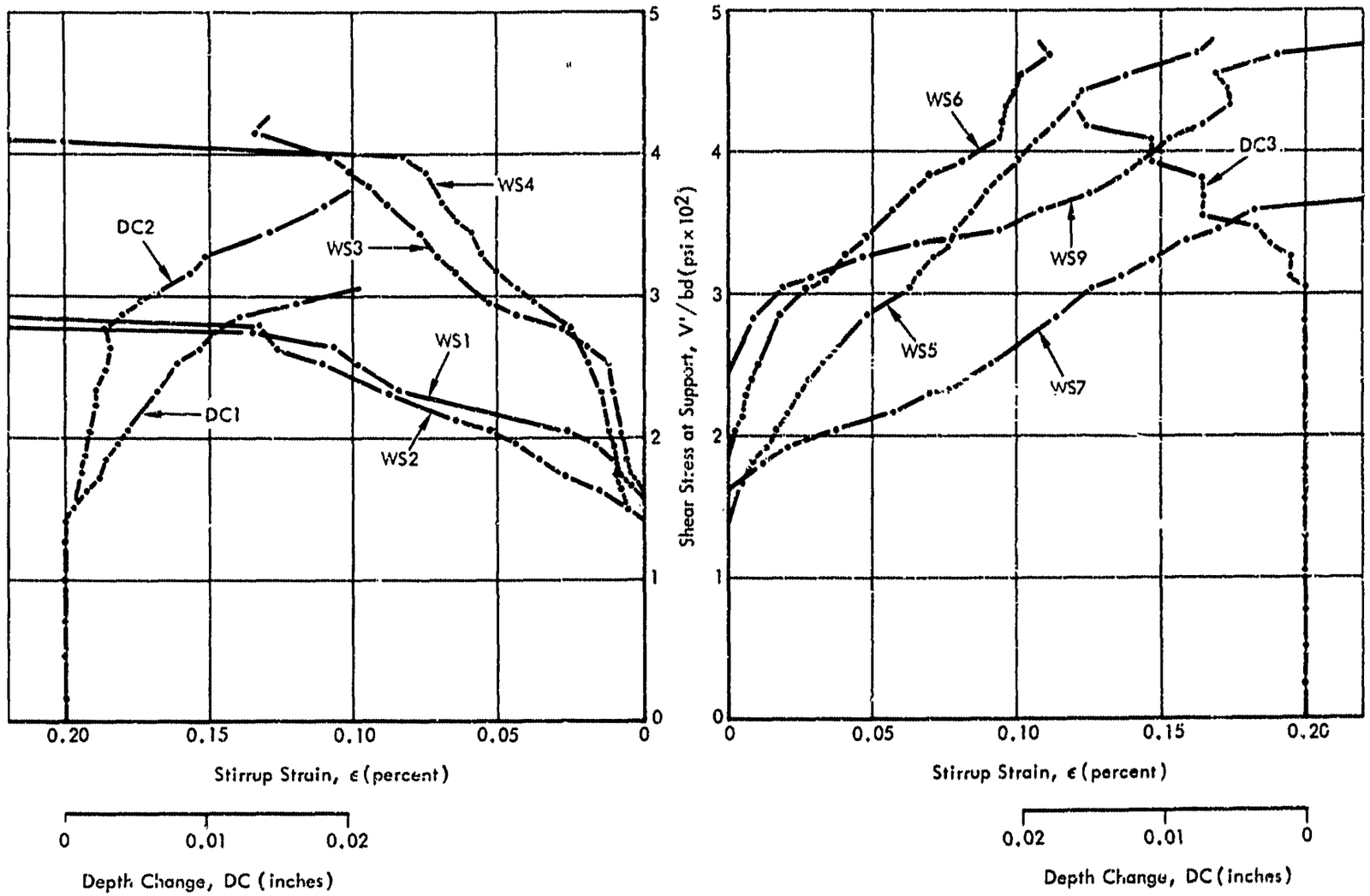

Figure 11. Shear stress at support versus stirrup strain - beam WD1.

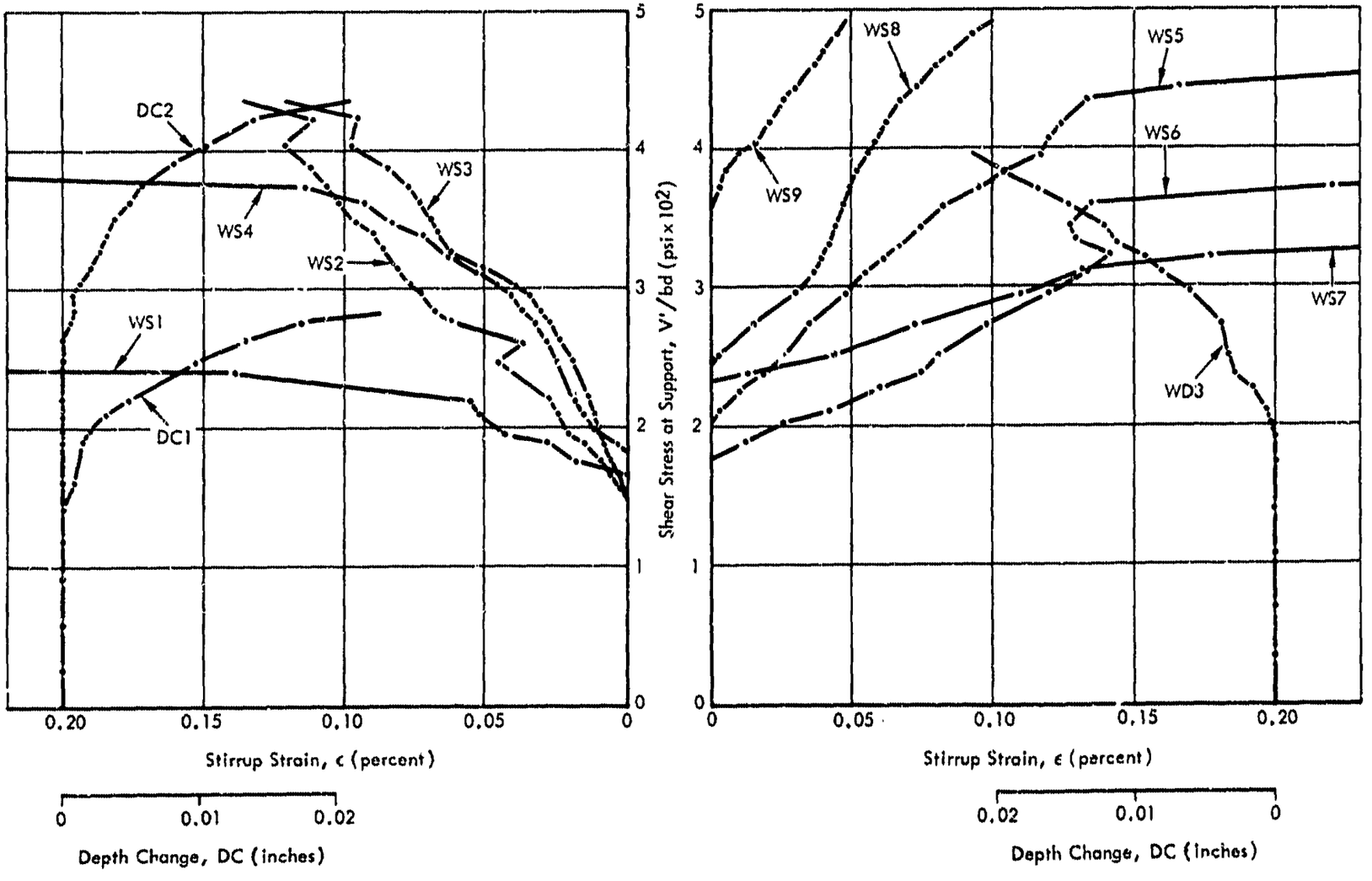

Figure 13. Shear stress at support versus stirrup strain - beam WD3.

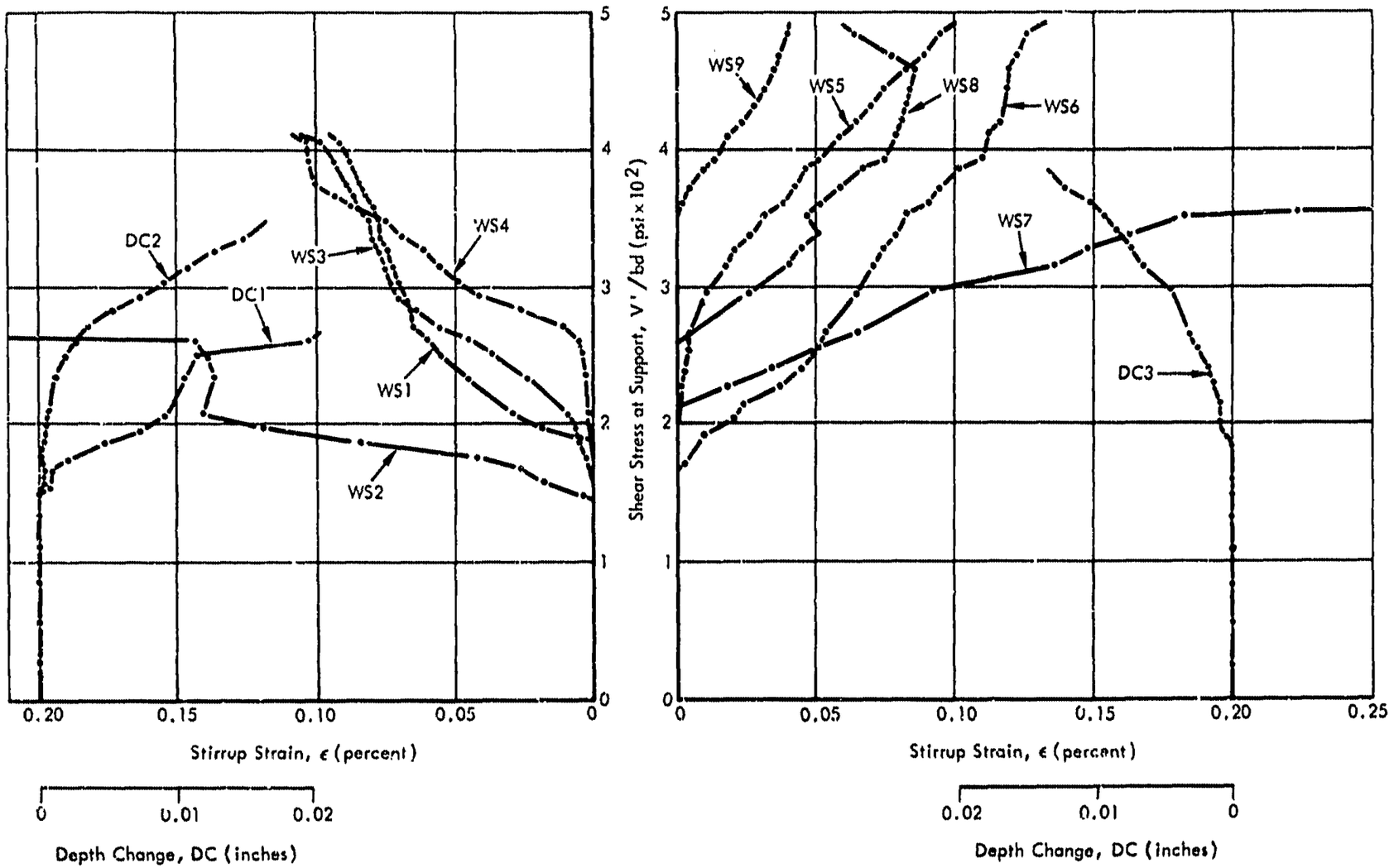

Figure 12. Shear stress at support versus stirrup strain - beam WD2.

Table VI. Measured Strain Rates in Tensile Steel and Stirrups

Beam No.	Measured Strain Rate, $\dot{\epsilon}$ (in./in./sec)										
	TS1	TS2	WS1	WS2	WS3	WS4	WS5	WS6	WS7	WS8	WS9
WD4-1	*	*	*	*	1.14	*	*	0.14	*	*	*
WD4-2	0.36	0.34	0.27	*	*	*	*	0.21	*	*	*
WD5	0.34	0.35	*	1.22	*	*	*	1.15	1.10	*	*
WD6	0.37	0.36	*	1.73	*	*	*	*	1.02	2.02	*
WD7-1	*	*	*	*	*	*	*	*	*	*	*
WD7-2	0.33	0.36	*	0.22	*	*	*	0.74	*	*	*
WD8-1	0.33	0.33	*	0.49	*	*	*	0.72	*	*	*
WD8-2	-	-	*	0.44	*	*	*	0.26	*	*	*
WD9-1	*	*	*	*	*	*	*	*	*	*	*
WD9-2	0.34	0.36	*	0.45	*	*	*	0.74	*	*	*

*$\epsilon_m < \epsilon_y$

The average strain rates in the stirrups which yielded are listed in Table VI. The values are the average strain rates prior to yielding. It is to be noted that the strain rates varied between beams and, except for three stirrups, were greater than the measured strain rates in the longitudinal tensile steel at midspan. In fact, the measured strain rates in some stirrups were four to six times greater. This means that the yield strength of the stirrups located near the critical section increased considerably in the beams subjected to dynamic loading. The exact increase is unknown since rapid load tests were not conducted on coupons from the stirrups. However, if the curve shown in Figure 3 is typical for the stirrups, the yield strength increased more than 40 percent. Even if Figure 3 is not typical, it indicates a smaller increase in yield strength than the stirrups actually experienced, since for a given strain rate the percent increase in yield strength increases as the static yield strength decreases[4] and the static yield strength of the stirrups was much less than for the No. 9 bars in Figure 3 (see Table I).

Ultimate Failure

All beams failed in flexure by yielding of the tension steel followed by crushing of the concrete at midspan. This is apparent from the strains TS1, TS2, and C1 shown in Appendixes C and F. Therefore, the ultimate shear resistance of the beams under static and dynamic load could not be measured.

THEORY VERSUS EXPERIMENTAL RESULTS

Shear at Supports

Calculating the shear forces produced by static loads presents no problem since it involves only principles of statics. However, calculating the shear forces produced by dynamic loads is tedious and laborious; one must consider the superposition of the contribution of an infinite number of normal modes of vibration. The contribution of each mode depends upon the spatial distribution and time variation of the load; the stiffness, resistance, mass, and damping capacity of the beam; and the support conditions. For the purpose of calculating either deflections or moments, the fundamental or first mode generally predominates, and accurate results can be easily obtained by considering only this mode. However, for the purpose of accurately calculating shears, the contribution of higher modes must be considered.

The effects of the higher modes of vibration, damping, load-duration, and time on shear are apparent in Figures 14 through 17. The curves in these figures are plots of equations developed in Appendix G for the shear at the supports of a simply supported beam under a uniform load. The equations were developed by assuming a triangular load-time function, elastic behavior, a uniformly distributed mass, and viscous damping. A detail study of these curves leads to interesting conclusions about the shear in uniformly loaded beams in the elastic range of response as follows:

1. The maximum shear is greatest under dynamic load, increases with peak load and load duration, and occurs at a time equal to one-half the fundamental period of vibration ($t/T_n = 0.5$) for long duration loads ($T/T_n \geq 6$).

2. The contribution from the fundamental mode of vibration accounts for 85 to 88 percent of the maximum shear at the supports for T/T_n between 1 and 20.

3. The curve for the average shear, the fundamental mode plus the average of all higher modes, follows very closely the curve for the exact shear.

4. The effect of the usual amount of damping present in beams (6 percent) is to decrease the shear at the supports to a value equal to the contribution from the first undamped mode of vibration for the time interval $0.35 \leq t/T_n \leq 0.60$.

Conclusion number 3 above led to the development of the chart for dynamic shear shown in Figure 17. The chart is based on the contribution to shear from the fundamental mode plus the average contribution of the higher modes, and on an elasto-plastic resistance diagram. The theory leading to the development of the chart is presented and discussed in Appendix G. The chart covers both the elastic and plastic range of response and is intended to aid the designer in the rapid computation of the maximum shear at the supports of a simply supported beam under a uniform dynamic load.

The utilization of the chart for dynamic shear is illustrated by the following calculations for beam WD6. From Table II, $w_0/r_y' = 0.943$ and $T/T_n = 13.5$. From Table VI and Figure 3 the ratio r_y/r_y' or factor F for WD6 is 1.26. Therefore,

$$\frac{w_0}{r_y} = \frac{w_0}{r_y'}\left(\frac{1}{F}\right) = \frac{0.943}{1.26} = 0.75$$

Entering Figure 17 with $w_0/r_y = 0.75$ and $T/T_n = 13.5$, the maximum dynamic shear factor for WD6 is

$$DSF_m = 1.26$$

The ratio V_m/V_y' is found by rearranging terms, or

$$\frac{V_m}{V_y'} = DSF_m \frac{V}{V_y'} = DSF_m \frac{w_0}{r_y'} = 1.26\ (0.943) = 1.19$$

The maximum dynamic shear factor (DSF_m) and ratio V_m/V_y' for each beam were computed from Figure 17 and are listed with the measured values in Table VII.

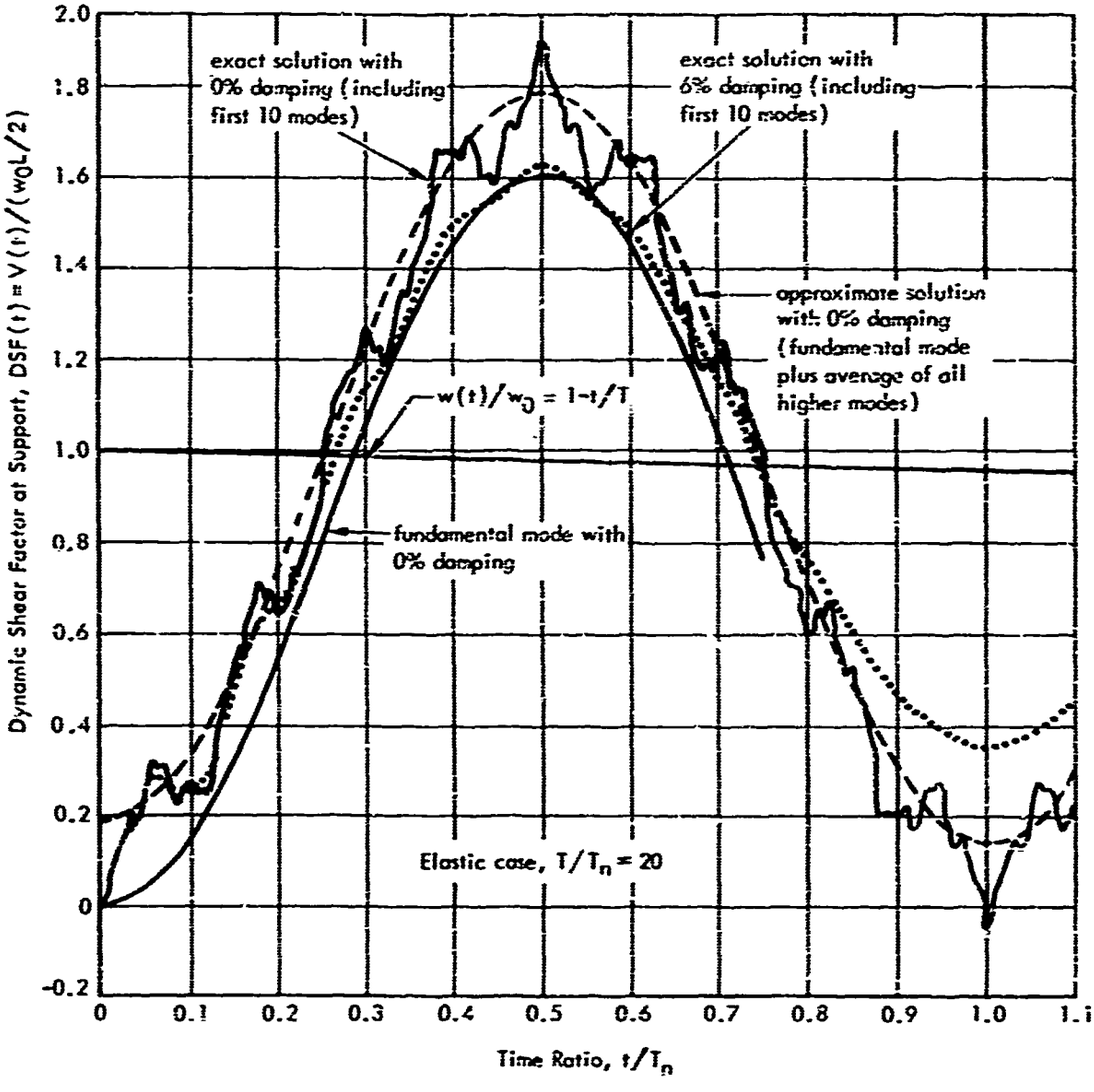

Figure 14. Dynamic shear factor at support of a simply supported beam under uniform load ($T/T_n = 20$).

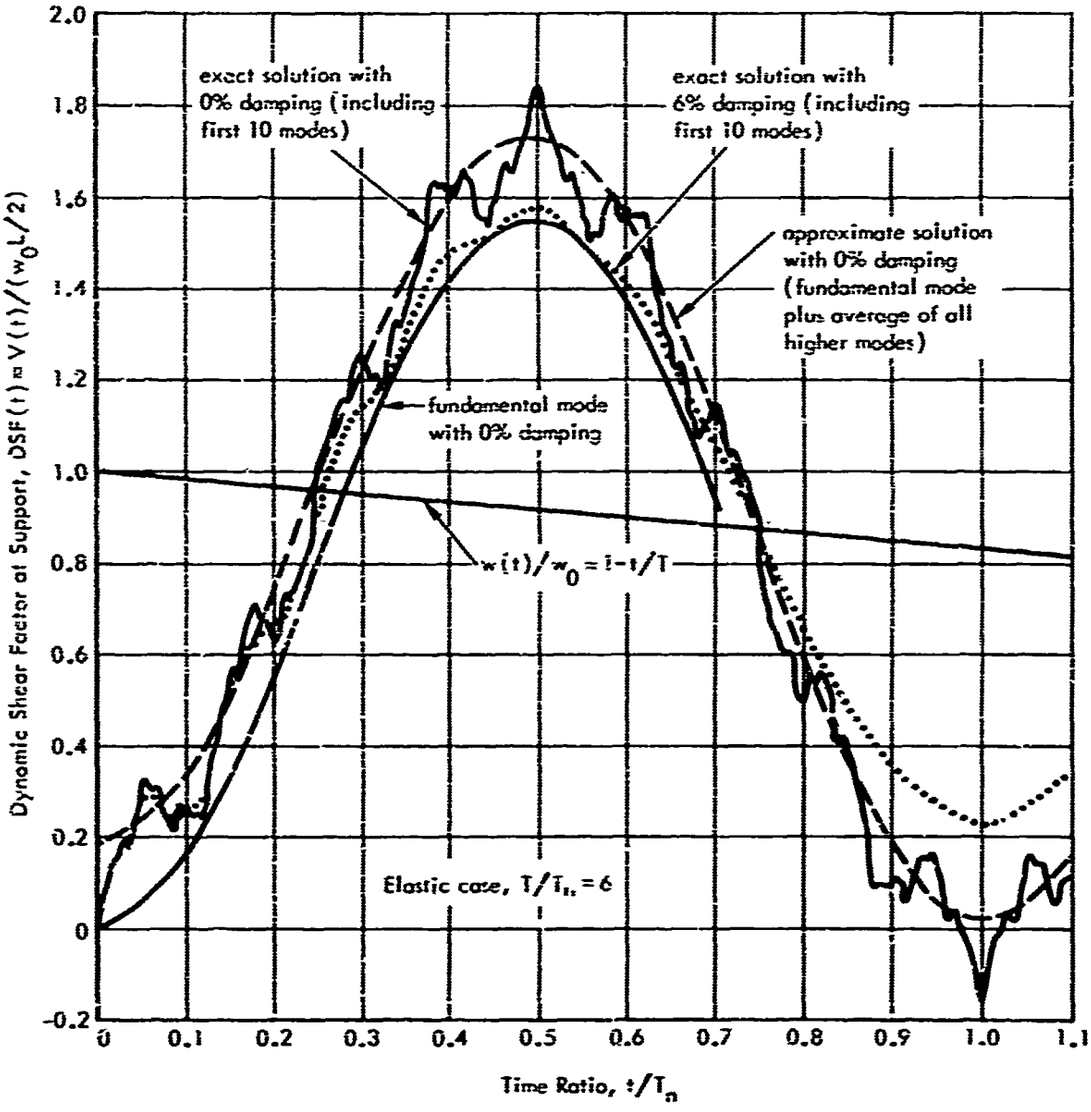

Figure 15. Dynamic shear factor at support of a simply supported beam under uniform load ($T/T_n = 6$).

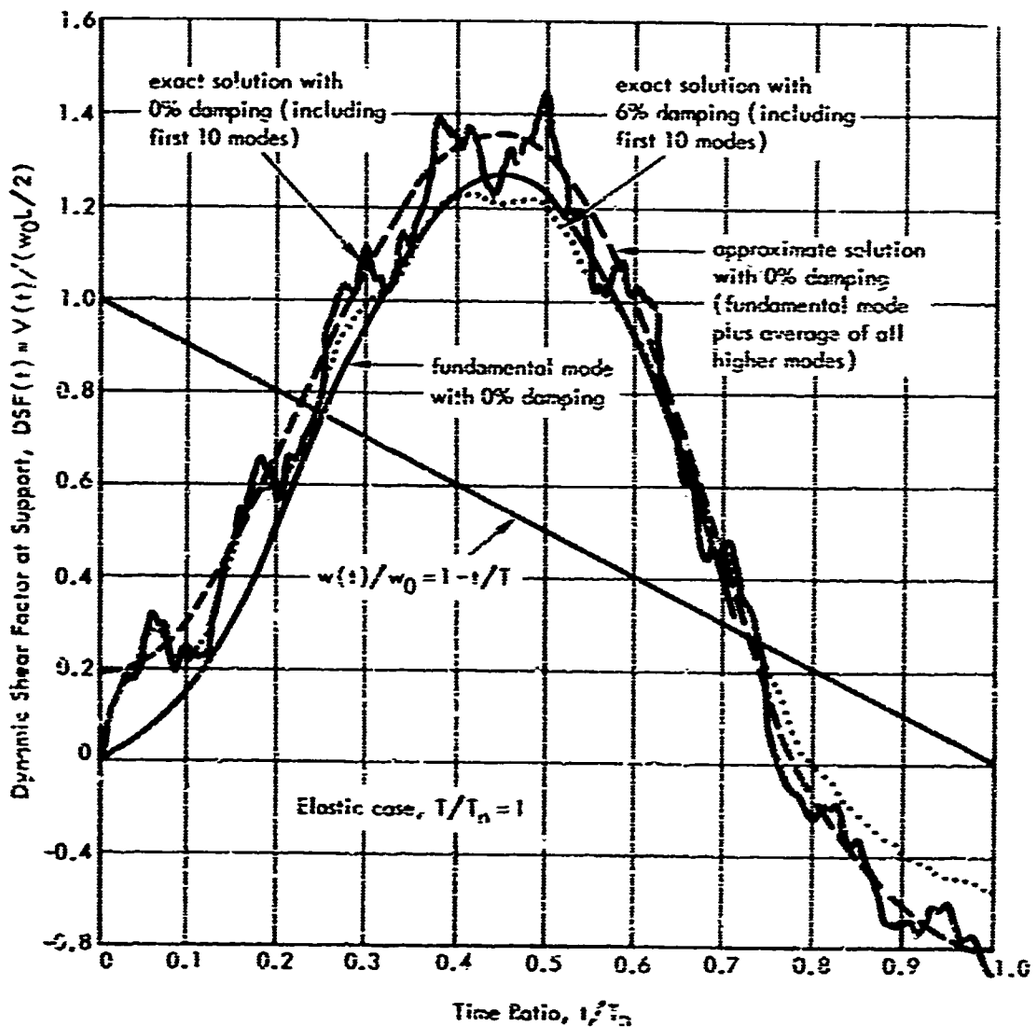

Figure 16. Dynamic shear factor at support of a simply supported beam under uniform load ($T/T_n = 1$).

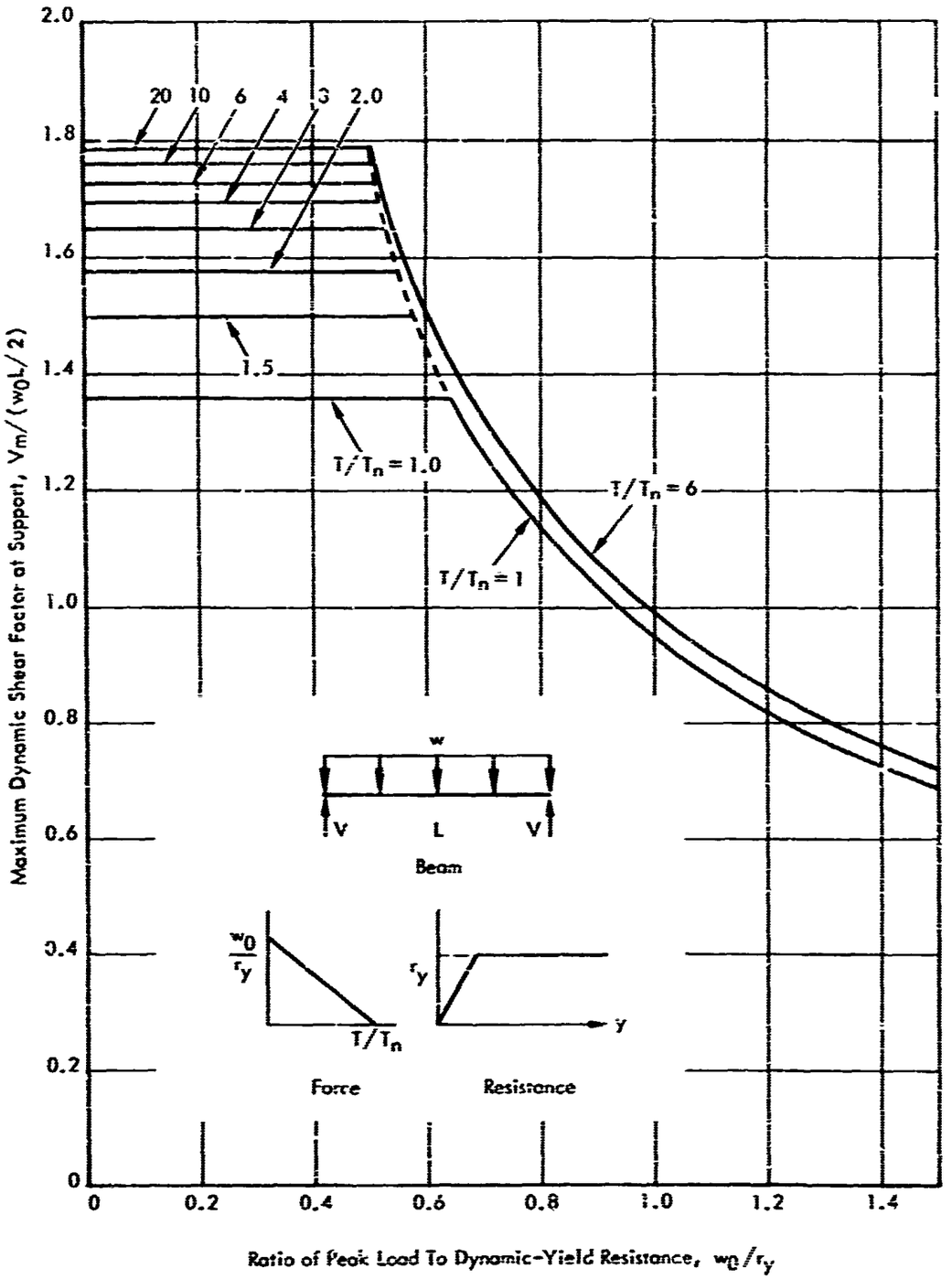

Figure 17. Maximum shear at supports of simple beam under uniform load.

Table VII. Comparison of Measured and Computed Maximum Shear

Beam No.	Loading Characteristics		Maximum Shear at Supports			
			Measured		Computed[2]	
	w_0/r_y[1]	T/T_n	DSF_m	V_m/V_y'	DSF_m	V_m/V_y'
WD4-1	0.500	14.3	1.62	1.02	1.77	1.11
WD4-2	0.675	10.3	1.43	1.21	1.38	1.17
WD5	0.728	14.4	1.35	1.25	1.29	1.25
WD6	0.749	13.5	1.27	1.20	1.25	1.18
WD7-1	0.465	21.2	1.64	0.96	1.78	1.04
WD7-2	0.741	14.7	1.37	1.28	1.27	1.19
WD8-1	0.706	4.1	1.32	1.17	1.30	1.16
WD8-2	0.643	4.1	1.35	1.09	1.39	1.12
WD9-1	0.425	1.4	1.49	0.80	1.48	0.79
WD9-2	0.710	1.4	1.34	1.20	1.26	1.13

[1] Assumes F = 1.25 based on Table VI and Figure 3.

[2] Based on Figure 17.

Shear Along Span

The critical diagonal crack forms or the stirrups yield when the nominal shear stress at the critical section exceeds some limiting value. To define this limiting value in terms of the shear at the support requires knowledge of the variation in shear along the span. If the variation under dynamic load is different from that under static load, the measured values of shear at the support listed in Tables IV and V are not a true measure of the dynamic shear resistance at diagonal cracking or first yielding of the stirrups. In fact, the dynamic shear resistance could be much greater or much less than the resistance indicated by the measured values of shear at the supports. This led to a study of the effect of dynamic load on the variation of shear along the span.

The variation of shear along a simply supported beam under a uniform dynamic load is shown in Figures G-4 and G-5, Appendix G. The curves in these figures represent the shear from the fundamental mode plus the average contribution from the higher modes. It is to be noted that the variation in shear changes with time but is nearly linear at the measured time when the critical diagonal crack formed (Table IV), $0.15 \leq t_c/T_n \leq 0.27$. This means that the ratios of V_c/V_c' given by the values listed in Table IV are probably a true measure of the increase in the diagonal cracking resistance under dynamic load provided, of course, the location of the critical section is the same under static as dynamic load.

In the literature, the critical section is usually defined as the section of diagonal tension cracking. In the experiments described here, the measured diagonal crack formed at about 0.60d and extended to about 2d from the support. Therefore, the critical section was located

somewhere between 0.60d and 2d from the support. However, the fact that the crack located within these limits under both static and dynamic loading suggests that the critical section did not shift appreciably under dynamic load.

Ratio of Moment to Shear

A major variable affecting the shear resistance is the ratio of moment to shear at the critical section.[1] A change in this ratio under dynamic loading could account for at least some of the increase in the measured shear resistance under dynamic loading as compared to static loading.

The effect of a uniform dynamic load on the ratio of moment to shear along the span of a simply supported beam is shown in Figure G-6, Appendix G. The curves in the figure show that the ratio of moment to shear changes with time and distance from the support. However, at no point along the span does the maximum ratio under dynamic load deviate more than about 20 percent from the ratio under static load.

Shear Resistance

The ACI-ASCE Committee 426(326) on Shear and Diagonal Tension[3], after an extensive study of test data from 194 beam tests, recommended semi-empirical equations as design criteria for resisting shear and diagonal tension in reinforced concrete beams. These equations are similar to those developed by Krefeld and Thurston at Columbia University[5] and were later adopted after a minor modification for inclusion in the ACI Building Code.[3] The equations are based on the hypothesis that the ultimate shear resistance of a beam with web reinforcement is the shear required to produce the diagonal tension crack plus the additional shear carried by the web reinforcement acting at its yield strength. For beams without web reinforcement, the ultimate shear resistance is the shear corresponding to formation of the diagonal tension crack. In terms of the nominal shear stress at the support, these equations lead to the following expressions for the ultimate shear resistance of simply supported beams under a static uniform load:

$$\frac{V_c'}{bd} = \frac{L}{L-2x_c}\left[1.9\sqrt{f_c'} + 2{,}500\,pd\left(\frac{V'}{M'}\right)_c\right] \qquad (1)$$

$$\frac{V_u'}{bd} = \frac{L}{L-2x_c}\left[1.9\sqrt{f_c'} + 2{,}500\,pd\left(\frac{V'}{M'}\right)_c + rf_y\right] \qquad (2)$$

where $\left(\frac{V'}{M'}\right)_c$ = the ratio of shear to moment at the critical section of the beam under a static uniform load

x_c = distance from the support to the critical section

The diagonal cracking resistance and ultimate shear resistance were computed from Equations 1 and 2, respectively, using the material properties listed in Table I. The computed values are compared with the measured resistance at diagonal cracking (Table IV) and the measured resistance at first yielding of the stirrups (Table V) in Table VIII and Figure 18. It is apparent from Figure 18 that Equations 1 and 2 adequately describe the static but grossly underestimate the dynamic shear resistance corresponding to diagonal cracking and first yielding of the stirrups. Actually, Equation 2 is a conservative measure of the static ultimate shear resistance, since the beams resisted greater shear forces than those corresponding to first yielding of the stirrups.

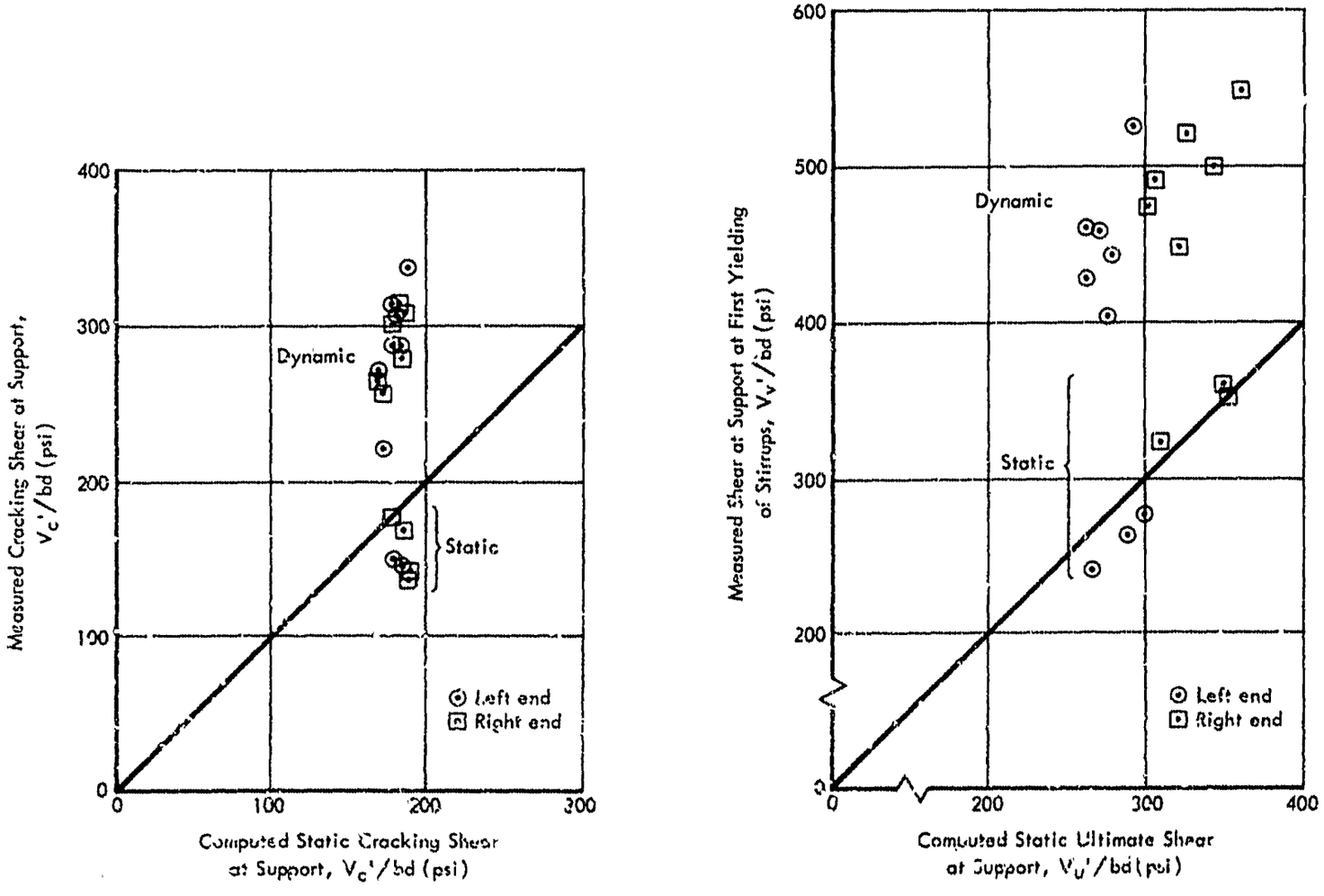

Figure 18. Comparison of measured and computed shear at support at cracking and at first yielding of stirrups.

Table VIII. Comparison of Measured and Computed Cracking and Ultimate Shear Stress

Beam No.	Computed Shear at Support				Measured Shear at Support				Measured ÷ Computed			
	Cracking, V_c/bd [1]		Ultimate, V_u/bd [2]		Cracking, V_c/bd		Stirrup Yield, V_v/bd		Cracking		Stirrup Yield	
	Left (psi)	Right (psi)	Left (psi)	Right (psi)	Left (psi)	Right (psi)	Left (psi)	Right (psi)	Left	Right	Left	Right
WD1	188	188	298	349	142	138	278	360	0.76	0.74	0.93	1.03
WD2	186	186	290	350	144	164	264	352	0.78	0.88	0.91	1.01
WD3	176	178	267	310	150	178	240	324	0.84	1.00	0.90	1.04
WD4	186	186	277	360	337	276	406	551	1.81	1.50	1.47	1.53
WD5	178	178	262	302	288	301	463	476	1.62	1.69	1.77	1.58
WD6	182	182	263	306	307	315	429	491	1.69	1.73	1.63	1.61
WD7	184	184	292	344	288	310	526	501	1.57	1.69	1.80	1.46
WD8	170	170	270	322	269	266	459	448	1.58	1.57	1.70	1.39
WD9	172	172	278	324	221	257	444	521	1.28	1.49	1.60	1.61

[1] Equation 1

[2] Equation 2

By accounting for the dynamic tensile strength of concrete and dynamic yield strength of the stirrups, one can readily modify Equations 1 and 2 to apply to the dynamic shear resistance:

$$\frac{V_c}{bd} = \frac{L}{L-2x_c}\left[1.7\left(1.9\sqrt{f_c'}\right) + 2{,}500\ pd\left(\frac{V'}{M'}\right)_c\right] \quad (3)$$

$$\frac{V_u}{bd} = \frac{L}{L-2x_c}\left[1.7\left(1.9\sqrt{f_c'}\right) + 2{,}500\ pd\left(\frac{V'}{M'}\right)_c + 1.4\ rf_y\right] \quad (4)$$

where 1.7 = factor to account for the increased tensile strength of concrete under dynamic load

1.4 = factor to account for the increased yield strength of the stirrups under rapid strain rates

The factor 1.7 in Equations 3 and 4 is based on the measured increase in the tensile splitting strength of molded concrete cylinders under rapid stress rates. (See Figure 4.) Actually, the value 1.7 is an arbitrary one since concrete strains near the critical section were not measured. The factor 1.4 is based on Figure 3, the measured strain rates in the stirrups, and the fact that for a given strain rate the percent increase in yield strength increases as the static yield strength decreases. Values computed from Equations 3 and 4 are compared with the measured dynamic shear resistance at diagonal cracking and at first yielding of stirrups in Figure 19. The figure shows good agreement between the measured and computed values of dynamic shear resistance, with a majority of the points representing higher measured than computed values.

FINDINGS AND CONCLUSIONS

1. The maximum dynamic shear at the supports was greater than the shear produced by the same peak load applied statically and increased with peak load and load duration. For $y_m \leq y_y$ the maximum shear occurred when the midspan deflection first reached a maximum value. For $y_m > y_y$ the maximum shear occurred when the tensile steel yielded at midspan.

2. Under both static and dynamic loading the web reinforcement was effective only after the formation of the critical diagonal crack. When the crack formed there was a pronounced increase in the magnitude and rate of straining in stirrups located near the crack.

3. There was no apparent change in the location of the critical diagonal crack under dynamic load, the variation in crack location was about the same for static and dynamic loads.

4. In general, the first stirrup to yield was located 18 inches (x/L = 0.12) from the left support and 16 inches (x/L = 0.11) from the right support. Yielding of the stirrups did not trigger collapse of the beam.

5. The strain rates in the stirrups crossed by the critical diagonal crack were greater than the strain rates in the longitudinal tension steel at midspan.

6. Values of rf_y as low as 65 (69 percent less than the value required by the ACI-ASCE formula) forced a flexural failure at midspan under static and dynamic loads.

7. The proposed ACI-ASCE formula for the ultimate shear resistance yielded values which were consistently less than the measured values.

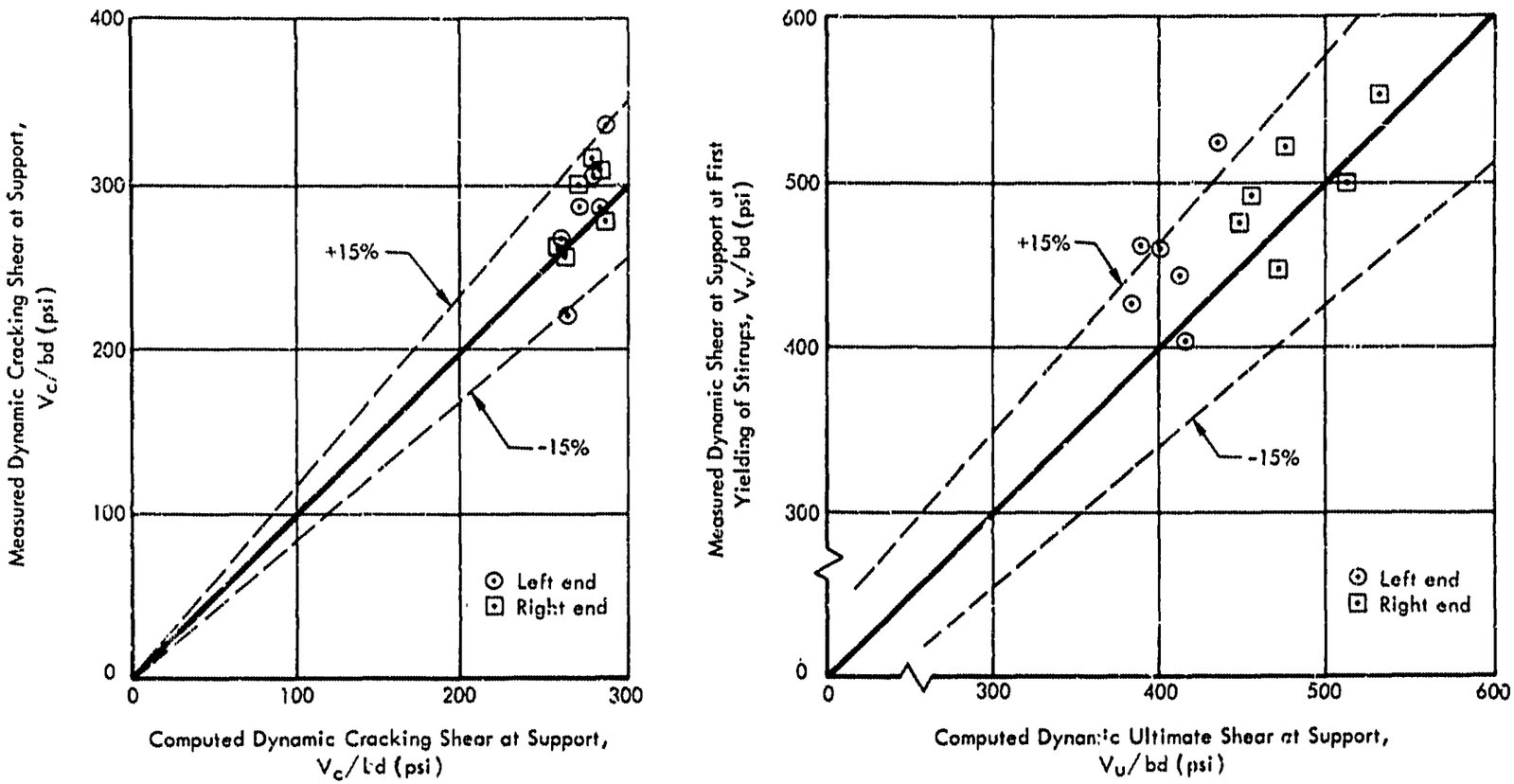

Figure 19. Comparison of measured and computed dynamic shear at support at cracking and at first yielding of stirrups.

8. The shears at the supports corresponding to diagonal cracking and first yielding of the stirrups were greater under dynamic load and were predictable from Equations 3 and 4. In these equations, as in the ACI-ASCE formulas, it is assumed that under dynamic load (1) the tensile strength of the concrete increases 70 percent, (2) the ratio of moment to shear along the span is that produced by the same load applied statically, and (3) the shear is a maximum at the support and decreases linearly to zero at midspan.

ACKNOWLEDGMENTS

Dr. C. P. Siess, Professor of Civil Engineering at the University of Illinois, provided guidance and advice during the course of this study. G. R. Swihart, Professor of Civil Engineering at the University of Nebraska, assisted in designing the test members and planning the test program. Dallas Forester, Research Assistant at the University of Illinois, was responsible for the dynamic split cylinder tests. Grateful acknowledgment is also due W. R. Ross and T. J. Landrum for casting the test members and carrying out the test program, and to W. Q. Ginn and M. Kurillo for reducing the data and preparing the figures for this report.

REFERENCES

1. ACI-ASCE Committee 426(326). "Shear and Diagonal Tension," Journal of the American Concrete Institute, Proceedings, Vol. 59, No. 1-3, January, February, and March 1962, pp. 1-30, 227-333, and 353-395.

2. Shaw, W. A., and J. R. Allgood. "An Atomic Blast Simulator," Proceedings of the Society for Experimental Stress Analysis, Vol. XVIII, No. 1, 1959.

3. American Concrete Institute, ACI 318-63: Standard Building Code Requirements for Reinforced Concrete, Detroit, June 1963.

4. Uzhik, G. V., and J. J. Voloshenko-Klimovitsky. "On the Elastic-Plastic Strain of Steels Under Longitudinal Impact," Proceedings of the Conference on the Properties of Materials at High Rates of Strain. The Institution of Mechanical Engineers (London), 1957, p. 239.

5. Columbia University. Studies of the Shear and Diagonal Tension Strength of Simply Supported Reinforced Concrete Beams, by W. J. Krefeld and C. W. Thurston, New York, June 1962.

6. U. S. Naval Civil Engineering Laboratory. Technical Report R-331, NCEL Dynamic Testing Machine, by W. L. Cowell. Port Hueneme, California, 30 October 1964.

7. U. S. Army Engineer Waterways Experiment Station. Miscellaneous Paper No. 6-609: Dynamic and Static Tests of Plain Concrete Specimens, by Lundeen and Saucier. Vicksburg, Mississippi, November 1963.

8. Cheney, James A. "Structural Analysis by Dynamic Load Parameters," Journal of the American Concrete Institute, Vol. 28, No. 1, (June 1956), pp. 99-111.

9. Norris, C. H., et al. Structural Design for Dynamic Loads. McGraw-Hill, New York, 1959.

LIST OF SYMBOLS

A_s	area of longitudinal tension reinforcement, in.^{2}
A_s'	area of longitudinal compression reinforcement, in.^{2}
A_v	area of web reinforcement, in.^{2}
b	width of beam, in.
C	concrete strain, in./in.
CS	compression steel strain, in./in.
d	effective depth of beam and diameter of cylinder, in.
DC	depth change displacement, in.
DSF	dynamic shear factor
DSF_m	maximum dynamic shear factor
E_s	modulus of elasticity of tension reinforcement, psi
E_s'	modulus of elasticity of compression reinforcement, psi
E_v	modulus of elasticity of stirrups, psi
f_c'	compressive strength of 6- by 12-inch concrete cylinder, psi
f_t	tensile stress, psi
f_t'	ultimate tensile strength of concrete, psi
f_{ts}'	static tensile strength of concrete, psi
f_{td}'	dynamic tensile splitting strength of concrete, psi
$\dot{f}_t$	tensile stress rate, psi/sec
f_y	yield stress of steel, psi
F	ratio of dynamic yield stress to static yield stress: f_y/f_y'
h	total depth of beam, in.
L	clear span of beam and length of cylinder, in.
M	dynamic moment, in.-lb
M'	static moment, in.-lb
MA	midspan acceleration, in./sec^2
MD	midspan displacement, in.
p	A_s/bd
p'	A_s'/bd

P	pressure, psi
r	dynamic flexural resistance, lb/in. and $A_v f_s$
r'	static load or static flexural resistance, lb/in.
r_y	dynamic flexural yield resistance, lb/in.
r_y'	static flexural yield resistance, lb/in.
R	reaction at support, kips
R*	mean reaction (Figure 10), kips
s	spacing of stirrups, in.
t	time, sec
t_c	time to diagonal tension cracking, sec
t_m	time to maximum, sec
t_y	time to first yielding of stirrups, sec
T	duration of load, sec
T_n	fundamental period of vibration, sec
TS	tension steel strain, in./in.
V(t)	dynamic shear at support at time, t, kips
V'	static shear at support, kips
V_c	dynamic shear at support corresponding to formation of critical diagonal crack, kips
V_c'	static shear at support corresponding to formation of critical diagonal crack, kips
V_m	maximum dynamic shear at support, kips
V_u	dynamic ultimate shear at support, kips
V_u'	static ultimate shear at support, kips
V_v	dynamic shear at support corresponding to first yielding of stirrups, kips
V_v'	static shear at support corresponding to first yielding of stirrups, kips
V_y'	static shear at support corresponding to static flexural yield resistance, kips
w	load, lb/in.
W	total applied load, lb
$\dot{W}$	load rate, lb/sec
WS	stirrup strain, in./in.
w_0	peak dynamic load, lb/in.

x	horizontal distance from center of support, in.
x_1	distance from center of support to intersection of diagonal crack and longitudinal tension reinforcement, in.
x_2	distance from center of support to intersection of diagonal crack and longitudinal compression reinforcement, in.
x_c	distance from center of support to critical section, in.
y	deflection at midspan, in.
y_m	maximum dynamic deflection, in.
y_y	dynamic flexural yield deflection, in.
y_y'	static flexural yield deflection, in.
ϵ	strain, in./in.
$\dot{\epsilon}$	strain rate, in./in./sec
ϵ_m	maximum strain, in./in.
ϵ_y	yield strain, in./in.

Appendix A

DYNAMIC YIELD STRENGTH OF BARS

SCOPE, OBJECTIVE, SPECIMENS, AND EQUIPMENT

Thirteen tensile specimens conforming to ASTM Specification E8-61T were machined from lengths of No. 9 bar used in the beams. Each specimen was subjected to a different strain rate and the yield strength observed. Five specimens were strained slowly (statically) and eight rapidly.

The objective of the tests was to determine the dynamic yield strength of the No. 9 bars used in the beams and to relate yield strength to strain rate.

The specimens were strained in tension with the NCEL rapid load machine[6] and continuous measurements were recorded of tensile strain and force in the specimen with CEC System D equipment and a CEC model 5-119 oscillograph. The force was measured with a 50-kip-capacity BLH load cell. The strain was measured with one SR-4 foil resistance strain gage (BLH-FA-50) placed midway between the ends of the specimen.

RESULTS AND DISCUSSION

The test results are listed in Table A-I and plotted in Figure 3. A typical oscillogram is shown in Figure A-1. As expected, the upper yield strength increased as a function of the strain rate (Figure 3). There was a slight increase in tensile strength with an increase in stress rate. The rupture stress listed in Table A-1 is only approximate. The point of actual fracture was very hard to determine from the oscillogram records.

Table A-I. Results of Rapid Load Tests on No. 9 Reinforcing Bar

Specimen No.	Strain Rate	Yield Stress		Tensile Strength	Rupture Strength	Elongation in 2 Inches	Reduction in Area
		Upper	Lower				
	$\dot{\epsilon}$ (in./in./sec)	f_{yu} (ksi)	f_{yl} (ksi)	f'_t (ksi)	f_{su} (ksi)	ϵ_u (%)	(%)
S1	static	82.5	79.5	122.5	105.0	16.5	29
S2	static	81.0	79.0	117.0	104.5	17.8	31
S3	static	82.0	79.0	117.5	105.5	17.0	32
S4	static	80.5	79.0	117.0	103.5	15.5	28
S5	static	81.5	78.5	117.0	104.0	18.0	33
D1	0.05	93.5	86.5	121.0	105.0	18.0	33
D2	0.12	94.5	86.0	123.0	104.0	-	36
D3	0.20	99.0	90.0	127.0	106.0	19.0	35
D4	0.36	102.0	93.5	128.5	110.5	17.0	33
D5	0.40	102.0	92.5	128.0	113.0	19.0	34
D6	0.41	102.0	92.5	127.5	107.0	19.0	37
D7	0.46	102.5	94.5	126.5	109.0	18.8	36
D8	0.86	105.0	94.0	128.0	109.0	16.8	37

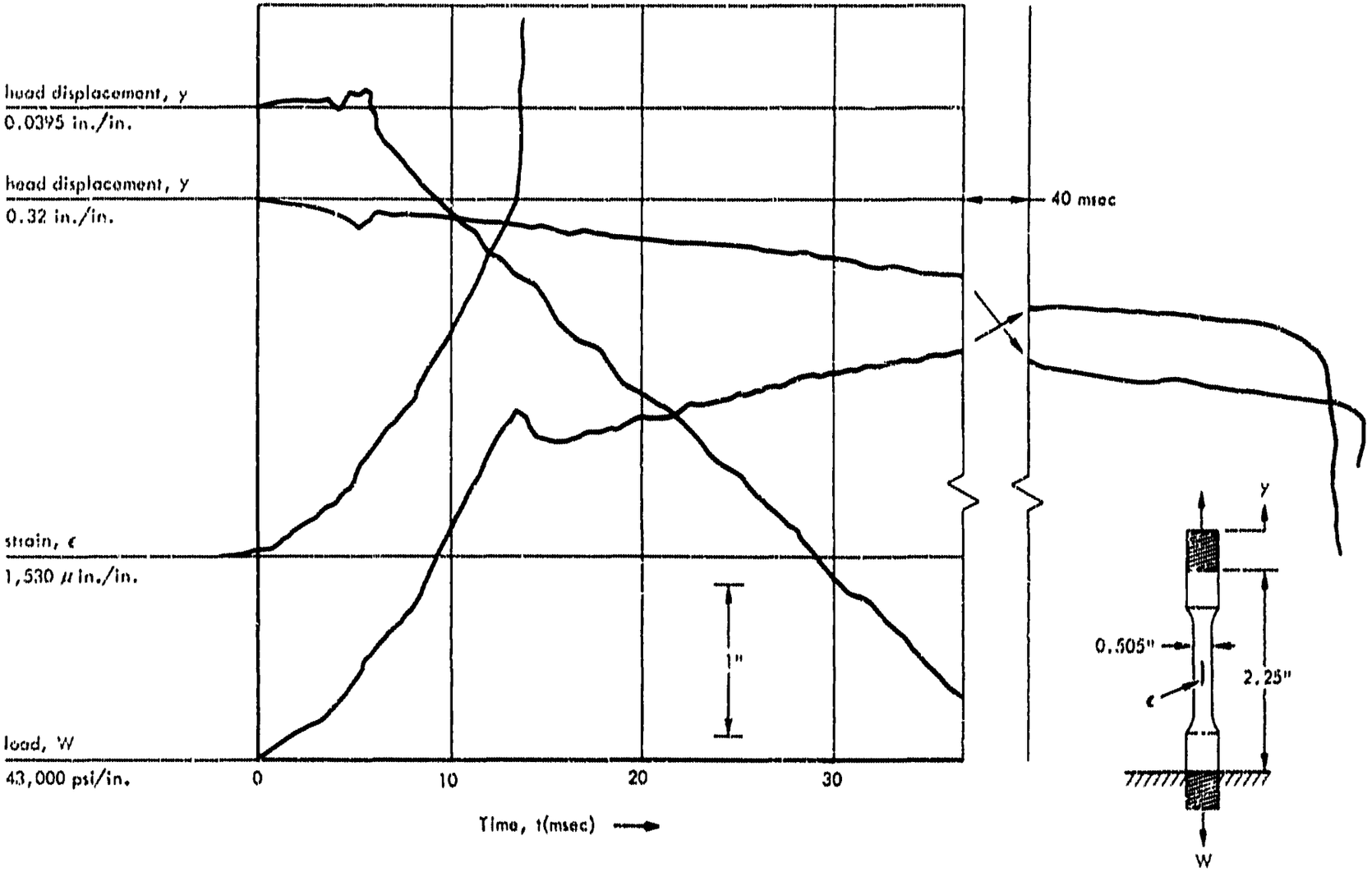

Figure A-1. Typical oscillogram, specimen D4.

Appendix B

DYNAMIC TENSILE SPLITTING STRENGTH OF CONCRETE

INTRODUCTION

The shear resistance of concrete beams increases with the tensile strength of the concrete.[1] Therefore, the increase in shear resistance observed in beams under dynamic load may be attributed partly to the increased tensile strength of the concrete.

Under dynamic load, the tensile splitting strength of concrete cylinders has been observed to increase 74 percent.[7] However, more data from split cylinder tests are needed to judge the value of such a test as a measure of the dynamic tensile strength of concrete and to relate tensile splitting strength to tensile stress rate.

OBJECTIVE

The objective of this portion of the work was to observe the effect of stress rate on the tensile splitting strength of molded concrete cylinders.

SCOPE

Seventeen concrete cylinders were tested under various loading rates in accordance with the recommended procedures outlined in ASTM Specification C496-62T, "Splitting Tensile Strength of Moulded Concrete Cylinders." The rate of loading was slow (static) on five cylinders and rapid on 12 cylinders. The materials and mix proportions for casting the cylinders were identical to those used to cast the beams described in this report.

SPECIMENS

All cylinders were 4 inches in diameter, 8 inches long, and cast from one batch of concrete. The concrete mix was made from Type I portland cement, 3/4-inch maximum size San Gabriel aggregate, and San Gabriel sand having a fineness modulus of 2.82. Mix proportions were 1.00:3.82:3.66 by weight, with a water-cement ratio of 0.71 by weight or 7.98 gallons per sack. The cement factor was 4.7 sacks per cubic yard. The average compressive strength of the concrete was 3,280 psi at 22 days for three standard 6- by 12-inch cylinders.

Four SR-4, Type A-12 wire resistance strain gages were bonded to the ends of each cylinder. Each strain gage formed one leg of a Wheatstone bridge circuit with three dummy gages. The exact locations of the gages are illustrated in Figure B-1.

TEST PROCEDURE

The specimen was lined with the marking apparatus specified in ASTM Specification C496-62T and positioned in the testing machine with two 1 by 8-1/2 by 1/8 inch-thick plywood strips. A plywood strip was placed on the top and one on the bottom of the cylinder along the line of contact (Figure B-1). A metal bar, 2-1/2 by 8-1/2 by 1-1/2 inches thick was placed between the top plywood strip and loading ram to assure a uniform distribution of pressure along the length of the cylinder (Figure B-1).

The static split cylinder tests were performed with a 400,000-pound Baldwin test machine. Strain readings were recorded at load increments of 2,000 pounds with CEC System D equipment and a CEC model 5-119 oscillograph. A typical setup for a static test is shown in Figure B-2.

The dynamic split cylinder tests were conducted with the NCEL rapid load machine.[6] Continuous measurements of load and strains were recorded with the same equipment used for the static tests. A typical setup for a dynamic test is shown in Figure B-3.

RESULTS AND ANALYSIS OF DATA

The results of the tensile splitting tests are summarized in Table B-I and plotted in Figure 4. A typical oscillogram for a dynamic test is shown in Figure B-4.

The load rate, $\dot{W}$, tensile stress rate, $\dot{f}_t$, and dynamic tensile splitting strength, f_{td}', were computed by the following relations:

$$\dot{W} = \frac{\Delta W}{\Delta t} \tag{B-1}$$

$$\dot{f}_t = \frac{2\dot{W}}{\pi dL} \tag{B-2}$$

$$f_{td}' = \frac{2W}{\pi dL} \tag{B-3}$$

Where $\frac{\Delta W}{\Delta t}$ = slope of linear portion of loading curve (Figure B-4) just prior to failure

L = length of cylinder

d = diameter of cylinder

W = maximum total applied load (Figure B-4)

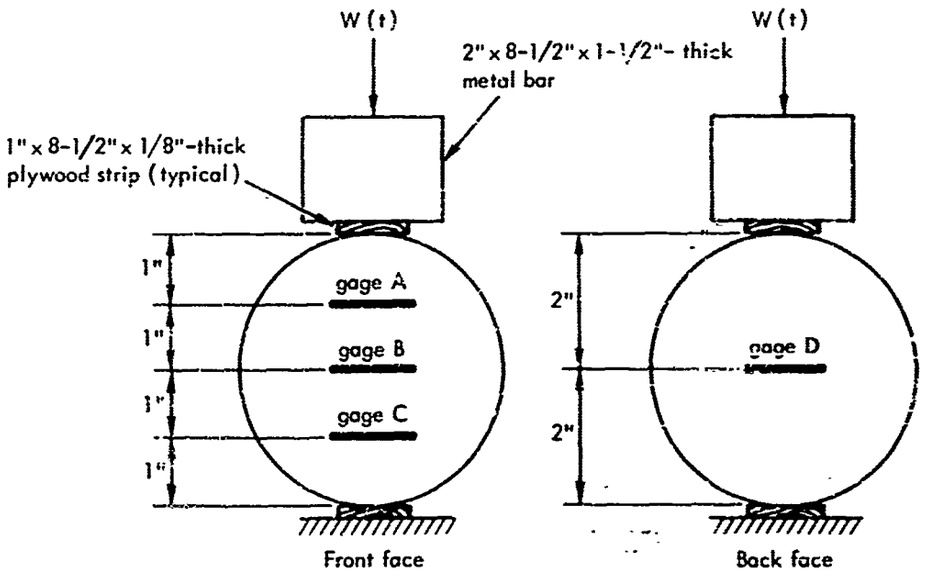

Figure B-1. Location of gages and plywood strips.

Figure B-2. Typical setup for static split cylinder test.

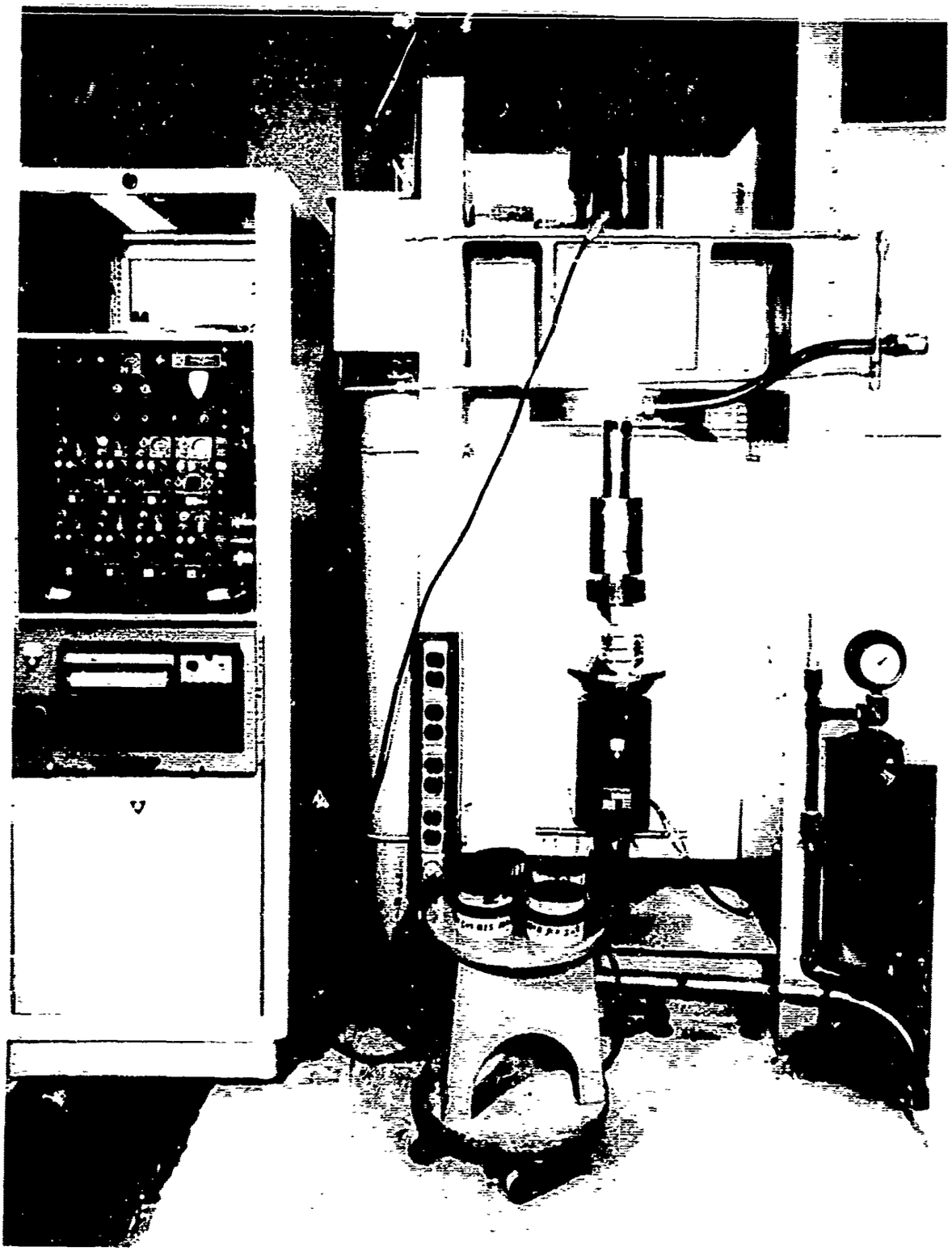

Figure B-3. Typical setup for dynamic split cylinder test.

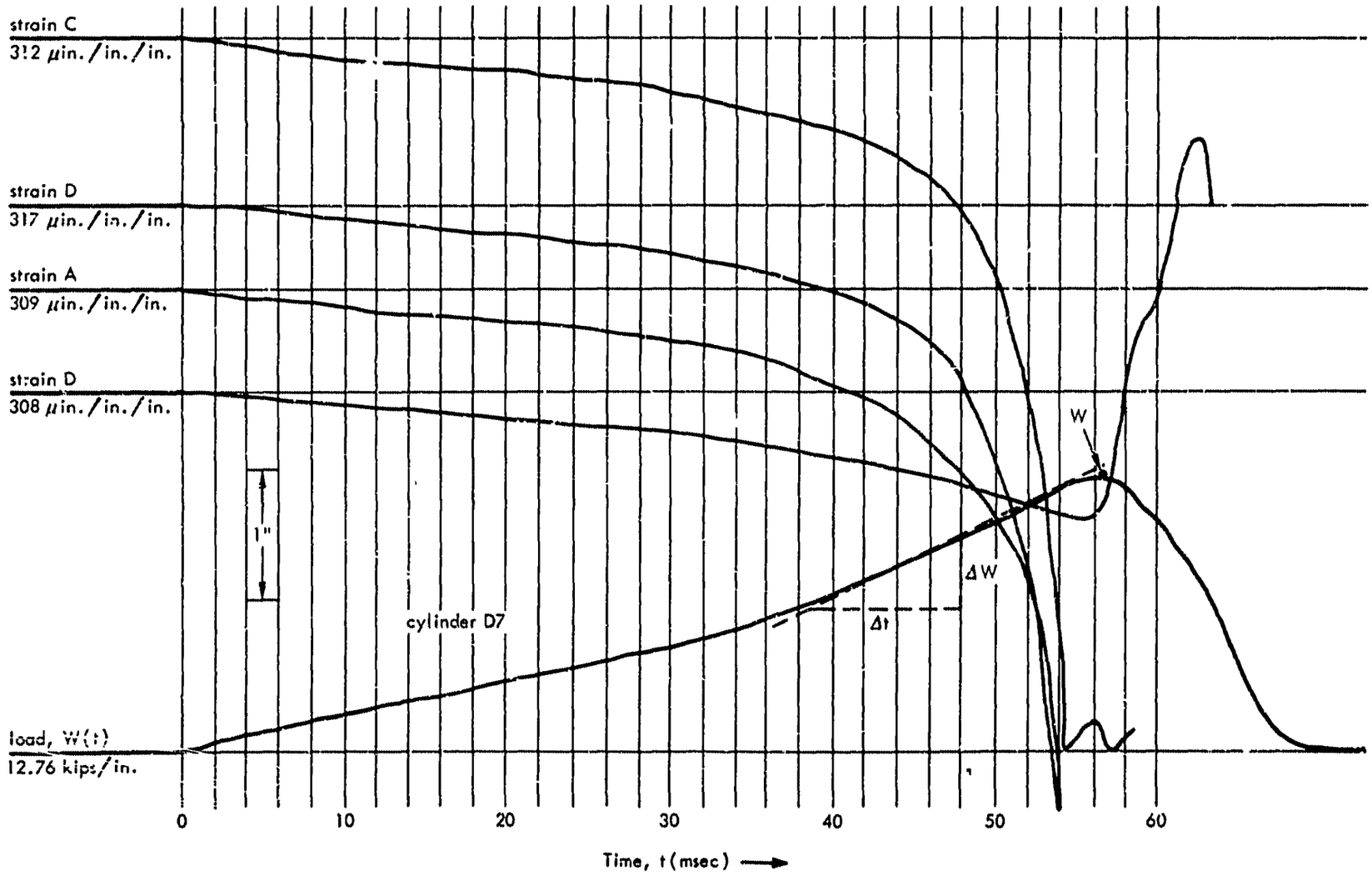

Figure B-4. Typical oscillogram for concrete tension test.

Table B-I. Results of Tensile Splitting Tests

Cylinder No.	Load Rate	Tensile Stress Rate	Tensile Splitting Strength	
	$\dot{W}$ (kips/in./sec)	$\dot{f}_t$ (psi/sec)	f_t' (psi)	f_{td}'/f_{ts}' [1]
S1	0.002	0.4	420	-
S2	0.002	0.4	420	-
S3	0.002	0.4	415	-
S4	0.003	0.6	450	-
S5	0.002	0.4	425	-
D1	440	87,800	570	1.34
D2	358	71,400	580	1.36
D3	333	66,300	605	1.42
D4	247	49,200	580	1.36
D5	173	34,400	600	1.40
D6	103	20,500	465	1.09
D7	77	15,300	530	1.25
D8	2.5	500	430	1.01
D9	21	4,100	525	1.23
D10	27	5,300	515	1.21
D11	1,060	210,200	685	1.61
D12	1,000	200,200	690	1.62

[1] f_{ts}' = average static tensile splitting strength of specimens, S1 - S5 = 425 psi

The tensile splitting strength increased with tensile stress rate (Table B-I). The static tensile strength varied from 415 to 450 psi, with an average strength of 425 psi. The dynamic tensile strength varied from 430 to 690 psi depending on the tensile stress rate. The maximum increase in dynamic tensile strength over the static tensile strength was 62 percent for a tensile stress rate of 210,000 psi/sec. The limitation of the rapid load machine limited the maximum stress rate to 210,000 psi/sec, but the trend of the curve shown in Figure 4 strongly suggests that greater stress rates would produce tensile strengths even greater than 62 percent. The shape of the curve also suggests that the rate of increase in tensile strength would be even greater at higher stress rates.

The breaks or fracture planes in the cylinders were clean, even, and passed through the center of the cylinder, all characteristics of a good break (Figure B-5). Stress rate had no apparent effect on the fracture except for a slight increase in the percent of coarse aggregate sheared in the cylinders stressed rapidly.

The strain distribution along the vertical diameter of the cylinders was similar and nearly uniform under slow and rapid stress rates, as shown in Figures B-6 and B-7. In other words, stress rate did not change the distribution of stress along the critical section. Therefore, the increase in tensile strength observed under rapid stress rates was indeed due to the increased tensile strength of the concrete and not to a change in the distribution of stress along the critical section.

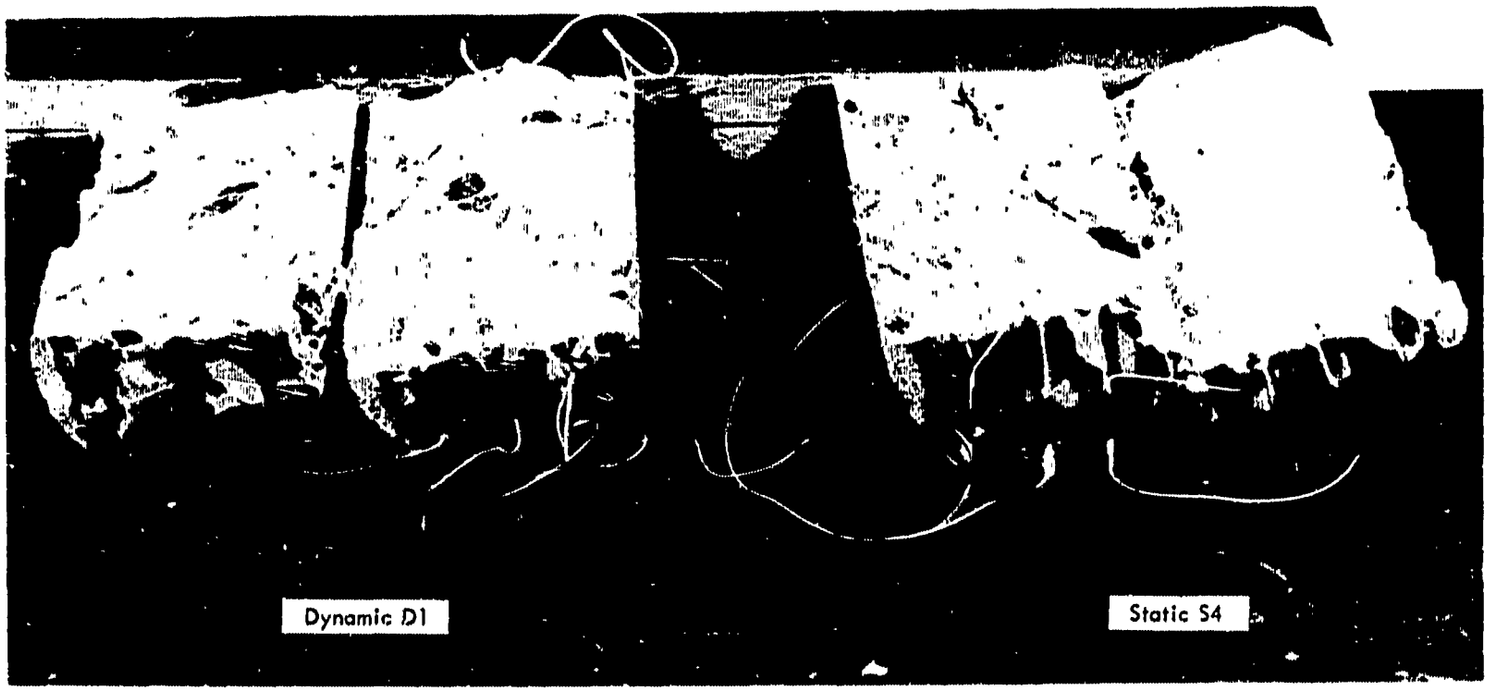

Figure B-5. Typical tensile splitting failure for static and dynamic loads.

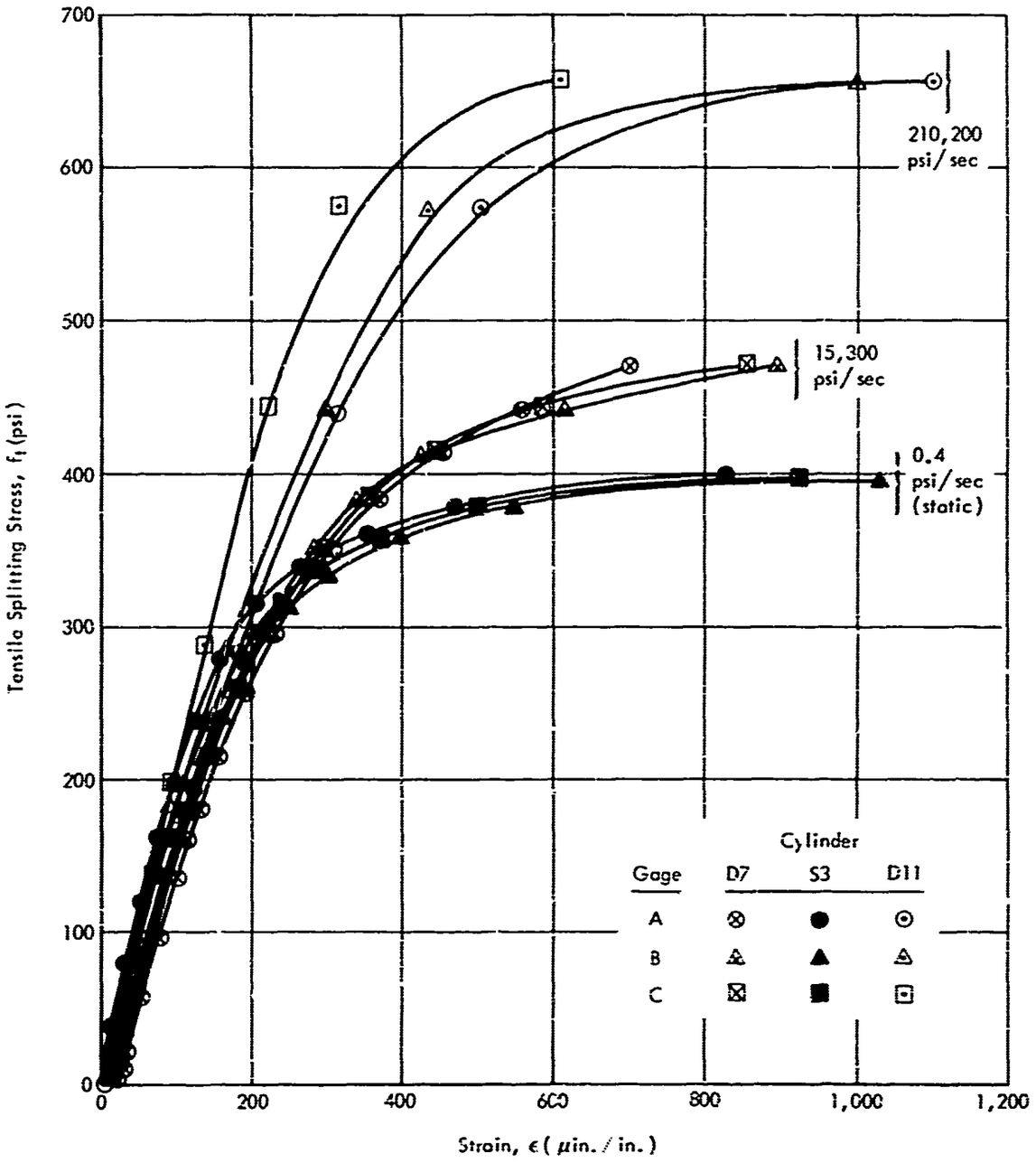

Figure B-6. Effect of stress rate on stress-strain relationship.

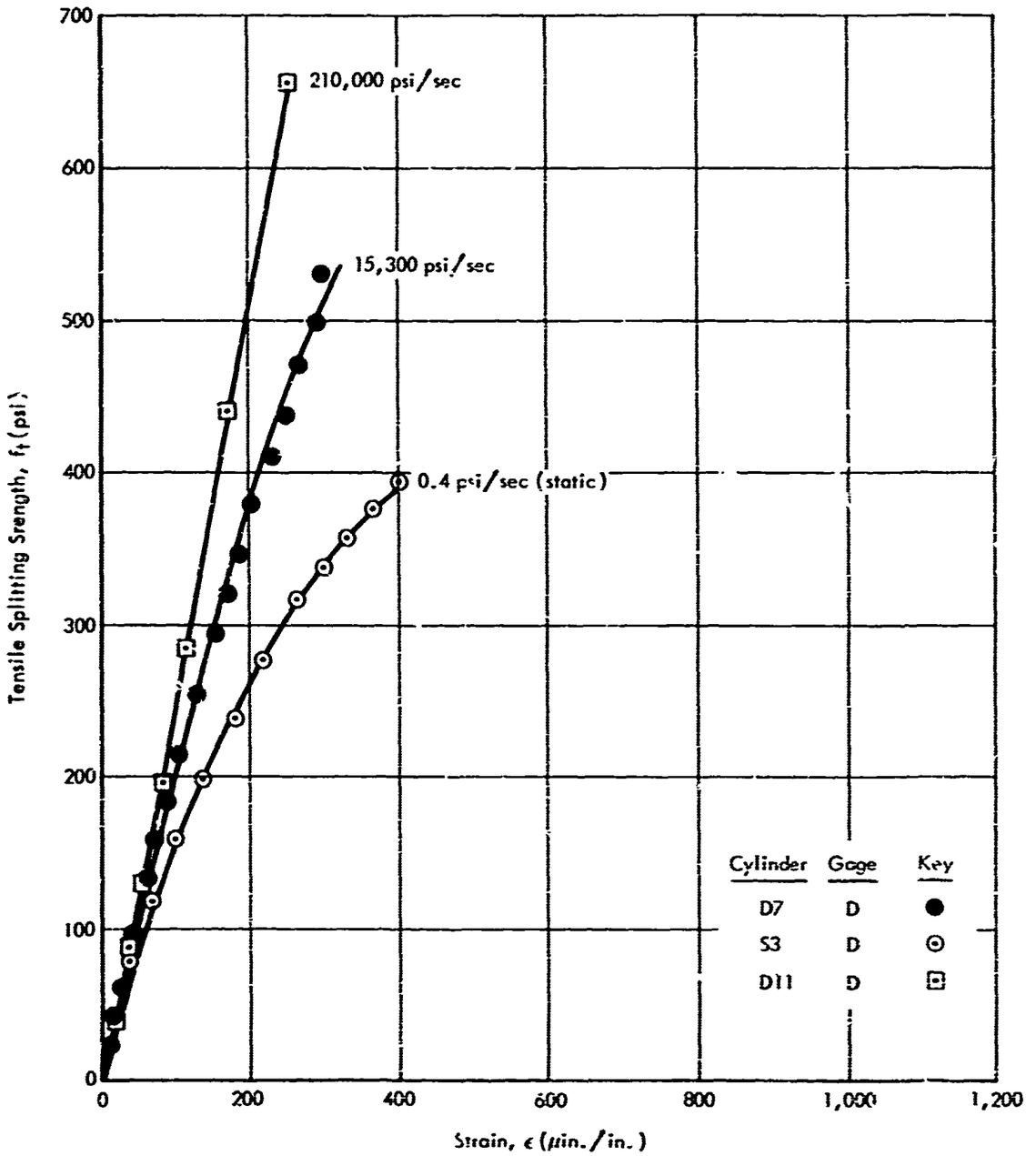

Figure B-7. Effect of stress rate on stress-strain relationship.

Although strains A, B, and C were compatible, strain D, located at the opposite end of the cylinder, was quite different. For a given load, strain D was invariably the least of the four strains. This difference is attributed to the fact that gage D was always bonded to the cylinder end exposed in the concrete mold. Segregated aggregate, lesser compaction, or misaligned mold walls at the end, resulting from vibrating the concrete, are possible reasons for the difference.

FINDINGS AND CONCLUSIONS

1. The distribution of strain along the vertical diameter of the cylinders did not change appreciably with changes in stress rate and was nearly uniform.

2. The tensile splitting strength increased with tensile stress rate as shown in Figure 4. The strength increased 62 percent when the stress was increased from 0.4 to 210,200 psi/sec.

3. Split cylinder tests appear to be as acceptable a method to measure the dynamic as the static tensile strength of concrete.

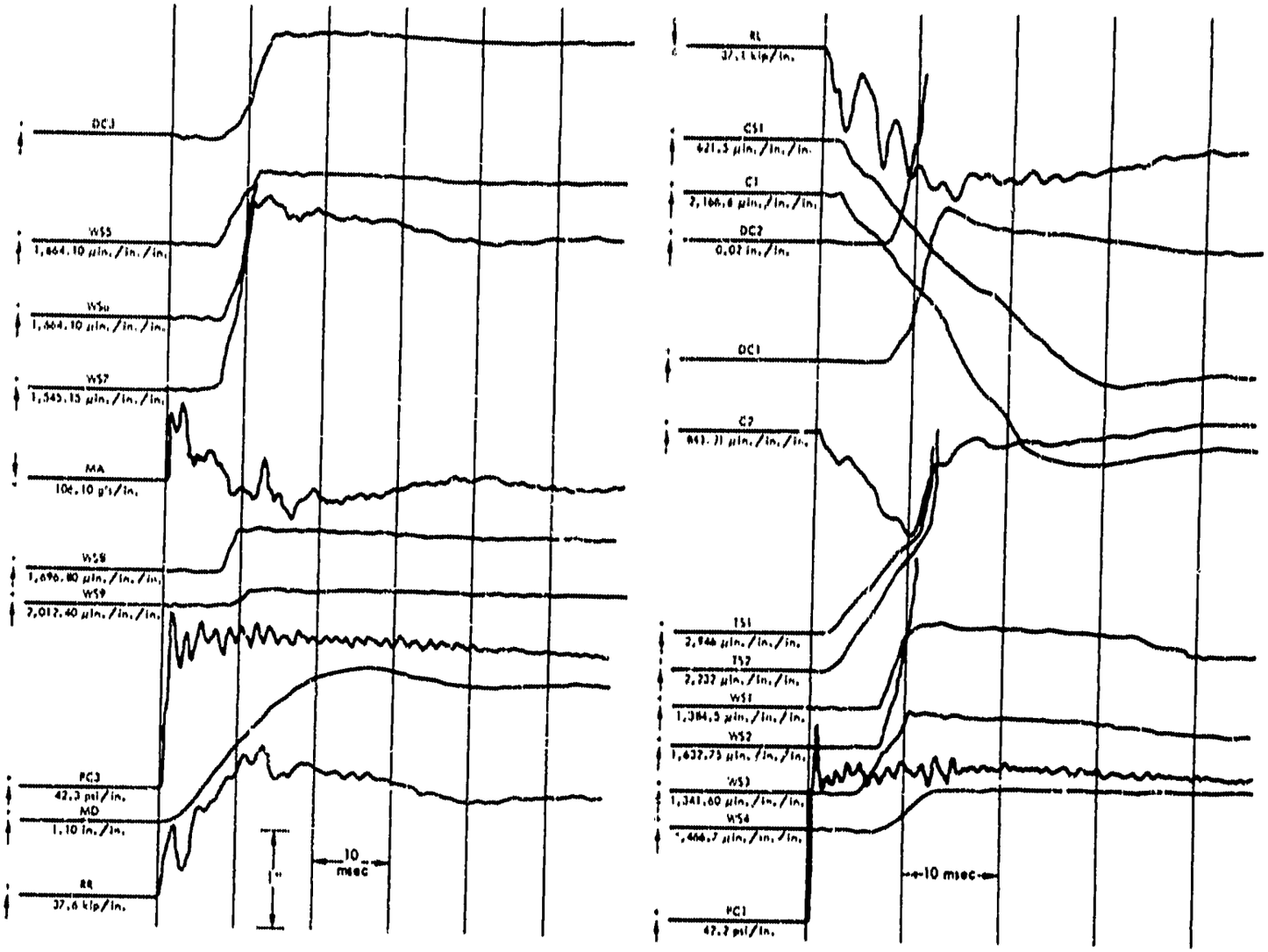

Figure C-2. Oscillogram for test WD5.

Appendix C

TYPICAL OSCILLOGRAMS FROM DYNAMIC TESTS

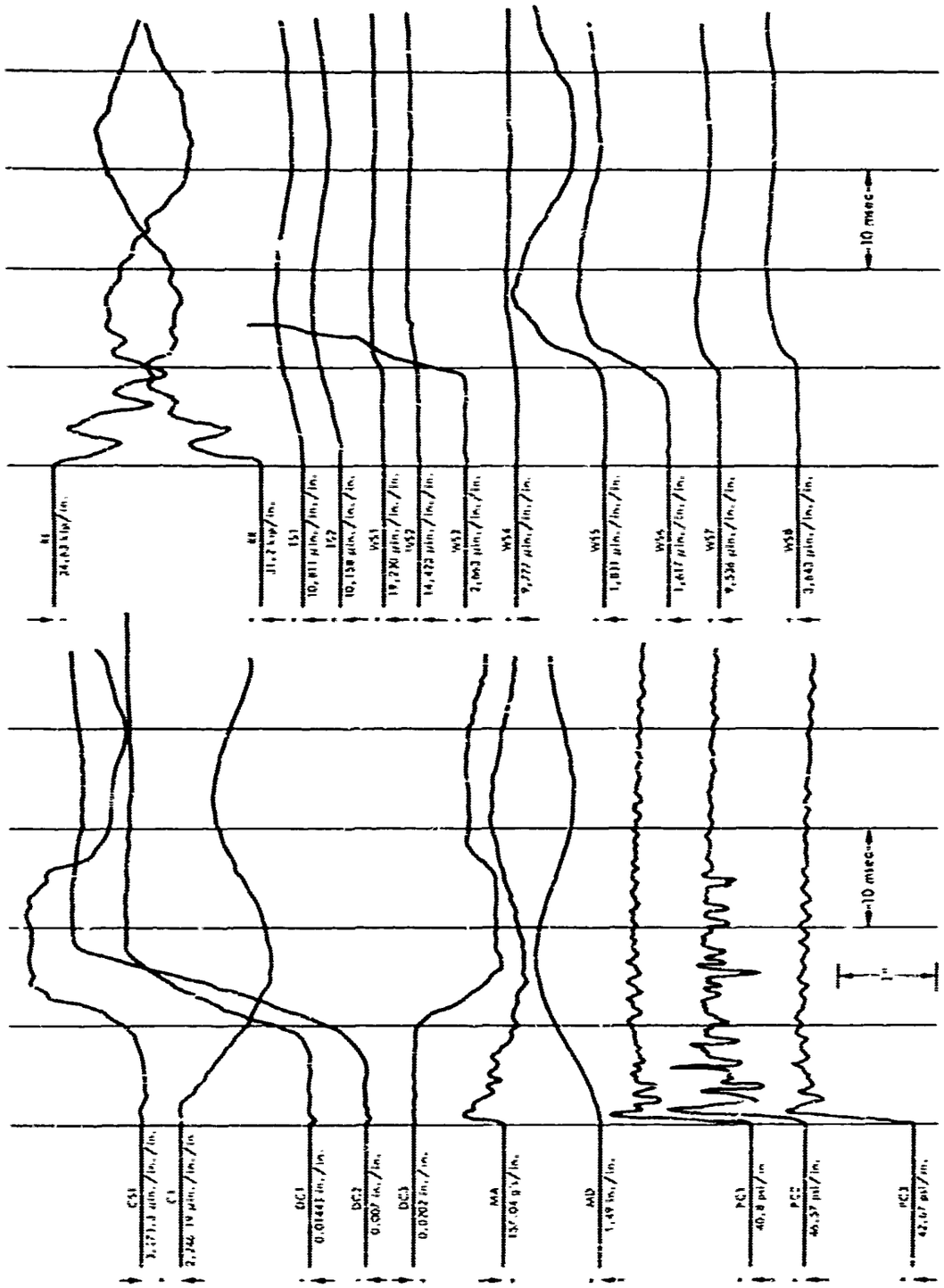

Figure C-1. Oscillogram for test WD4-1.

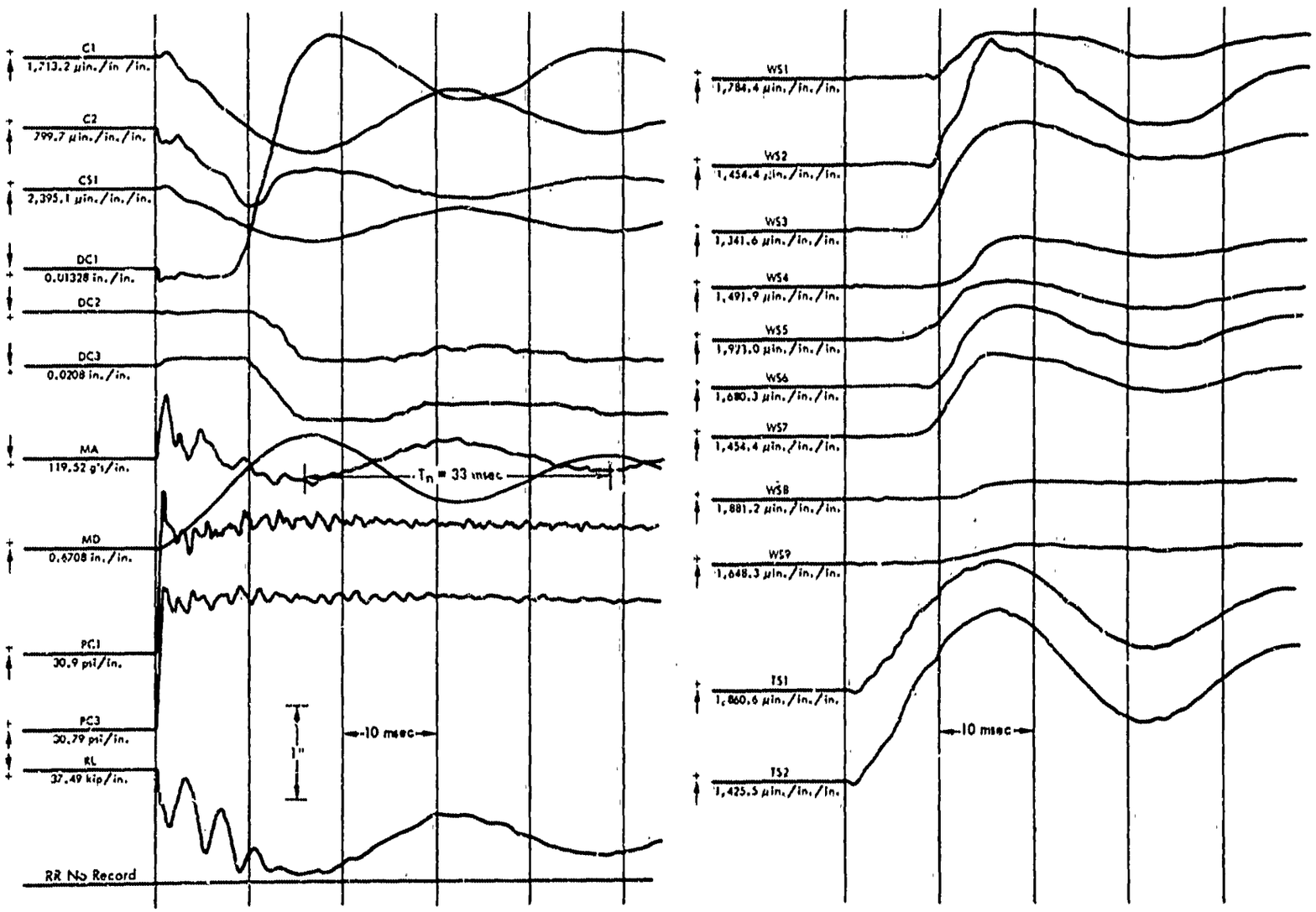

Figure C-4. Oscillogram for test WD7-1.

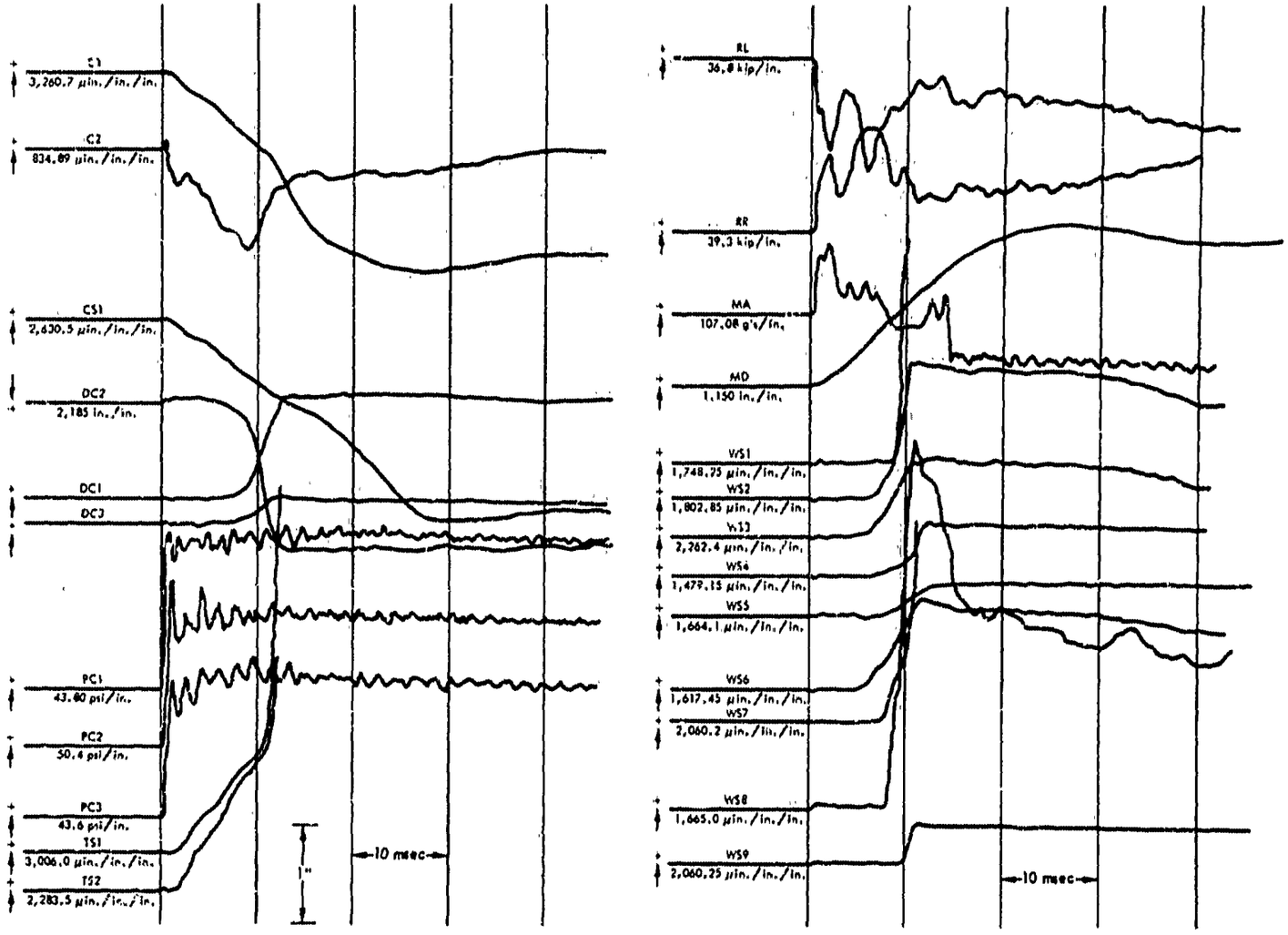

Figure C-3. Oscillogram for test WD6.

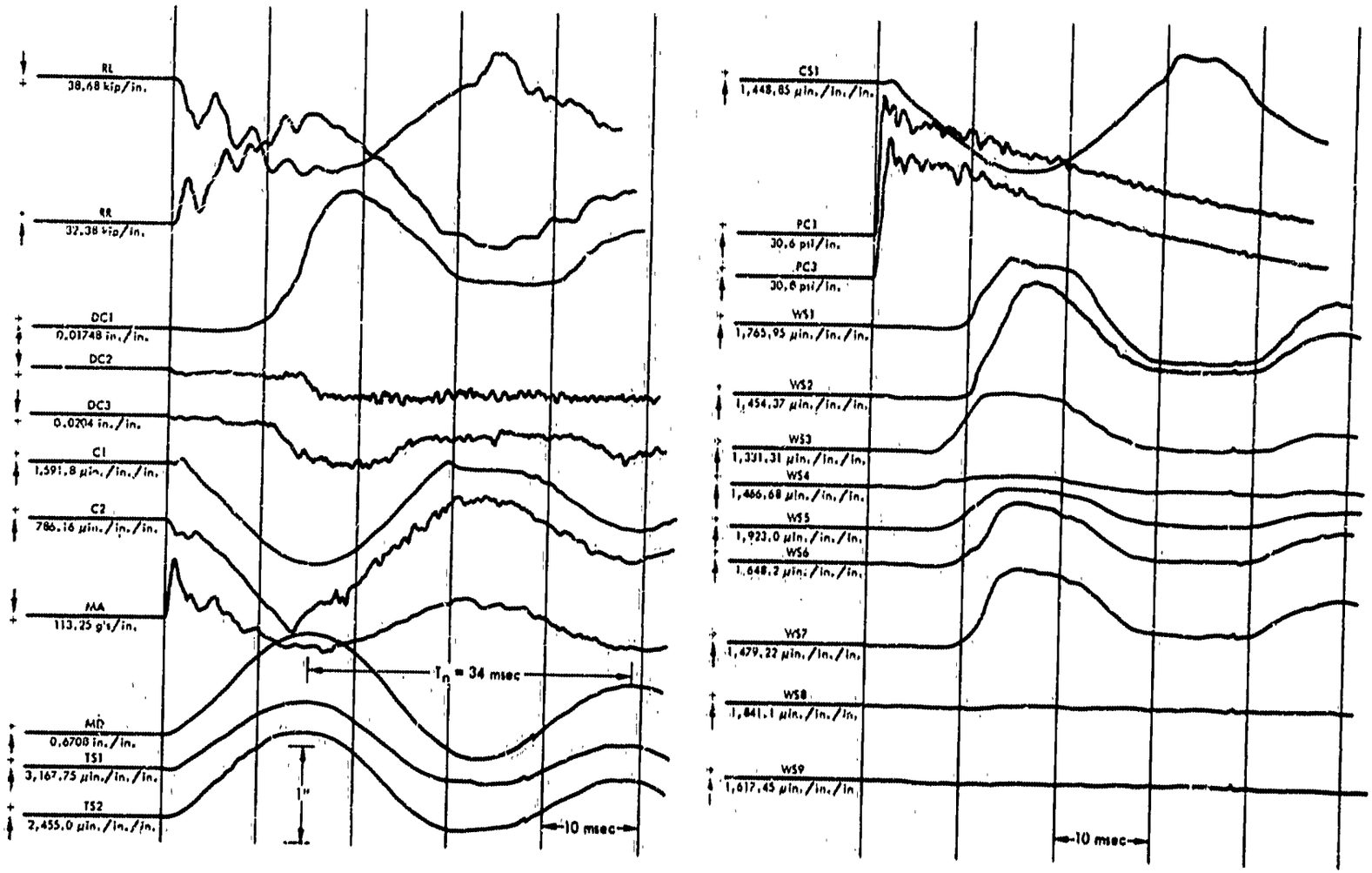

Figure C-6. Oscillogram for test WD9-1.

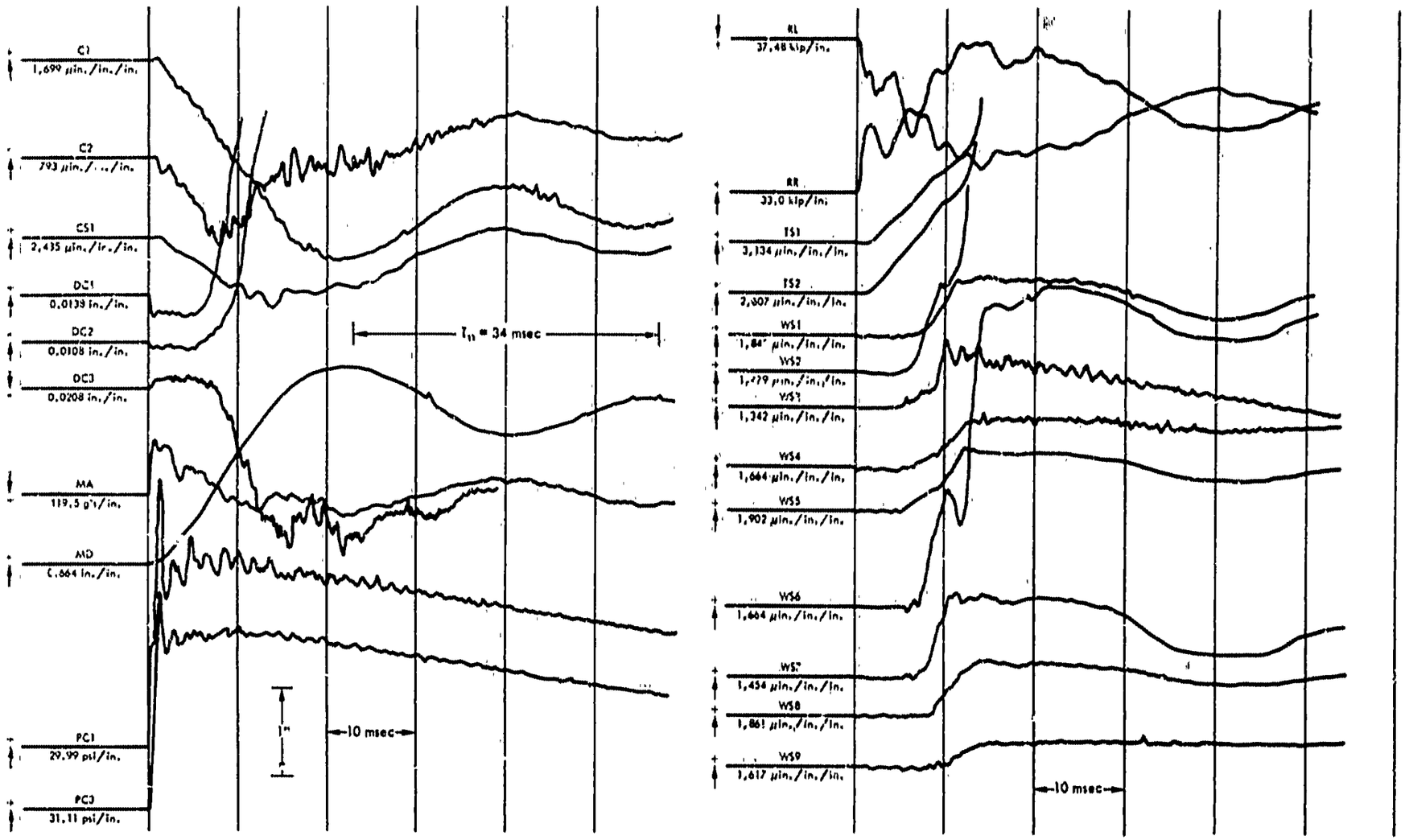

Figure C-5. Oscillogram for test WD8-1.

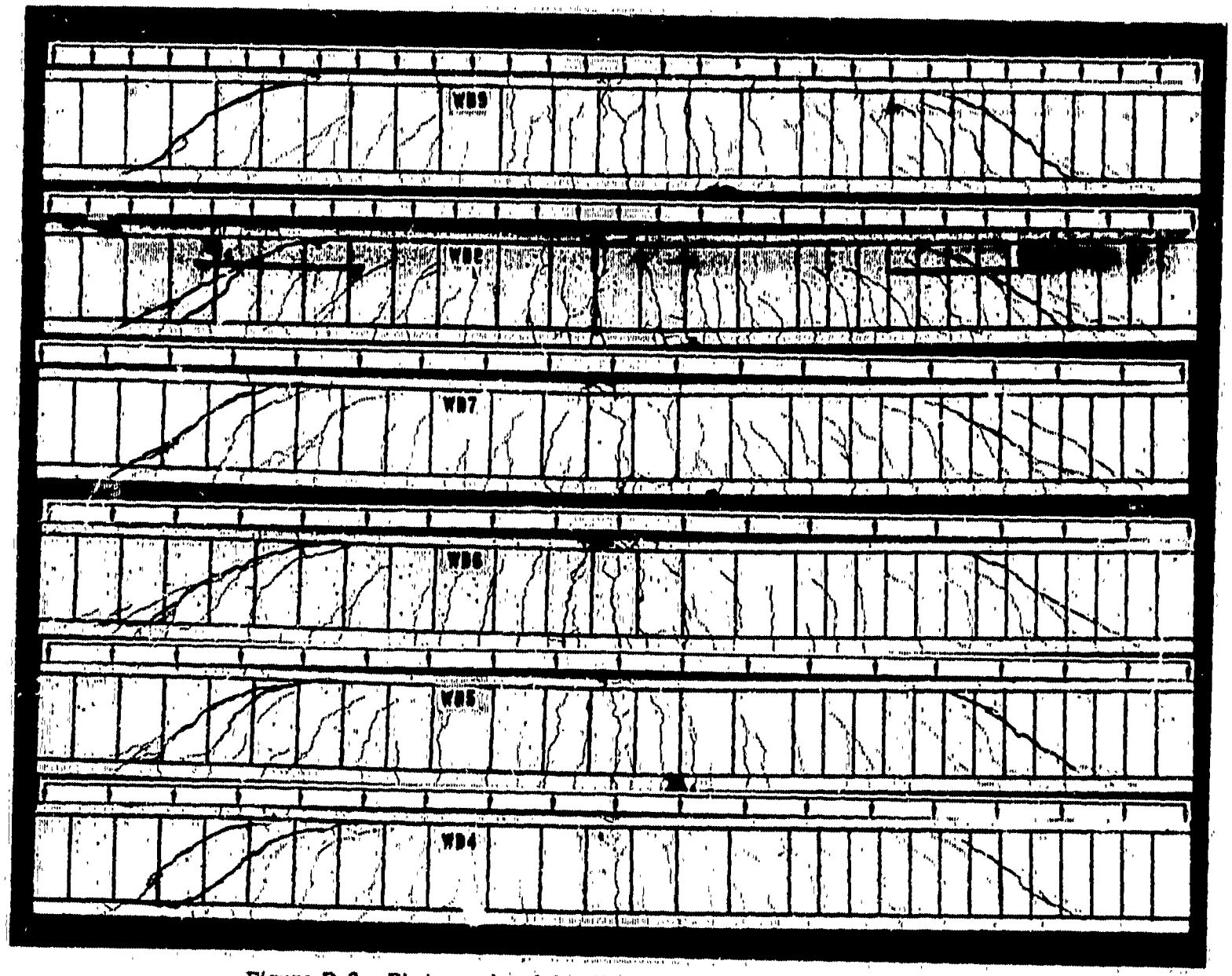

Figure D-2. Photographs of dynamically loaded beams after failure.

Appendix D

PHOTOGRAPHS OF BEAMS AFTER FAILURE

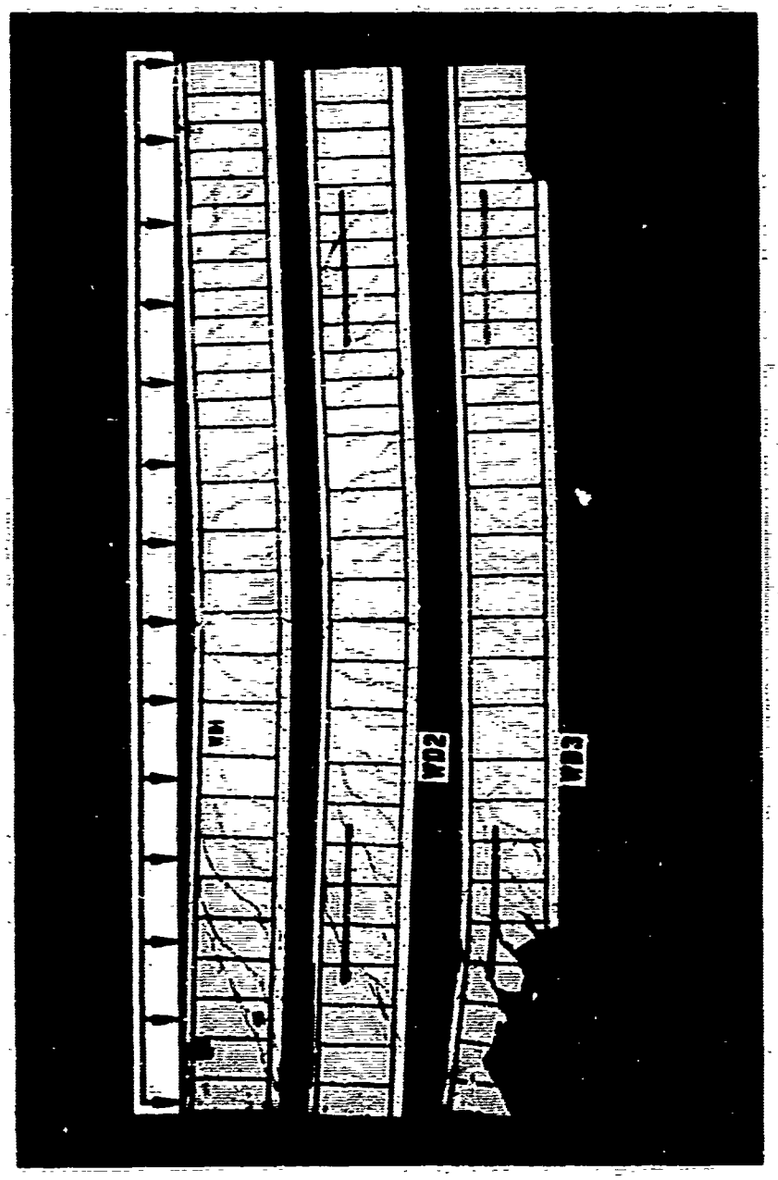

Figure D-1. Photographs of statically loaded beams after failure.

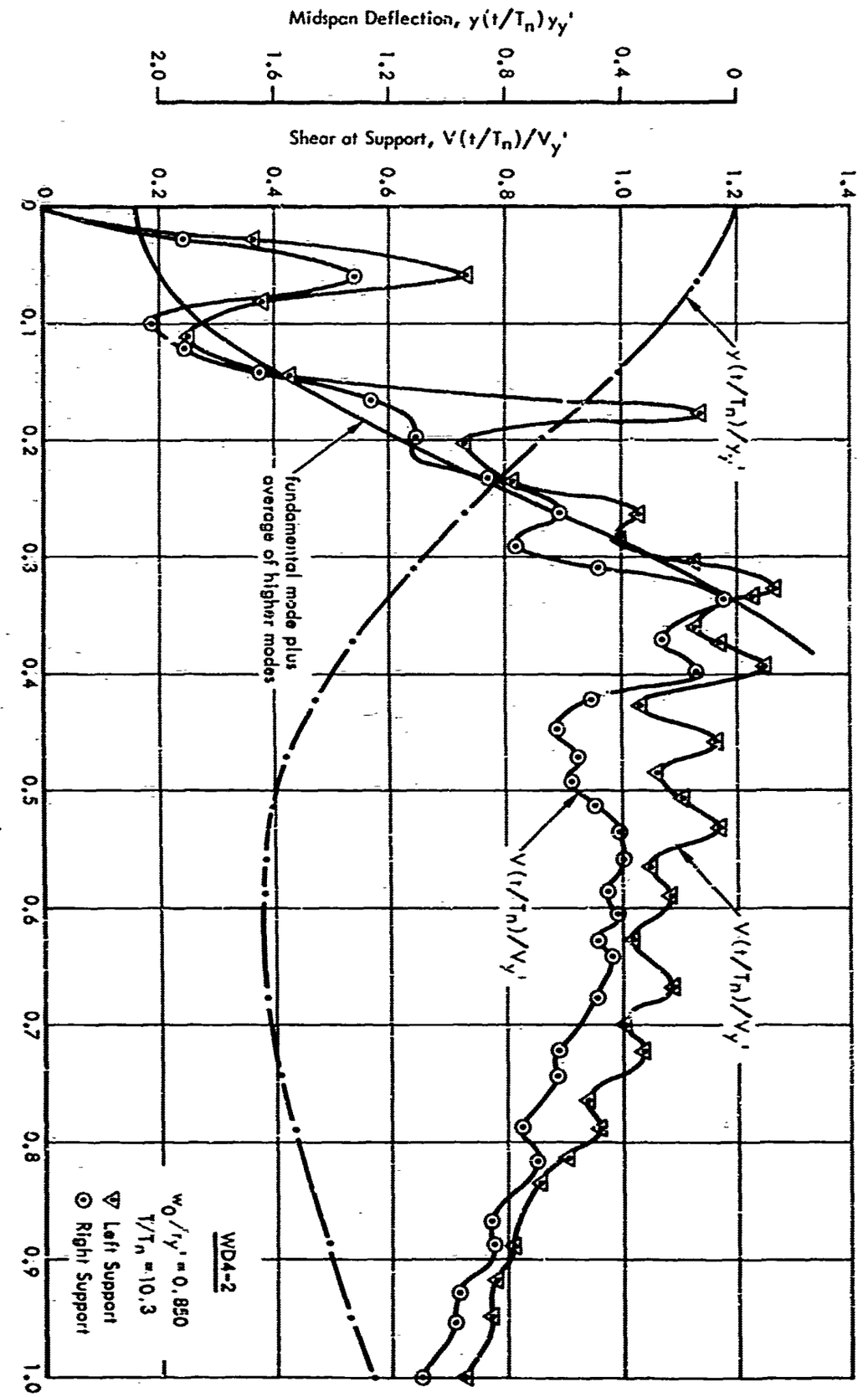

Figure E-2. Measured midspan deflection and shear at support versus time, WD4-2.

Appendix E

SUPPORT SHEAR AND MIDSPAN DEFLECTION-TIME CURVES

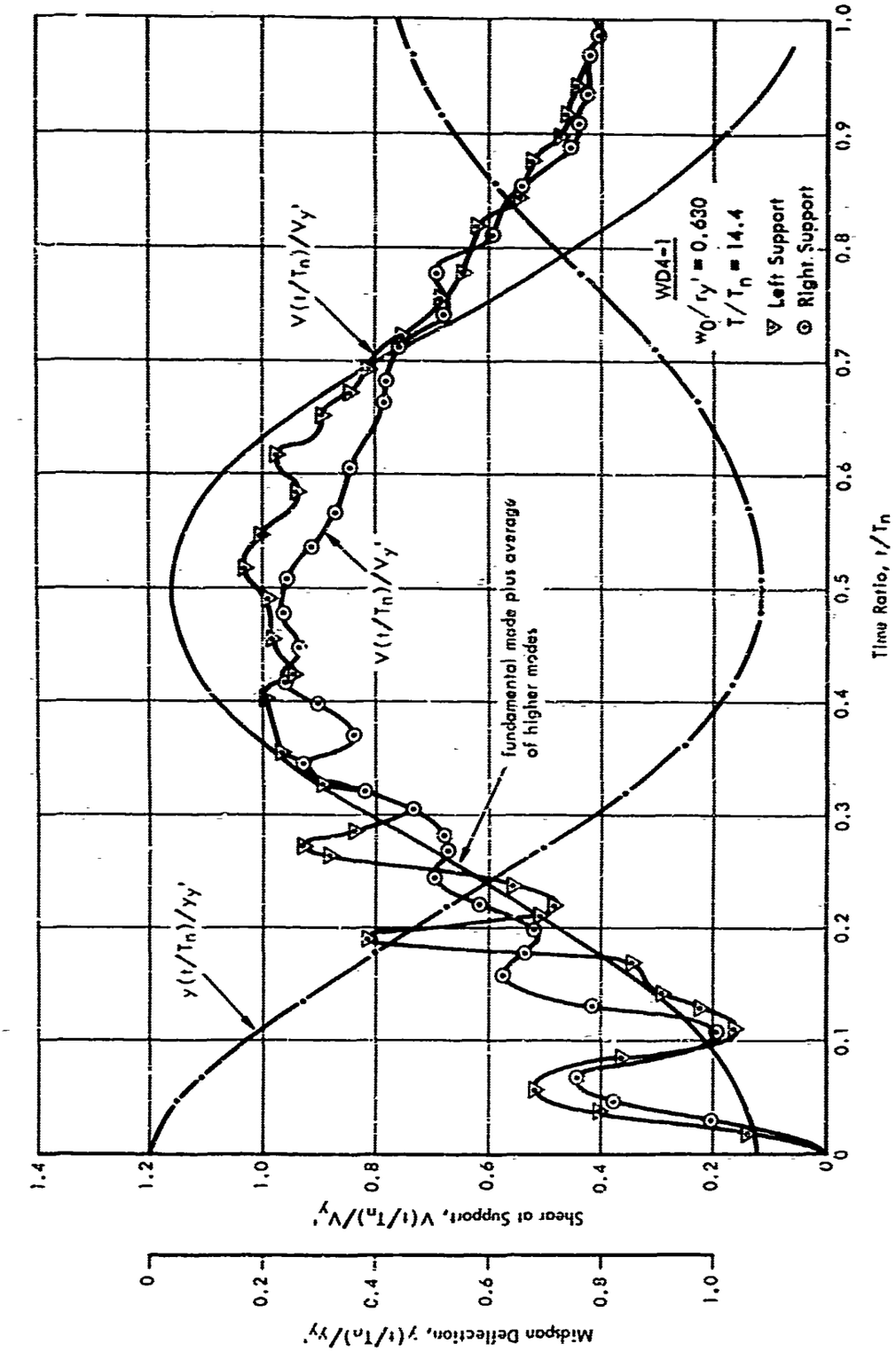

Figure E-1. Measured midspan deflection and shear at support versus time, WD4-1.

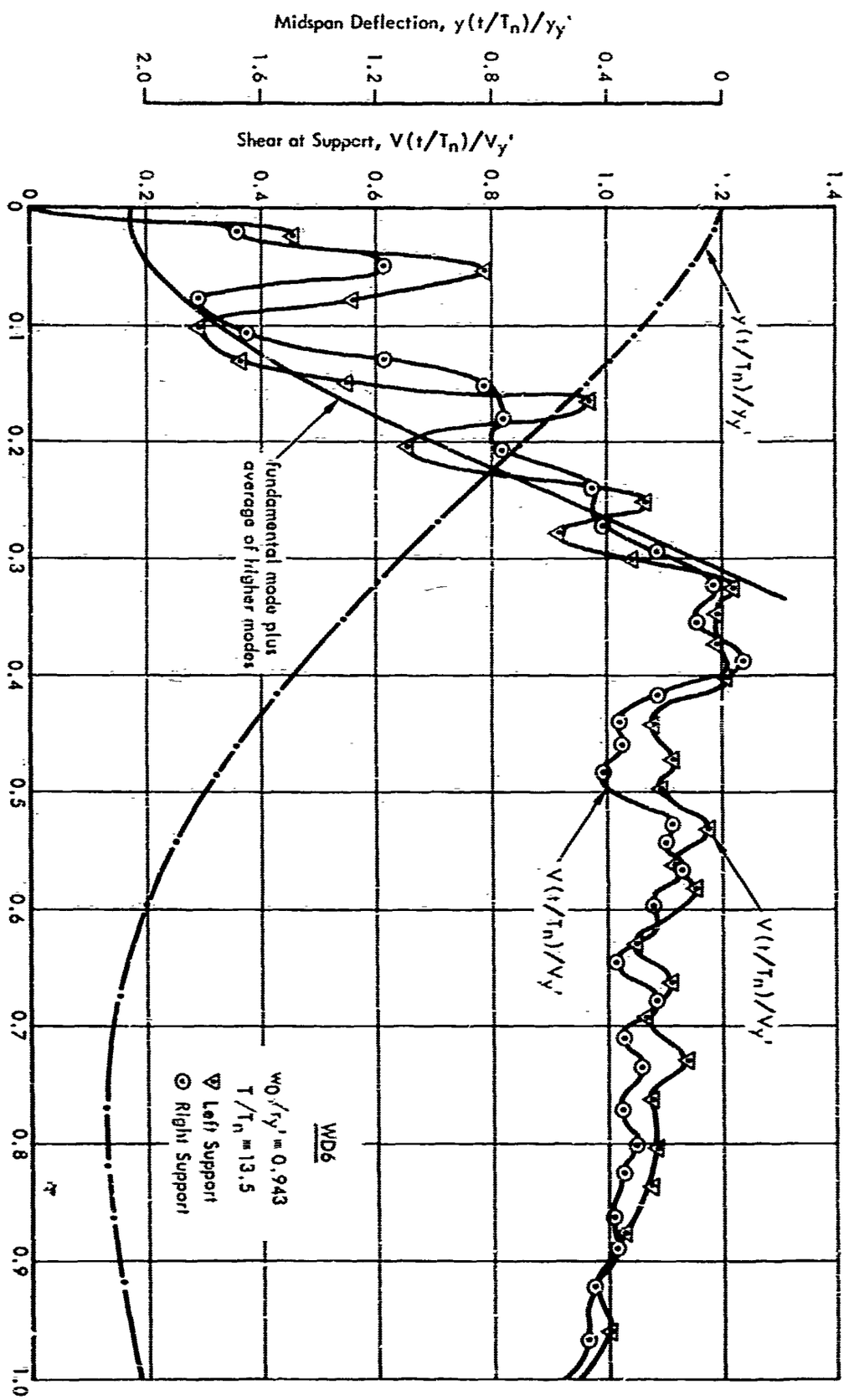

Figure E-4. Measured midspan deflection and shear at support versus time, WD6.

Figure E-3. Measured midspan deflection and shear at support versus time, WD5.

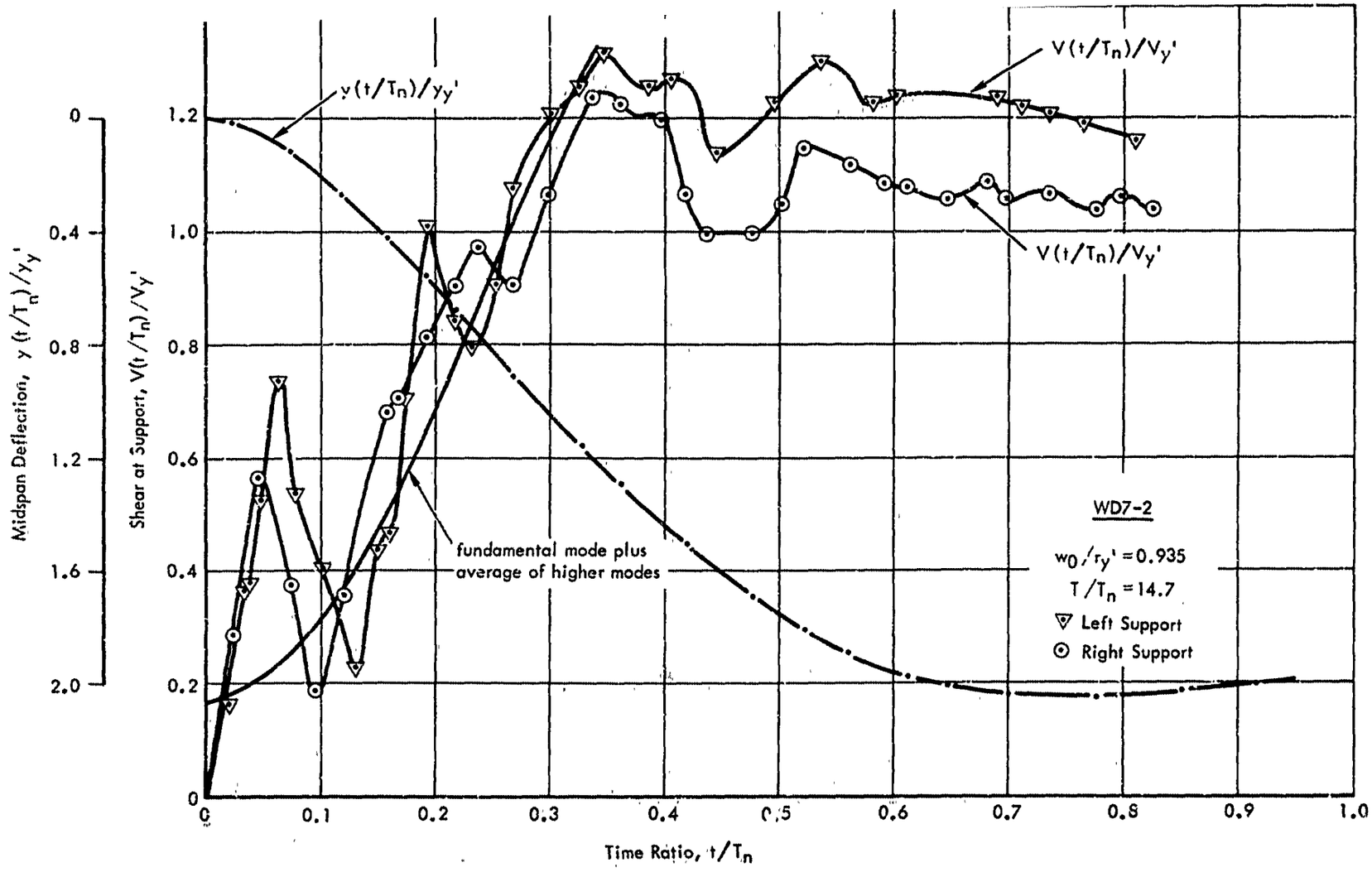

Figure E-6. Measured midspan deflection and shear at support versus time, WD7-2.

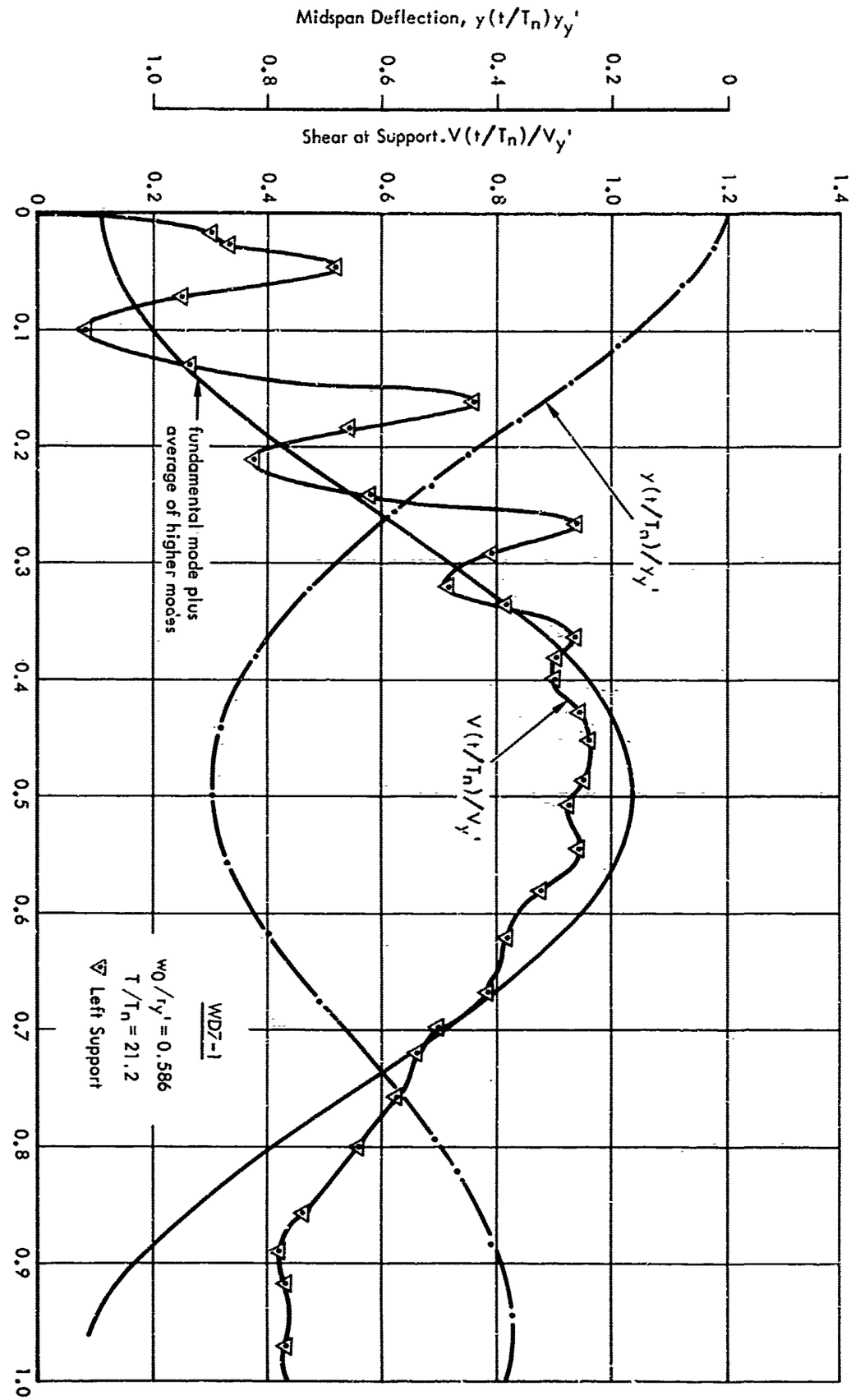

Figure E-5. Measured midspan deflection and shear at support versus time, WD7-1.

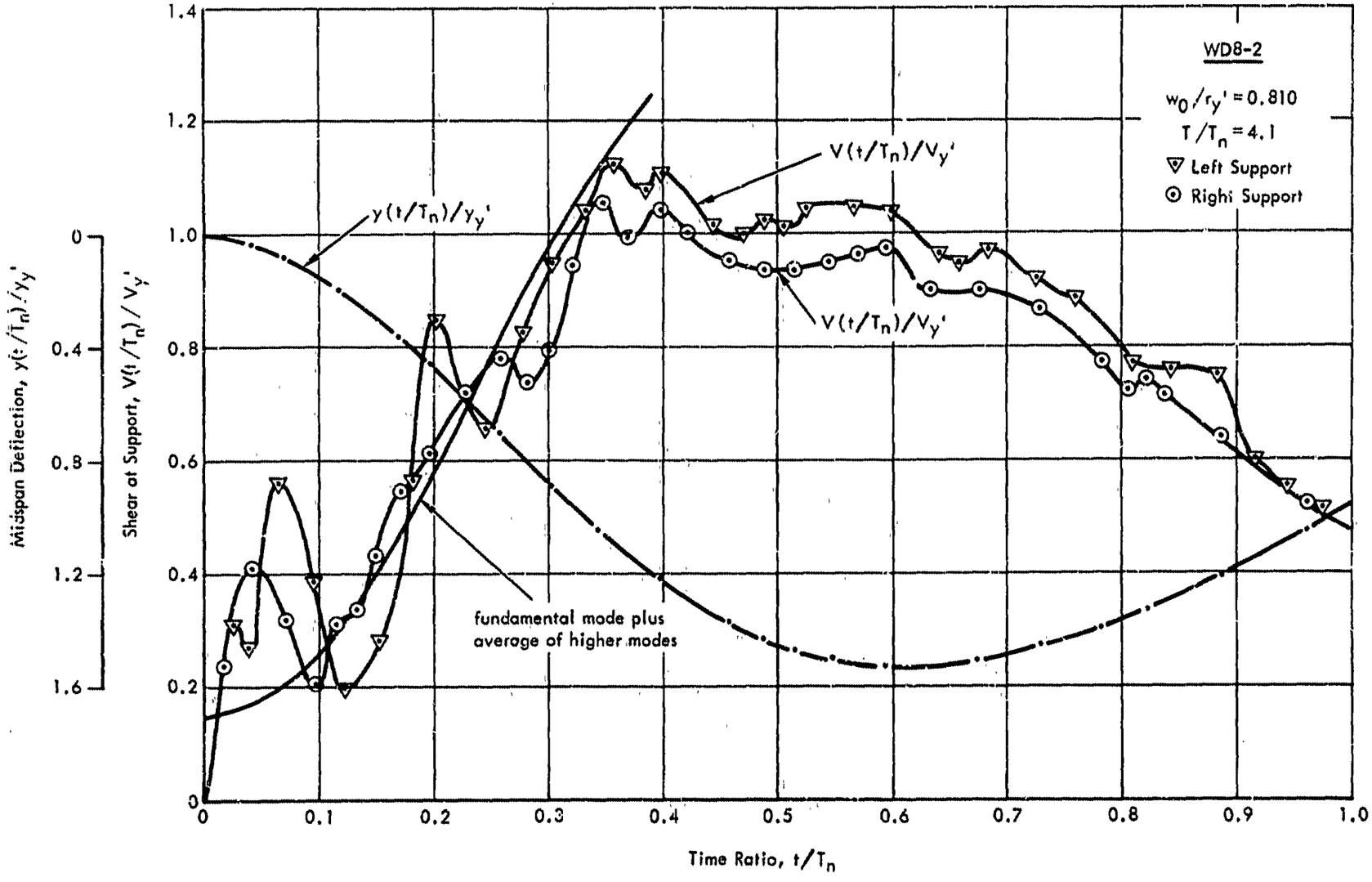

Figure E-8. Measured midspan deflection and shear at support versus time, WD8-2.

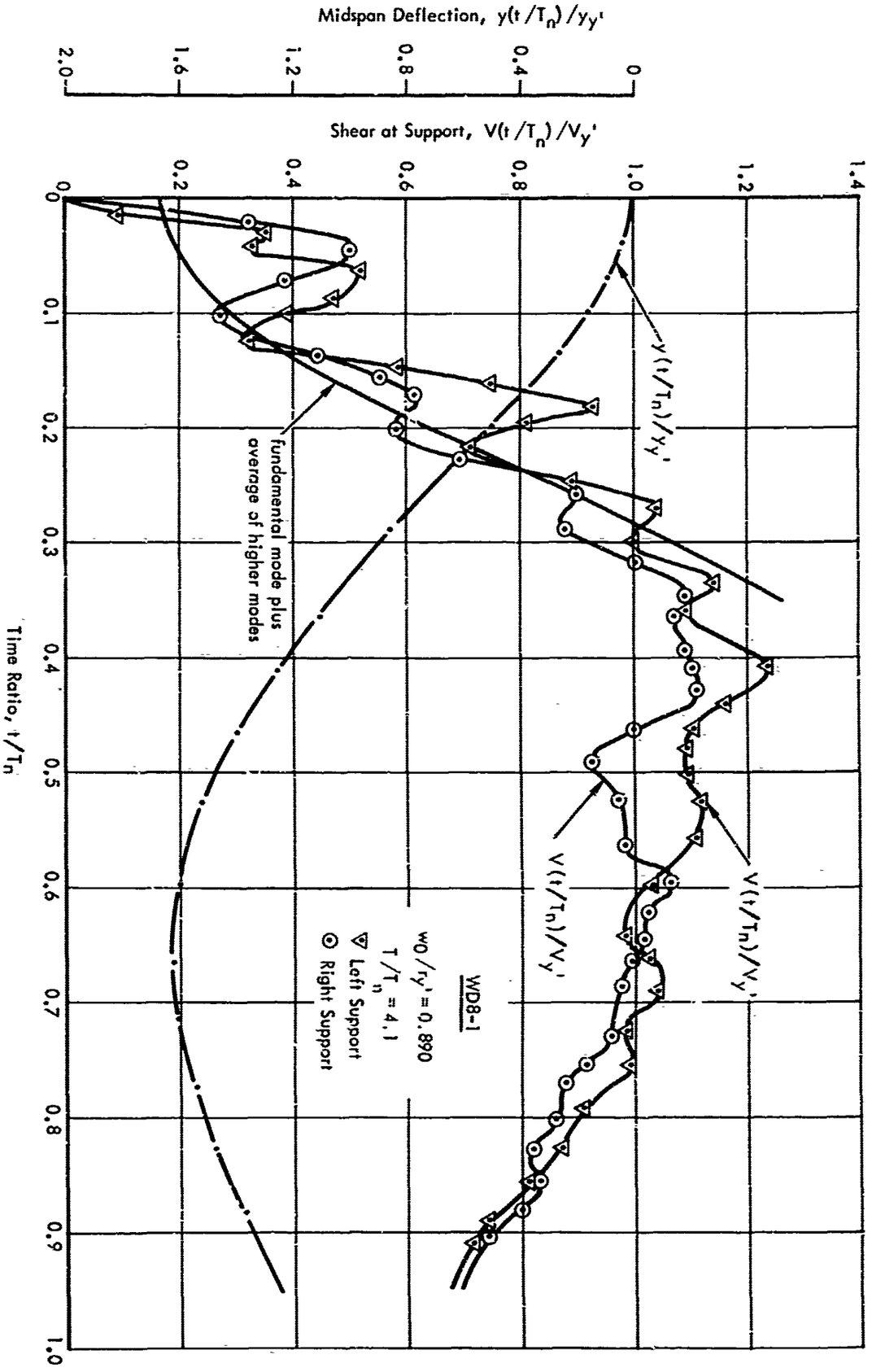

Figure E-7. Measured midspan deflection and shear at support versus time, WD8-1.

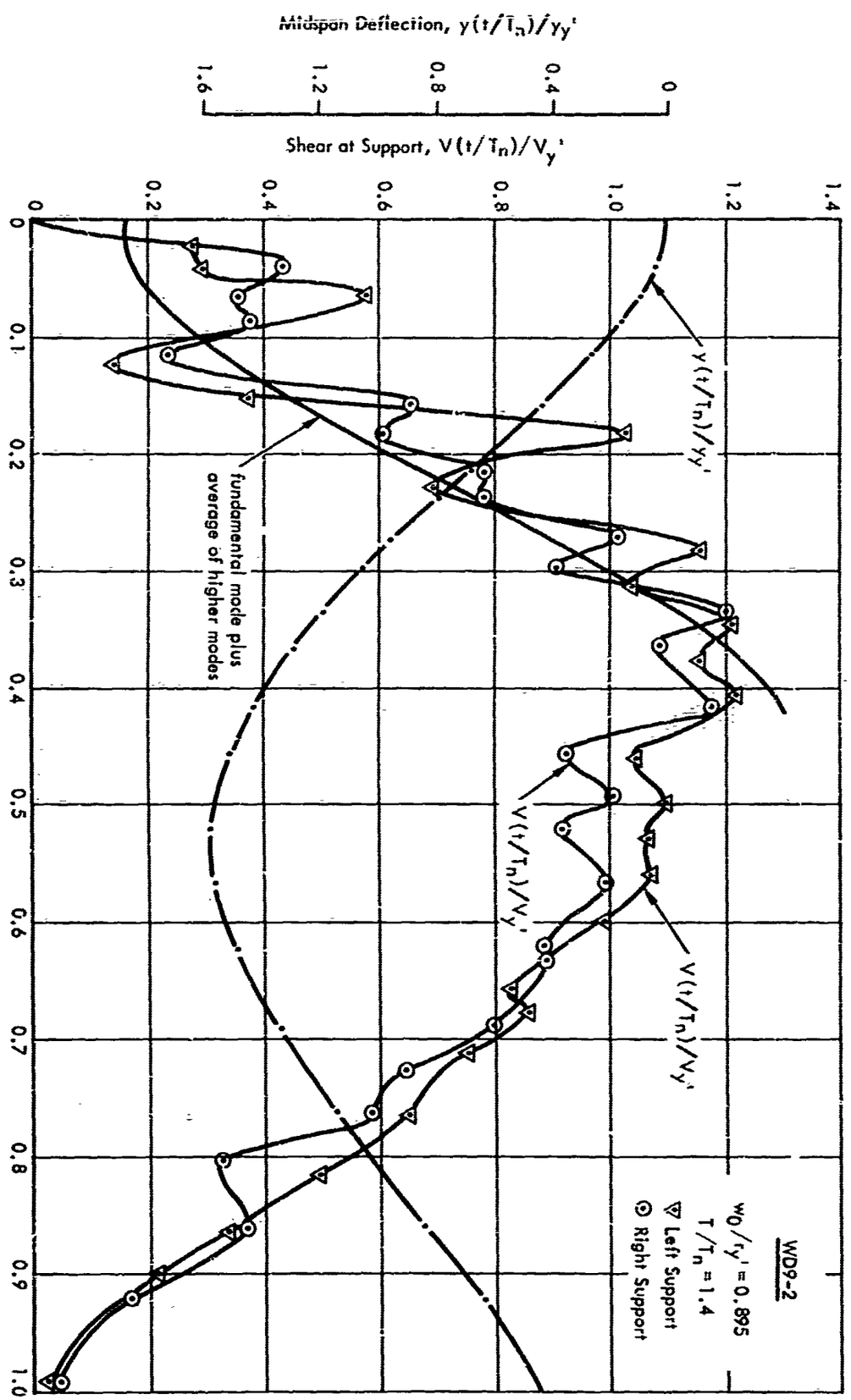

Figure E-10. Measured midspan deflection and shear at support versus time, WD9-2.

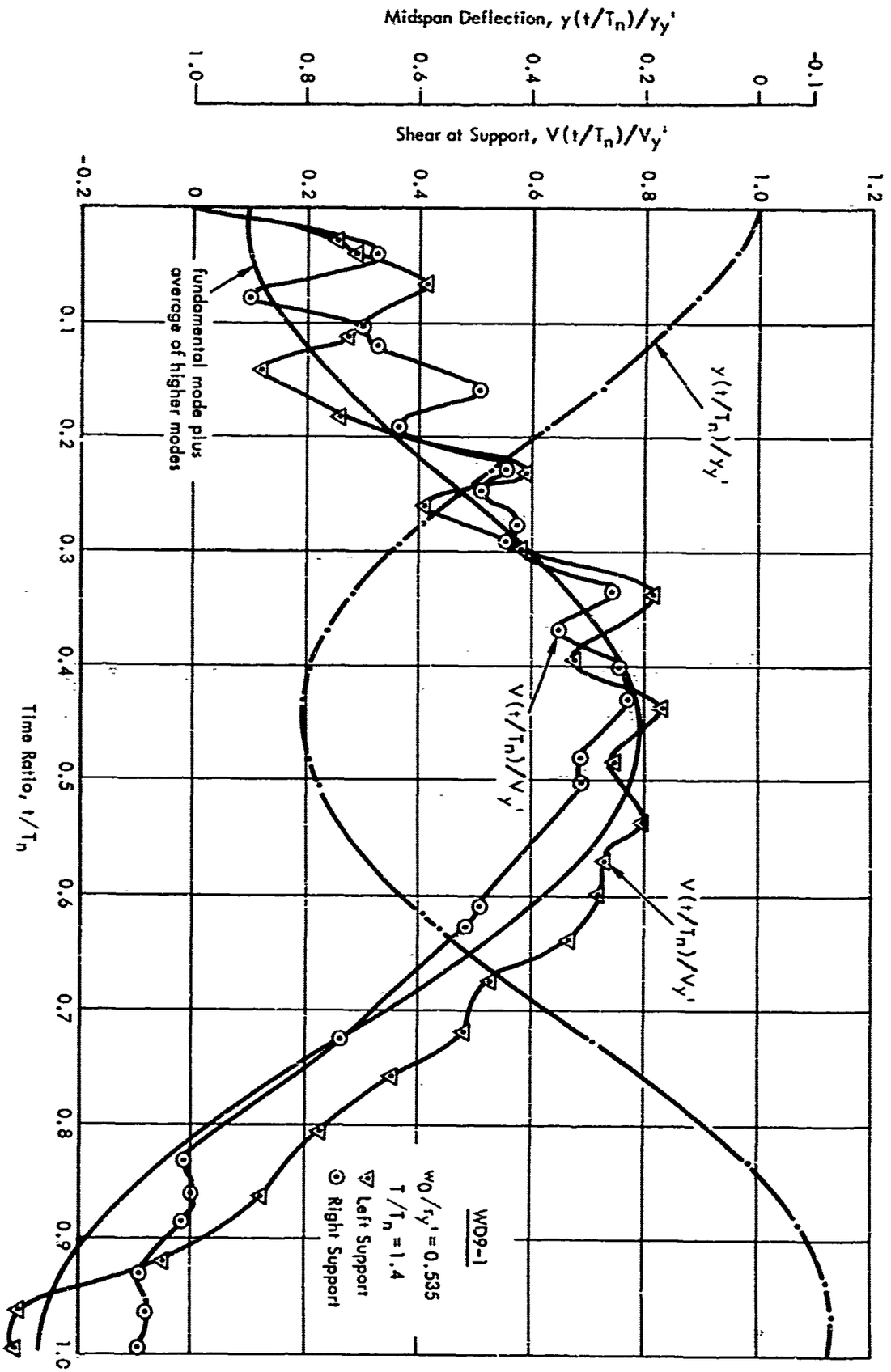

Figure E-9. Measured midspan deflection and shear at support versus time, WD9-1.

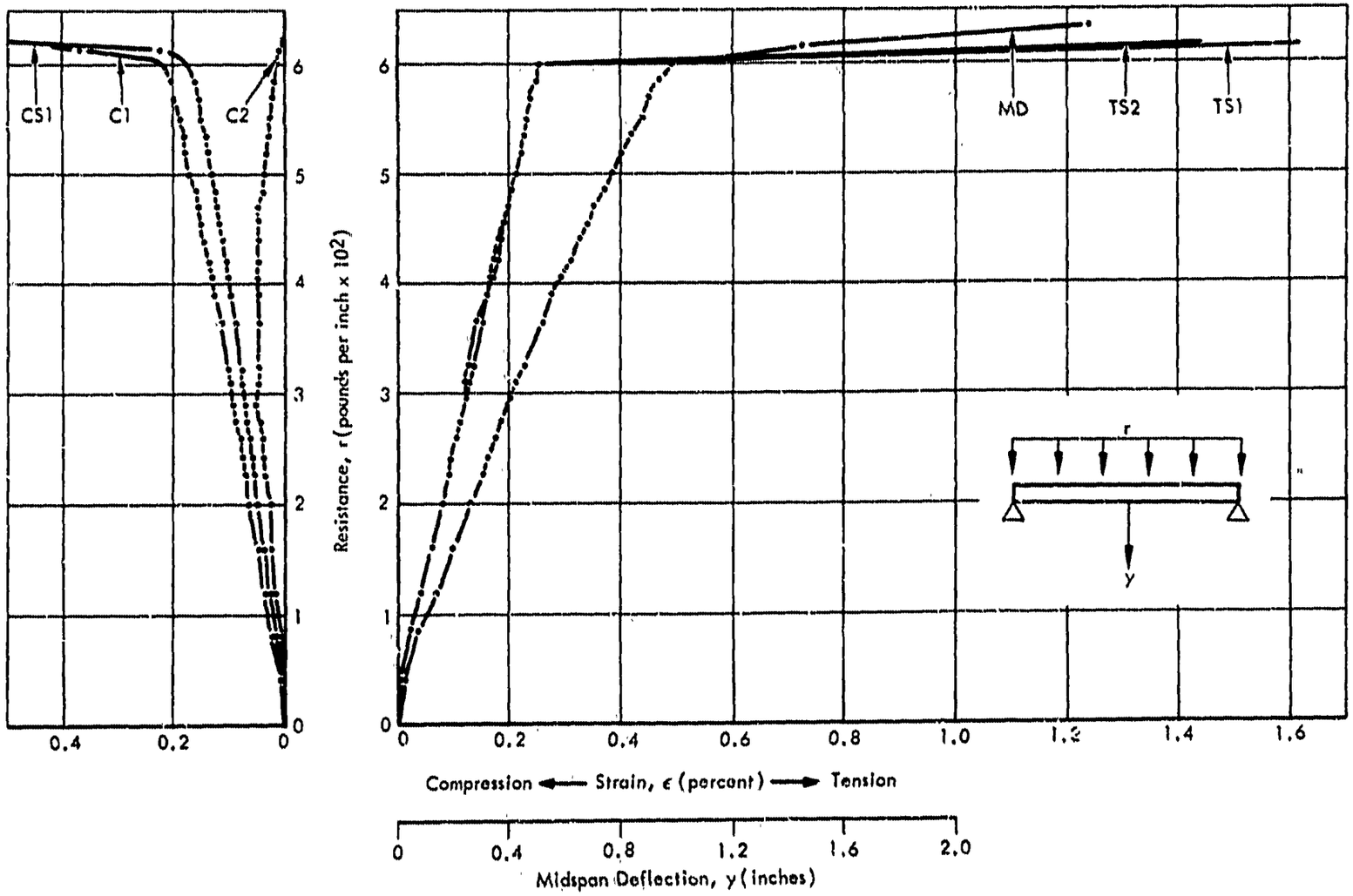

Figure F-2. Resistance-strain curves - beam WD2.

Appendix F

STATIC LOAD-DEFLECTION AND LOAD-STRAIN CURVES

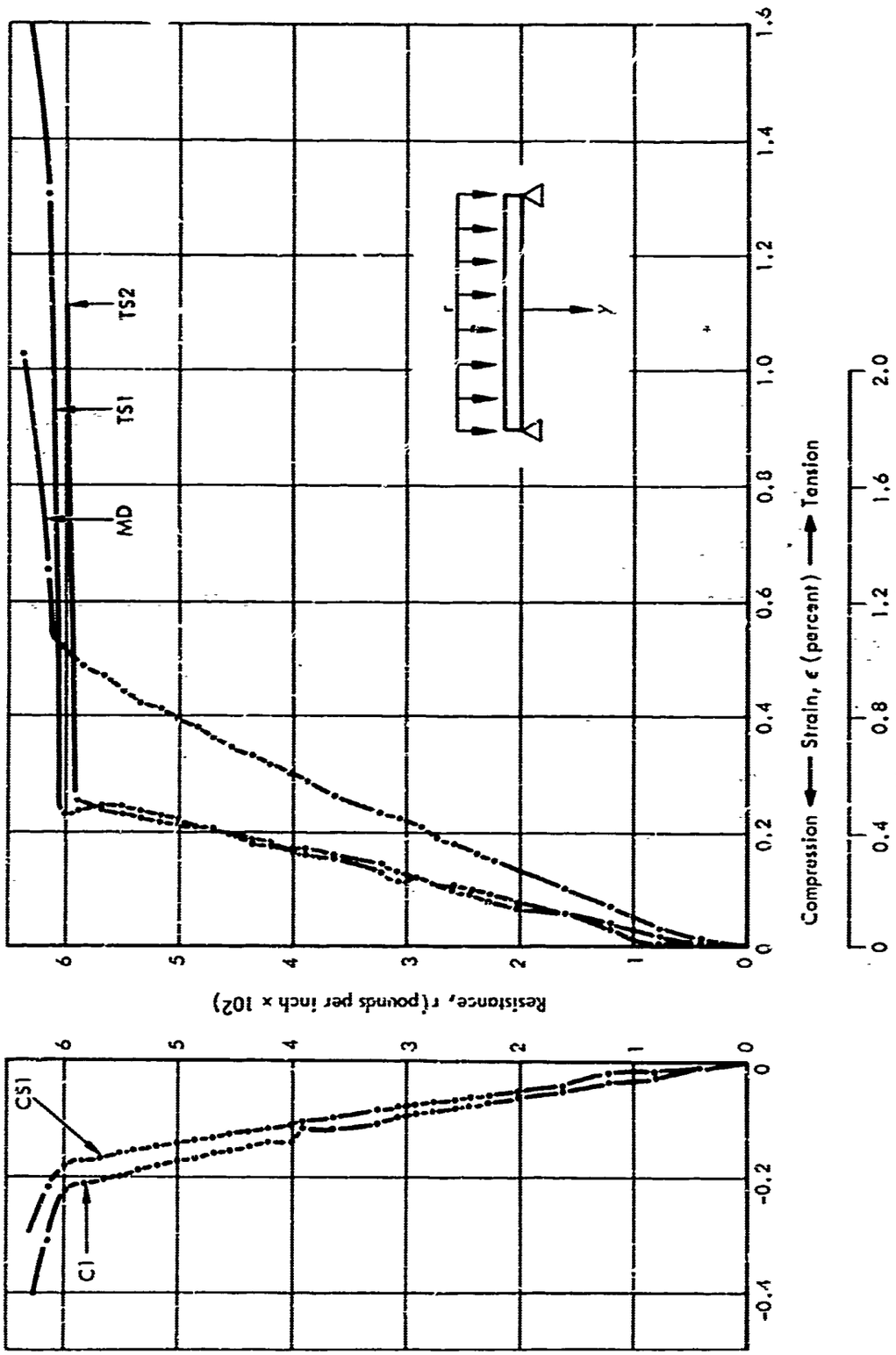

Figure F-1. Resistance-strain curves - beam WD1.

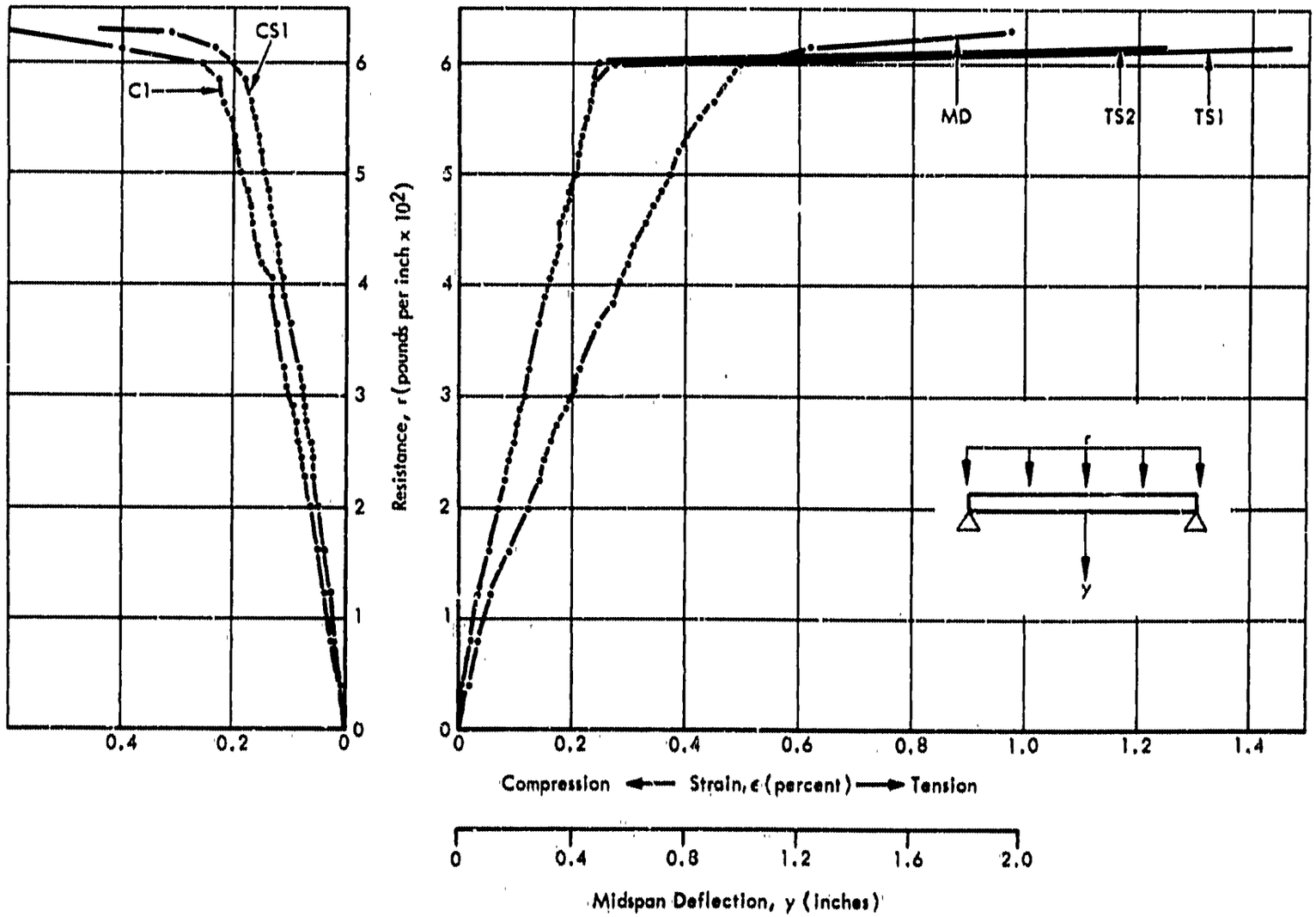

Figure F-3. Resistance-strain curves - beam WD3.

Appendix G

MODAL ANALYSIS OF A SIMPLY SUPPORTED BEAM UNDER A UNIFORM LOAD

OBJECTIVE

A modal analysis of a simply supported beam under a uniformly distributed dynamic load was made to (1) determine the influence of the dynamic parameters (peak load, load-duration and damping) on the transient variation in shear and moment-shear ratio along the span, and (2) develop a dynamic response chart for quickly determining the maximum shear forces a beam must resist to fail in flexure.

SCOPE AND APPROACH

Exact solutions for the transient variation in shear and moment at any point along the beam are developed and compared with approximate solutions. From the approximate solutions, a chart for the maximum dynamic shear factor at the supports was developed for various ratios of peak load to dynamic yield resistance and load-duration to fundamental period of vibration.

EXACT SOLUTION FOR DEFLECTION, MOMENT, AND SHEAR

In Figure G-1, the uniform beam is to be considered subjected to a uniformly distributed load of the type shown in Figure G-2. The beam has a uniformly distributed mass (m) and a constant stiffness (EI). The time variation in the load at each point along the span is the same. The damping force at any point along the span is assumed to be proportional to the velocity at that point, and the constant of proportionality (c) is the same at any point.

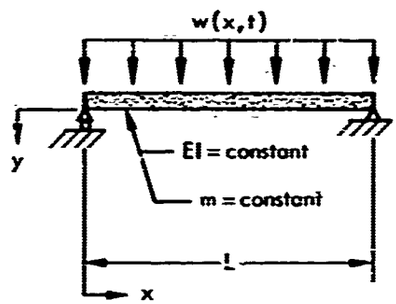

Figure G-1. Simply supported beam.

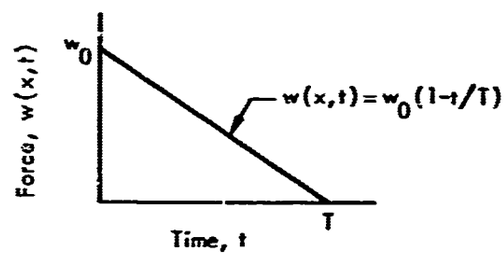

Figure G-2. Force function.

A free-body diagram showing the forces acting along an incremental length (dx) of the beam at any time (t) is shown in Figure G-3.

Assuming that the time variation in the load along the entire length of the beam is the same, the forcing function may be expressed as

$$w(x,t) = W(x)f(t)$$

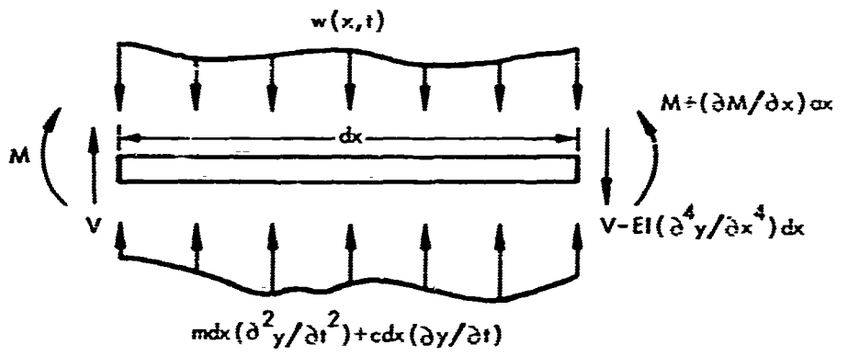

Figure G-3. Free-body diagram.

Summing the forces acting on the free body (Figure G-3), the governing equation of motion for the system is

$$m\frac{\partial^2 y}{\partial t^2} + c\frac{\partial y}{\partial t} + EI\frac{\partial^4 y}{\partial x^4} = W(x)\,f(t) \qquad \text{(G-1)}$$

Deflection

Solving Equation G-1, the exact solution for the deflection at any point on the beam of Figure G-1 produced by the forcing function of Figure G-2 for $0 \le t \le T$ is [8,9]

$$y(x,t) = \sum_{j=1} C_j \phi_j(x)\, AF_j(t) \qquad \text{(G-2)}$$

where $C_j = \dfrac{4w_0 L^4}{j^5 \pi^5 EI}$, j = odd

$$\phi_j(x) = \sin\left(j\frac{\pi x}{L}\right)$$

$$AF_j(t) = 1 - \frac{t}{T} + \frac{2\beta}{\omega_j T} + e^{-\beta\omega_j t}\left[\frac{1}{\omega_j\sqrt{1-\beta^2}}\left(\frac{1}{T} - \beta\omega_j - \frac{2\beta^2}{T}\right)\sin\left(\omega_j\sqrt{1-\beta^2}\,t\right)\right.$$

$$\left. - 1 + \frac{2\beta}{\omega_j T}\cos\left(\omega_j\sqrt{1-\beta^2}\,t\right)\right]$$

j = jth mode

ω_j = circular frequency of the jth mode = $j^2 \frac{\pi^2}{L^2}\sqrt{\frac{EI}{m}}$

β = damping ratio = $\frac{c}{c_{cr}} = \frac{c}{2m\omega_j}$

Moment

The moment at any point and time is

$$M(x,t) = -EI\frac{\partial^2 y}{\partial x^2}$$

Therefore, from Equation G-2, the exact solution for the moment at any point along the beam for $0 \le t \le T$ is

$$M(x,t) = \frac{4w_0 L^2}{\pi^3}\sum_{j=\text{odd}}\frac{1}{j^3}\sin\left(j\frac{\pi x}{L}\right)\left[1 - \frac{t}{T} + \frac{2\beta}{\omega_j T} + e^{-\beta\omega_j t}\left[\frac{1}{\omega_j\sqrt{1-\beta^2}}\right.\right.$$

$$\left.\left. \cdot \left(\frac{1}{T} - \beta\omega_j - \frac{2\beta^2}{T}\right)\sin\left(\omega_j\sqrt{1-\beta^2}\,t\right) - \left(1 + \frac{2\beta}{\omega_j T}\right)\cos\left(\omega_j\sqrt{1-\beta^2}\,t\right)\right]\right] \qquad \text{(G-3)}$$

Shear

The shear at any point and time is

$$V(x,t) = -EI\frac{\partial^3 y}{\partial x^3}$$

Therefore, from Equation G-2, the exact solution for the shear at any point and time for $0 \leq t \geq T$ is

$$V(x,\ t) = \frac{4w_0 L}{\pi^2} \sum_{j=\text{odd}} \frac{1}{j^2} \cos\left(j\pi\frac{x}{L}\right)\left\{1 - \frac{t}{T} + \frac{2\beta}{\omega_j T} + e^{-\beta\omega_j t}\left[\frac{1}{\omega_j\sqrt{1-\beta^2}}\left(\frac{1}{T} - \beta\omega_j - \frac{2\beta^2}{T}\right)\right.\right.$$

$$\left.\left. \cdot \sin\left(\omega_j\sqrt{1-\beta^2}\,t\right) - \left(1 + \frac{2\beta}{\omega_j t}\right)\cos\left(\omega_j\sqrt{1-\beta^2}\,t\right)\right]\right\} \qquad \text{(G-4)}$$

The shear at the ends (x = 0, L) of a simply supported beam under a uniform static load, w_0, is

$$V' = \frac{w_0 L}{2}$$

Therefore, the dynamic shear factor at each end of the beam is

$$DSF(o,t) = \frac{V(o,t)}{V'} = \frac{8}{\pi^2}\sum \frac{1}{j^2}\left\{1 - \frac{t}{T} + \frac{\beta T_n}{j^2\pi T} + e^{-2\pi\beta j^2 \frac{t}{T_n}}\left[\frac{1}{\sqrt{1-\beta^2}}\left(\frac{T_n}{2\pi T j^2} - \beta - \frac{T_n\beta^2}{\pi T j^2}\right)\right.\right.$$

$$\left.\left. \cdot \sin\left(2\pi j^2\sqrt{1-\beta^2}\,\frac{t}{T_n}\right) - \left(1 + \frac{\beta T_n}{\pi T j^2}\right)\cos\left(2\pi j^2\sqrt{1-\beta^2}\,\frac{t}{T_n}\right)\right]\right\} \qquad \text{(G-5)}$$

where T_n = fundamental period of vibration = $\dfrac{2\pi j^2}{\omega_j}$

Solutions to Equation G-5 are plotted in Figures 14, 15, and 16 for ratios of T/T_n equal to 20, 6, and 1, respectively.

APPROXIMATE SOLUTION FOR SHEAR AT SUPPORTS

For an undamped beam ($\beta = 0$), Equation G-5 can be expressed as

$$DSF(o,t) = \frac{8}{\pi^2}\left[1 - \frac{t}{T} + \frac{T_n}{2\pi T}\sin\left(2\pi\frac{t}{T_n}\right) - \cos\left(2\pi\frac{t}{T_n}\right)\right]$$

$$+ \frac{8}{\pi^2}\sum_{j=3,5\ldots}\frac{1}{j^2}\left[1 - \frac{t}{T} + \frac{T_n}{2\pi j^2 T}\sin\left(2\pi j^2\frac{t}{T_n}\right) - \cos\left(2\pi j^2\frac{t}{T_n}\right)\right] \quad \text{(G-4)}$$

but

$$\sum_{j=3,5\ \ldots}\frac{1}{j^2} = \frac{\pi^2}{8} - 1$$

Therefore,

$$DSF(o,t) = \frac{8}{\pi^2}\left[1 - \frac{t}{T} + \frac{T_n}{2\pi T}\sin\left(2\pi\frac{t}{T_n}\right) - \cos\left(2\pi\frac{t}{T_n}\right)\right] + \frac{8}{\pi^2}\left(\frac{\pi^2}{8} - 1\right)\left(1 - \frac{t}{T}\right)$$

$$+ \frac{8}{\pi^2}\sum_{j=3,5\ldots}\frac{1}{j^2}\left[\frac{T_n}{2\pi j^2 T}\sin\left(2\pi j^2\frac{t}{T_n}\right) - \cos\left(2\pi j^2\frac{t}{T_n}\right)\right]$$

The average magnitude of the last term in the above equation is zero and can be neglected. Therefore, an approximate solution for the dynamic shear factor at the supports of a simply supported beam with no damping for $0 \leq t \leq T$ is[9]

$$DSF(o,t) \cong 0.810\left[1 - \frac{t}{T} + \frac{T_n}{T}\sin\left(2\pi\frac{t}{T_n}\right) - \cos\left(2\pi\frac{t}{T_n}\right)\right] + 0.190\left(1 - \frac{t}{T}\right) \quad \text{(G-6)}$$

Solutions to Equation G-6 are plotted in Figures 15, and 16.

MAXIMUM DYNAMIC SHEAR FACTOR AT SUPPORTS

Elastic Range ($y_m \leq y_y$)

The dynamic shear factor at the supports is a maximum when

$$\frac{\partial}{\partial t}\left[DSF(o,t)\right] = 0$$

Combining Equation G-6 with the above equation and rearranging, the time corresponding to the maximum dynamic shear factor at the supports of an undamped beam under a uniform load is

$$\frac{t_m}{T_n} = \frac{1}{2\pi}\left\{\cos^{-1}\left[\frac{0.50}{0.4053\sqrt{1 + 4\pi^2\left(\frac{T}{T_n}\right)^2}}\right] + \tan^{-1}\left(2\pi\frac{T}{T_n}\right)\right\} \qquad \text{(G-7)}$$

Equations G-6 and G-7 were used to plot the portion corresponding to the elastic case of the response chart for maximum shear shown in Figure 17. The elastic case corresponds to that portion of the chart to the left of the dashed line shown in Figure 17.

Plastic Range ($y_m \geq y_y$)

The maximum shear forces in a beam subjected to plastic deflections are a function of the resistance developed by the beam and the distribution of the applied load. By assuming the spanwise distribution of inertia forces acting on the beam and applying the laws of statics, an approximate solution for the shear at the supports of a beam with any type of boundary conditions is of the form

$$V(o,t) = C_1 r(x,t) + C_2 w(x,t)$$

For simply supported beam, the constant C_2 is less than C_1 for any reasonable assumption for the spanwise distribution of inertia forces[9]. This suggests that the maximum shear at the supports of a simply supported beam having an elasto-plastic resistance diagram will occur when the flexural yield hinge first forms at the midspan. Beam tests described in this report support this conclusion. Therefore, the approach used for calculating the maximum dynamic shear factor for the plastic range was to evaluate Equation G-6 at the time corresponding to first yielding of the beam at midspan.

The midspan deflection of a beam can be accurately described by considering only the contribution from the first mode. Therefore, from Equation G-2 the yield deflection at midspan of an undamped beam can be expressed as

$$y_y\left(\frac{L}{2}, t_y\right) = \frac{4w_0 L^4}{\pi^5 EI}\left[1 - \frac{t_y}{T} + \frac{T_n}{2\pi T}\sin\left(2\pi\frac{t_y}{T_n}\right) - \cos\left(2\pi\frac{t_y}{T_n}\right)\right]$$

The yield deflection of a simply supported beam under a uniform load in terms of the flexural yield resistance (r_y) is

$$y_y = \frac{5r_y L^4}{384\,EI}$$

Combining the above two equations and rearranging,

$$\frac{t_y}{T_n}\left(\frac{T_n}{T}\right) + \cos\left(2\pi\frac{t_y}{T_n}\right) - \frac{T_n}{2\pi T}\sin\left(2\pi\frac{t_y}{T_n}\right) = 1 - \frac{5\pi^5}{1,536}\left(\frac{r_y}{w_0}\right) \qquad \text{(G-8)}$$

Evaluating Equation G-8 at the time corresponding to first yielding of the beam at midspan, the maximum dynamic shear factor for the plastic case is

$$DSF_m(o,t) = 0.810\left[1 - \frac{t_y}{T} + \frac{T_n}{2\pi T}\sin\left(2\pi\frac{t_y}{T_n}\right) - \cos\left(2\pi\frac{t_y}{T_n}\right)\right] + 0.190\left(1 - \frac{t_y}{T}\right) \qquad \text{(G-9)}$$

SHEAR DISTRIBUTION ALONG BEAM

From Equation G-4 and the simplifying assumptions leading to Equation G-6, an approximate solution for the shear along the length of an undamped beam in terms of the equivalent static shear at the support is

$$\frac{V(x,t)}{\frac{w_0 L}{2}} = 0.810\cos\left(\frac{\pi x}{L}\right)\left[\frac{T_n}{2\pi T}\sin\left(2\pi\frac{t}{T_n}\right) - \cos\left(2\pi\frac{t}{T_n}\right)\right] + \left(1 - \frac{2x}{L}\right)\left(1 - \frac{t}{T}\right) \qquad \text{(G-10)}$$

Equation G-10 is plotted in Figure G-4 and shows the variation in shear along the beam at various times.

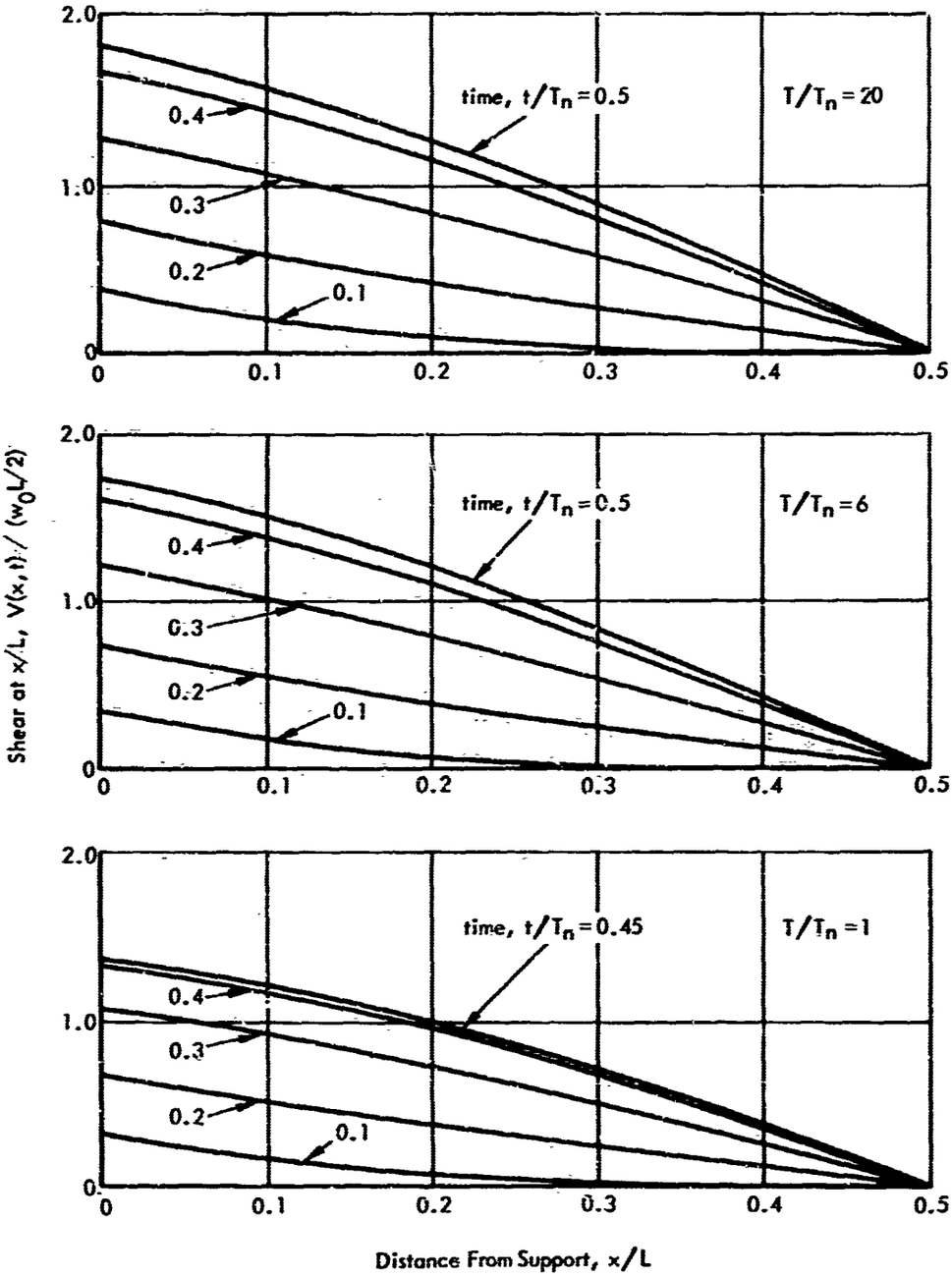

Figure G-4. Distribution of shear along length of beam, elastic case.

The shear along the beam under a uniform static load, w_0, is

$$V'(x) = \frac{w_0 L}{2}\left(1 - \frac{2x}{L}\right).$$

The above two relationships lead to the following approximate solution for the dynamic shear factor at any point and time along the beam:

$$DSF(x,t) = \frac{0.810}{\left(1 - \frac{2x}{L}\right)} \cos\left(\frac{\pi x}{L}\right)\left[\frac{T_n}{2\pi T}\sin\left(\frac{2\pi t}{T_n}\right) - \cos\left(\frac{2\pi t}{T_n}\right)\right] + \left(1 - \frac{2x}{L}\right)\left(1 - \frac{t}{T}\right) \quad \text{(G-11)}$$

Equation G-11 is plotted in Figure G-5.

MOMENT-SHEAR RATIO ALONG SPAN

From Equations G-3 and G-4 and neglecting terms with an average of zero, an approximate solution for the moment-shear ratio at any time and point is $(M/V)(x,t)$

$$= \frac{L}{\pi}\left\{\frac{\sin\left(\pi\frac{x}{L}\right)\left[1 - \frac{t}{T} + \frac{T_n}{2\pi T}\sin\left(2\pi\frac{t}{T_n}\right) - \cos\left(2\pi\frac{t}{T_n}\right)\right] + \left(1 - \frac{t}{T}\right)\sum_{j=3,5,\ldots}\frac{1}{j^2}\sin\left(j\pi\frac{x}{L}\right)}{\cos\left(\pi\frac{x}{L}\right)\left[1 - \frac{t}{T} + \frac{T_n}{2\pi T}\sin\left(2\pi\frac{t}{T_n}\right) - \cos\left(2\pi\frac{t}{T_n}\right)\right] + \left(1 - \frac{t}{T}\right)\sum_{j=3,5,\ldots}\frac{1}{j^2}\cos\left(j\pi\frac{x}{L}\right)}\right\} \quad \text{(G-12)}$$

Solutions to Equation G-12 are plotted in Figure G-6.

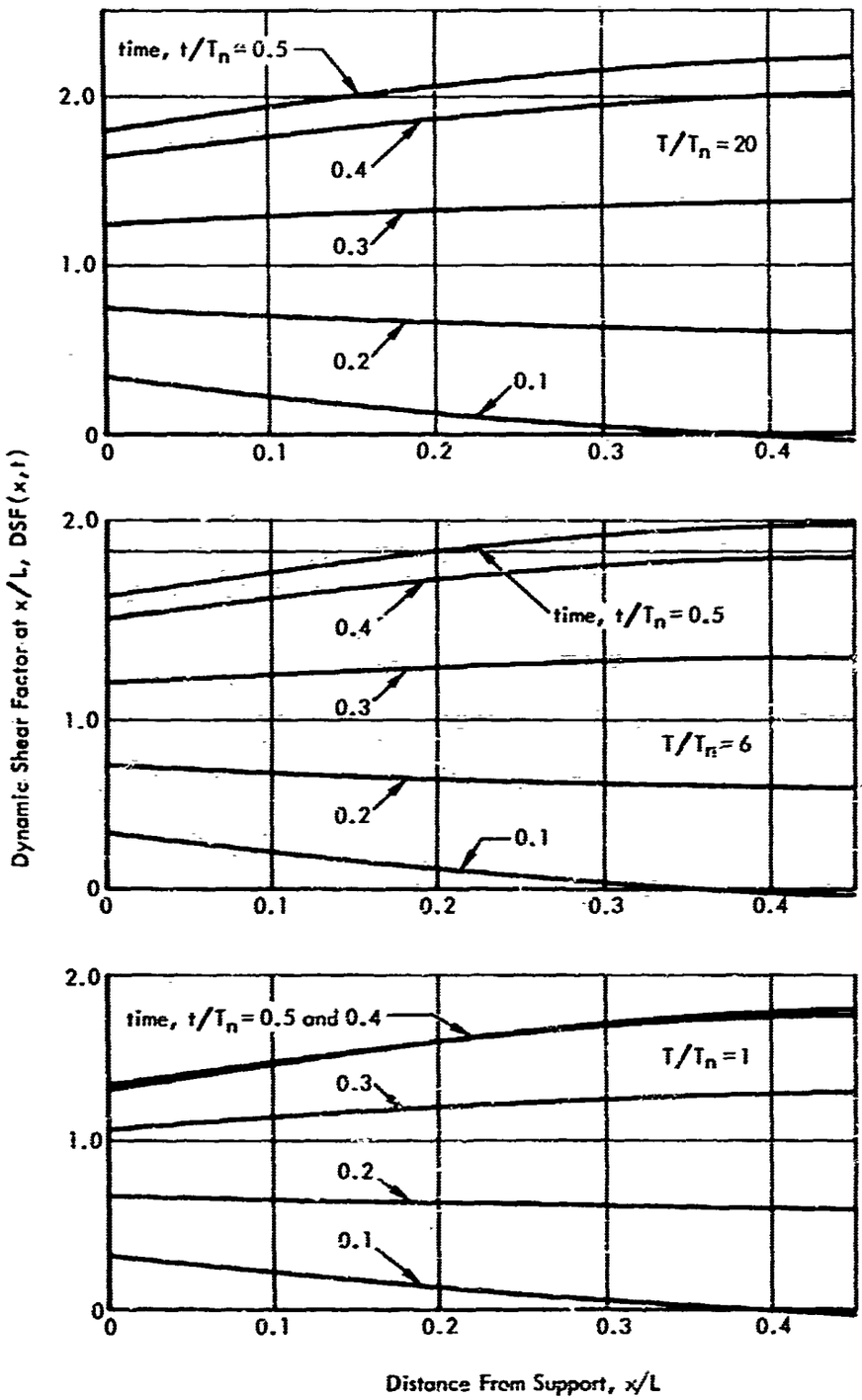

Figure G-5. Variation in dynamic shear factor along length of beam, elastic case.

Figure G-6. Moment-shear ratio along span of a simply supported beam under a uniform dynamic load, elastic case.

Unclassified
Security Classification

DOCUMENT CONTROL DATA - R&D

(Security classification of title, body of abstract and indexing annotation must be entered when the overall report is classified)

1. ORIGINATING ACTIVITY *(Corporate author)*
U. S. Naval Civil Engineering Laboratory
Port Hueneme, California 93041

2a. REPORT SECURITY CLASSIFICATION
Unclassified

2b GROUP

3. REPORT TITLE
Dynamic Shear Strength of Reinforced Concrete Beams — Part I

4. DESCRIPTIVE NOTES *(Type of report and inclusive dates)*
June 1962 - May 1965

5. AUTHOR(S) *(Last name, first name, initial)*
Keenan, William A.

6. REPORT DATE	7a. TOTAL NO. OF PAGES	7b. NO. OF REFS
December 1965	91	9

8a. CONTRACT OR GRANT NO.	9a. ORIGINATOR'S REPORT NUMBER(S)
b. PROJECT NO. Y-F008-08-02-110	TR-395
c.	9b. OTHER REPORT NO(S) *(Any other numbers that may be assigned this report)*
d.	

10. AVAILABILITY/LIMITATION NOTICES
Distribution of this document is unlimited.

11. SUPPLEMENTARY NOTES	12. SPONSORING MILITARY ACTIVITY
	BUDOCKS

13. ABSTRACT

A series of reinforced concrete beams were tested to study shear and diagonal tension in beams under dynamic load. The tests constitute the first phase of a study designed (1) to determine criteria for the minimum amount of web reinforcement required for developing the ultimate flexural resistance of beams and (2) to evaluate the difference between these criteria for static and dynamic loading.

It was found that (1) the shear resistance at diagonal tension cracking and at first yielding of the stirrups increased under dynamic load, and (2) the formulas presented in a definitive report by a joint committee of the American Concrete Institute (ACI) and the American Society of Civil Engineers (ASCE) adequately predicted the static shear resistance but grossly underestimated the dynamic shear resistance. Evidence is cited which attributes the increase in shear resistance under dynamic load to an increase in the tensile strength of the concrete and yield strength of the stirrups. An effective amount of web reinforcement (rf_y), 69 percent less than the amount required by the ACI-ASCE formula, resulted in flexure failures under static and dynamic load.

Equations are presented which permit prediction of the dynamic shear resistance corresponding to diagonal tension cracking and first yielding of the stirrups. A dynamic response chart is developed for estimating the maximum shear at the supports of a simple supported beam under a uniform dynamic load.

DD FORM 1 JAN 64 1473 0101-807-6800

Unclassified
Security Classification

Unclassified

Security Classification

14. KEY WORDS	LINK A		LINK B		LINK C	
	ROLE	WT	ROLE	WT	ROLE	WT
Dynamic tests						
Static tests						
Shear strength						
Reinforced concrete						
Beams (structural)						
Determination						
Reinforcing steel						
Mechanical properties						
Requirements						

INSTRUCTIONS

1. ORIGINATING ACTIVITY: Enter the name and address of the contractor, subcontractor, grantee, Department of Defense activity or other organization *(corporate author)* issuing the report.

2a. REPORT SECURITY CLASSIFICATION: Enter the overall security classification of the report. Indicate whether "Restricted Data" is included. Marking is to be in accordance with appropriate security regulations.

2b. GROUP: Automatic downgrading is specified in DoD Directive 5200.10 and Armed Forces Industrial Manual. Enter the group number. Also, when applicable, show that optional markings have been used for Group 3 and Group 4 as authorized.

3. REPORT TITLE: Enter the complete report title in all capital letters. Titles in all cases should be unclassified. If a meaningful title cannot be selected without classification, show title classification in all capitals in parenthesis immediately following the title.

4. DESCRIPTIVE NOTES: If appropriate, enter the type of report, e.g., interim, progress, summary, annual, or final. Give the inclusive dates when a specific reporting period is covered.

5. AUTHOR(S): Enter the name(s) of author(s) as shown on or in the report. Enter last name, first name, middle initial. If military, show rank and branch of service. The name of the principal author is an absolute minimum requirement.

6. REPORT DATE: Enter the date of the report as day, month, year; or month, year. If more than one date appears on the report, use date of publication.

7a. TOTAL NUMBER OF PAGES: The total page count should follow normal pagination procedures, i.e., enter the number of pages containing information.

7b. NUMBER OF REFERENCES: Enter the total number of references cited in the report.

8a. CONTRACT OR GRANT NUMBER: If appropriate, enter the applicable number of the contract or grant under which the report was written.

8b, 8c, & 8d. PROJECT NUMBER: Enter the appropriate military department identification, such as project number, subproject number, system numbers, task number, etc.

9a. ORIGINATOR'S REPORT NUMBER(S): Enter the official report number by which the document will be identified and controlled by the originating activity. This number must be unique to this report.

9b. OTHER REPORT NUMBER(S): If the report has been assigned any other report numbers *(either by the originator or by the sponsor)*, also enter this number(s).

10. AVAILABILITY/LIMITATION NOTICES: Enter any limitations on further dissemination of the report, other than those imposed by security classification, using standard statements such as:

(1) "Qualified requesters may obtain copies of this report from DDC."

(2) "Foreign announcement and dissemination of this report by DDC is not authorized."

(3) "U. S. Government agencies may obtain copies of this report directly from DDC. Other qualified DDC users shall request through _____."

(4) "U. S. military agencies may obtain copies of this report directly from DDC. Other qualified users shall request through _____."

(5) "All distribution of this report is controlled. Qualified DDC users shall request through _____."

If the report has been furnished to the Office of Technical Services, Department of Commerce, for sale to the public, indicate this fact and enter the price, if known.

11. SUPPLEMENTARY NOTES: Use for additional explanatory notes.

12. SPONSORING MILITARY ACTIVITY: Enter the name of the departmental project office or laboratory sponsoring *(paying for)* the research and development. Include address.

13. ABSTRACT: Enter an abstract giving a brief and factual summary of the document indicative of the report, even though it may also appear elsewhere in the body of the technical report. If additional space is required, a continuation sheet shall be attached.

It is highly desirable that the abstract of classified reports be unclassified. Each paragraph of the abstract shall end with an indication of the military security classification of the information in the paragraph, represented as (TS), (S), (C), or (U).

There is no limitation on the length of the abstract. However, the suggested length is from 150 to 225 words.

14. KEY WORDS: Key words are technically meaningful terms or short phrases that characterize a report and may be used as index entries for cataloging the report. Key words must be selected so that no security classification is required. Identifiers, such as equipment model designation, trade name, military project code name, geographic location, may be used as key words but will be followed by an indication of technical context. The assignment of links, roles, and weights is optional.

Unclassified

Security Classification